Liquid crystalline polymer membranes for gas separation

Liquid crystalline polymer membranes for gas separation

PROEFSCHRIFT

ter verkrijging van de graad van doctor aan de Technische Universiteit Eindhoven, op gezag van de rector magnificus prof.dr.ir. F.P.T. Baaijens, voor een commissie aangewezen door het College voor Promoties, in het openbaar te verdedigen op woensdag 14 december 2022 om 16:00 uur

door

Joey Joseph Hubertina Kloos

geboren te Maastricht

Dit proefschrift is goedgekeurd door de promotoren en de samenstelling van de promotiecommissie is als volgt:

Voorzitter:	prof.dr.ir. E.J.M. Hensen
1e promotor:	prof.dr.ir. D.C. Nijmeijer
2e promotor:	dr.ing. Z. Borneman
Copromotor(en):	prof.dr. A.P.H.J. Schenning
Leden:	prof.dr.ir. I.F.J. Vankelecom (KU Leuven)
	prof.dr. J.L. Serrano (University of Zaragoza)
	prof.dr. R.P. Sijbesma
	dr.ir. J.P.A. Heuts

Het onderzoek of ontwerp dat in dit proefschrift wordt beschreven is uitgevoerd in overeenstemming met de TU/e Gedragscode Wetenschapsbeoefening.

“Don’t adventures ever have an end? I suppose not. Someone else always has to carry on the story.”

— Bilbo Baggins

A catalogue record is available from the Eindhoven University of Technology Library

ISBN: 978-90-386-5610-6

Printing: Ridderprint | www.ridderprint.nl

The research in this thesis was conducted in the Membrane Materials and Processes group at the Eindhoven University of Technology, The Netherlands.

This research was part of the research program START-UP with project number 740.018.005, which is financed by the Dutch Organization for Scientific Research (NWO).

Summary

Liquid crystalline polymer membranes for gas separation

In this thesis the structure-property relationships of liquid crystalline (LC) membranes for gas separation applications were investigated. The aspects under study were (1) the effect of molecular order and orientation of the LC nanostructures, (2) the layer spacing and tilt angle of the nanostructures, (3) the operating temperature and chemical composition of the LC monomers and (4) the steric size of the LC substituents. As a result, this work shows the opportunities of using LCs to fabricate nanostructured membranes for gas separation by showing how and to what extent the above-mentioned aspects can be used to control the gas separation performance of LC membranes.

First, a general introduction of LC materials and their applications is provided in **Chapter 1**. The history and developments in LC materials are briefly discussed and this is followed by a section that provides the relevant theory on the self-assembly properties, alignment and fabrication processes of LC polymer materials. Subsequently, the use of LC materials for fabricating membranes with distinct and well-controlled morphologies for various membrane processes is addressed. Then the opportunities and motivation for using LC polymer membranes for gas separation membranes are discussed, followed by a section that provides the relevant theory regarding polymer membrane-based gas separation. Lastly, the aim and outline of this thesis are provided.

In **Chapter 2** the effect of molecular order and orientation on the gas separation performance of free-standing LC polymer membranes is investigated. LC membranes are fabricated with various, distinct morphologies that differ in type and degree of molecular order (isotropic, nematic cybotactic, and smectic C) and orientation (planar and homeotropic) while using the same chemical composition. Single gas permeation data show that the gas permeability decreases with increasing molecular order while the ideal gas selectivity of He and CO_2 over N_2 increases tremendously when going from randomly ordered to the highly ordered smectic C morphology. The solubility coefficient is similar for all membranes while the diffusion coefficient of the ordered smectic C membranes is found to be 10 times lower compared to the randomly ordered membranes, demonstrating that

gas permeation through LC membranes mainly depends on diffusivity rather than solubility. It is proposed that with increasing molecular order, the free volume elements in the membrane become smaller, which hinders gasses with larger kinetic diameters more than gasses with smaller kinetic diameters, inducing selectivity. The effect of molecular orientation is shown by a 3-fold reduction of the diffusion coefficient of homeotropic aligned smectic C membranes compared to planar aligned smectic C membranes.

In **Chapter 3** the effect of chemical composition and temperature on gas permeability and solubility of free-standing smectic LC polymer membranes is investigated. Planar aligned smectic LC membranes with various compositions of a mono-methacrylate LC with a crown ether functionality (M1) to enhance CO_2 solubility and a di-acrylate LC cross-linker (M2) are fabricated. The layer spacing and tilt angle of the layered structures are found to be independent of preparation temperature but are highly dependent on the chemical composition of the membrane. Increasing the M1 content decreases the layer spacing while the tilt angle of the layered structures increases. This is because the molecular length of M1 is smaller than that of M2, resulting in smaller layer spacings for membranes with higher M1 contents. Single gas permeation data measured below the glass transition temperatures (T_g) of the membranes demonstrate that the CO_2 permeability for all M1/M2 compositions is mainly dependent on the difference in CO_2 solubility. For membranes that contain 30 wt% M1 both the CO_2 solubility and permeability increase compared to membranes without M1, leading to improved ideal gas selectivities towards CO_2 and showing the favorable effect of the crown ether functionalities on the CO_2 gas separation performances. However, for membranes that contained more than 30 wt% M1, a decreasing layer spacing with increasing M1 content results in reduced gas solubilities leading to lower gas permeabilities without additional selectivity gain towards CO_2. Gas permeation data measured at respectively 20 °C, 40 °C and 70 °C show that the permeabilities of all gasses increase with increasing temperature while the selectivities decrease. Above the T_g of the membranes, the diffusion coefficient increases with increasing M1 content leading to higher CO_2 permeabilities and selectivities for the membranes with higher M1 contents, showing that above the T_g the differences in CO_2 permeability between the different M1/M2 compositions is mainly dependent on the diffusivity of gasses rather than the solubility.

In **Chapter 4** the effect of layer spacing on the gas separation performance of free-standing smectic LC polymer membranes is investigated more in-depth. Additionally, the effect of

halogenation on the gas transport properties of smectic LC membranes is investigated. Planar aligned smectic LC membranes with various layer spacings and halogenated LCs are fabricated by using LCs with different alkyl spacer lengths, to tune the layer spacing of the smectic structure, and LCs that contain various halogen substituents to improve the gas performances towards CO_2. The tilt angle of the smectic structures is similar for all membranes but the layer spacing is found to be highly dependent on the length of the alkyl spacer of the LC monomers. Single gas permeation data demonstrate that the permeability of all membranes increases with increasing layer spacing while the ideal gas selectivity towards He decreases with increasing layer spacing. The solubility coefficient is very similar for all membranes while the diffusion coefficient of the membranes with a layer spacing of 31.9 Å is found to be 6 times lower compared to the membranes with a layer spacing of 45.2 Å, demonstrating that the layer spacing in smectic LC membranes mainly affects the diffusivity of gasses rather than the solubility. Comparing permeation data of smectic LC membranes with and without halogenated LCs shows only a slight improvement of the gas permeabilities and selectivities towards CO_2 because of the relatively low halogen content that can be used for maintaining a smectic morphology.

In **Chapter 5** the gas permeation performance of free-standing nematic LC polymer membranes with various substituents that differ in steric size is investigated. Planar aligned nematic LC membranes are fabricated consisting of LCs with the same chemical backbone but with respective cyano, chloro, methyl and phenyl substituents on the central aromatic cores of the LC monomers. Single gas permeation data show increasing gas permeabilities with increasing steric size of the substituent while the ideal gas selectivity of He over CH_4 and He over CO_2 decreases. The solubility coefficient of all membranes is independent of the LC substituents while the diffusion coefficient for the membranes with the largest (phenyl) substituent is found to be 3 times higher compared to the membranes with the smallest (cyano) substituent, showing that the steric size of the LC substituents mainly affects the diffusivity of gasses rather than the solubility. The effect of the kinetic diameter of different gas species on the gas permeation properties of nematic LC membranes is demonstrated by a 20 times lower diffusion coefficient for the larger Xe compared to the smaller CO_2, which results in considerably lower Xe permeabilities.

Lastly, **Chapter 6** reflects on the results obtained and proposes several future research directions for LC membranes for gas separations.

Samenvatting

Vloeibaar kristallijne polymeermembranen voor gasscheiding

In dit proefschrift zijn de structuur-eigenschappenrelaties van vloeibaar kristallijne (LC) polymeermembranen voor gasscheidingstoepassingen onderzocht. De onderzochte aspecten zijn (1) het effect van de moleculaire orde en oriëntatie van de LC-nanostructuren, (2) de laagafstand en hellingshoek van de nanostructuren, (3) de bedrijfstemperatuur en chemische samenstelling van de LC-monomeren en (4) de sterische grootte van de LC-substituenten. Als gevolg hiervan toont dit werk de mogelijkheden aan van het gebruik van LC's om op nanometerschaal gestructureerde membranen voor gasscheiding te maken, door te laten zien hoe en in welke mate de bovengenoemde aspecten kunnen worden gebruikt om de gasscheidingsprestaties van deze membranen te regelen.

Allereerst wordt in **Hoofdstuk 1** een algemene introductie van LC-materialen en hun toepassingen gegeven. De geschiedenis en ontwikkelingen in LC-materialen worden kort besproken en dit wordt gevolgd door een sectie die de relevante theorie geeft over de zelfassemblage-eigenschappen, uitlijning en het maakproces van LC-polymeermaterialen. Vervolgens wordt het gebruik van LC-materialen voor het maken van membranen met verschillende en goed gecontroleerde morfologieën voor verschillende membraanprocessen besproken. Vervolgens worden de mogelijkheden en motivatie voor het gebruik van LC-polymeermembranen voor gasscheiding besproken, gevolgd door een sectie die de relevante theorie biedt met betrekking tot op polymeermembraan gebaseerde gasscheiding. Ten slotte worden het doel en de opzet van dit proefschrift gegeven.

In **Hoofdstuk 2** wordt het effect van moleculaire orde en oriëntatie op de gasscheidingsprestaties van vrijstaande LC-polymeermembranen onderzocht. Er zijn LC-membranen gemaakt met dezelfde chemische samenstelling, maar met verschillende type en mate van moleculaire orde (isotroop, nematisch cybotactisch en smectisch C) en oriëntatie (planair en homeotroop). Gaspermeatiedata tonen aan dat de gaspermeabiliteit afneemt met toenemende moleculaire orde, terwijl de ideale gasselectiviteit van He en CO_2

ten opzichte van N_2 enorm toeneemt, wanneer men van niet geordende naar een hoog geordende smectisch C-morfologie gaat. De oplosbaarheidscoëfficiënt is vergelijkbaar voor alle membranen, terwijl de diffusiecoëfficiënt van de geordende smectisch C-membranen 10 keer lager is dan die van de niet geordende membranen, wat aantoont dat de gaspermeatie van deze LC-membranen voornamelijk afhangt van de diffusie van gas door het membraan en niet van de oplosbaarheid van het gas in het membraan. Dit komt waarschijnlijk doordat de vrije volume-elementen in het membraan kleiner worden met toenemende moleculaire ordening. Hierdoor worden gassen met grotere kinetische diameters meer tegengehouden dan gassen met kleinere kinetische diameters, wat leidt tot selectiviteit tussen verschillende gassen. Het effect van de moleculaire oriëntatie wordt aangetoond met een 3 keer lagere diffusiecoëfficiënt voor de homeotrope uitgelijnde smectisch C-membranen in vergelijking met de planair uitgelijnde smectisch C-membranen.

In **Hoofdstuk 3** wordt het effect van de chemische samenstelling en de temperatuur op de gaspermeatie en de oplosbaarheid van vrijstaande smectische LC-polymeermembranen onderzocht. Er zijn planair uitgelijnde smectische LC-membranen gemaakt met verschillende samenstellingen van een mono-methacrylaat LC met een kroonetherfunctionaliteit (M1) om de oplosbaarheid van CO_2 in het membraan te verhogen en een di-acrylaat cross-linker (M2). De laagafstand en hellingshoek van de smectische structuren zijn onafhankelijk van de bereidingstemperatuur, maar zijn sterk afhankelijk van de chemische samenstelling van het membraan. Wanneer het M1-gehalte toeneemt, neemt de laagafstand af, terwijl de hellingshoek van de smectische structuren toeneemt. Dit komt doordat de moleculaire lengte van M1 kleiner is dan die van M2, waardoor de laagafstanden kleiner worden voor membranen met een hoger M1-gehalte. Gaspermeatiedata gemeten onder de glasovergangstemperaturen (T_g) van de membranen tonen aan dat de CO_2-permeabiliteit voor alle M1/M2-samenstellingen voornamelijk afhangt van het verschil in CO_2-oplosbaarheid. Voor membranen met 30 wt% M1 nemen zowel de CO_2-oplosbaarheid als de permeabiliteit toe in vergelijking met membranen zonder M1, wat leidt tot een betere ideale gasselectiviteit voor CO_2 en het positieve effect aantoont van de kroonetherfunctionaliteiten op de CO_2-gasscheidingsprestaties. Voor membranen die meer dan 30 wt% M1 bevatten, resulteert een afnemende laagafstand met toenemend M1-gehalte in verminderde gasoplosbaarheid, wat leidt tot lagere gaspermeabiliteiten zonder dat de selectiviteit ten aanzien van CO_2 verbetert. Uit gaspermeatiedata gemeten bij respectievelijk 20 °C, 40 °C

en 70 °C blijkt dat de permeabiliteit van alle gassen toeneemt bij een toenemende temperatuur, terwijl de selectiviteit afneemt. Boven de T_g van de membranen neemt de diffusiecoëfficiënt toe met toenemend M1-gehalte, wat leidt tot hogere CO_2-permeabiliteiten en selectiviteiten voor de membranen met een hoger M1-gehalte, waaruit blijkt dat boven de T_g de verschillen in CO_2-permeabiliteit tussen de verschillende M1/M2-samenstellingen hoofdzakelijk afhangen van de diffusie van gassen en niet van de oplosbaarheid van het gas in het membraan.

In **Hoofdstuk 4** wordt het effect van de laagafstand op de gasscheidingsprestaties van vrijstaande smectische LC-polymeermembranen nader onderzocht. Daarnaast wordt het effect van halogenering op de gastransporteigenschappen van smectische LC-membranen onderzocht. Er zijn planair uitgelijnde smectische LC-membranen gemaakt met verschillende laagafstanden en gehalogeneerde LC's door gebruik te maken van LC's met verschillende alkylstaartlengten, om de laagafstand van de smectische structuur te variëren, en LC's die verschillende halogeensubstituenten bevatten om de gasprestaties ten aanzien van CO_2 te verbeteren. De hellingshoek van de smectische structuren is voor alle membranen gelijk, maar de laagafstand blijkt sterk afhankelijk te zijn van de lengte van de alkylstaart van de LC-monomeren. Gaspermeatiedata tonen aan dat de gaspermeabiliteiten van alle membranen toeneemt met toenemende laagafstand, terwijl de ideale gasselectiviteit voor He afneemt met toenemende laagafstand. De oplosbaarheidscoëfficiënt is voor alle membranen vergelijkbaar, terwijl de diffusiecoëfficiënt van de membranen met een laagafstand van 31.9 Å 6 keer lager is in vergelijking met de membranen met een laagafstand van 45.2 Å, wat aantoont dat de laagafstand in smectische LC-membranen vooral de diffusie van gassen beïnvloedt in plaats van de oplosbaarheid. Uit een vergelijking van de permeatiegegevens van smectische LC-membranen met en zonder gehalogeneerde LC's blijkt dat de toevoeging van gehalogeneerde LC's slechts tot een geringe verbetering leidt van de gaspermeabiliteit en de selectiviteit voor CO_2 vanwege het relatief lage halogeengehalte dat kan worden gebruikt om een smectische morfologie te behouden.

In **Hoofdstuk 5** worden de gaspermeatieprestaties onderzocht van vrijstaande nematische LC-polymeermembranen met verschillende substituenten die verschillen in sterische grootte. Er zijn planair uitgelijnde nematische LC-membranen gemaakt van LC's met dezelfde chemische structuur, maar met respectieve cyano-, chloor-, methyl- en fenylsubstituenten op de centrale aromatische kernen van de LC-monomeren.

Gaspermeatiedata tonen aan dat de gaspermeatie toeneemt met toenemende sterische grootte van de substituent, terwijl de ideale gasselectiviteit van He over CH_4 en He over CO_2 afneemt. De oplosbaarheidscoëfficiënt van alle membranen is onafhankelijk van de LC-substituenten, terwijl de diffusiecoëfficiënt voor de membranen met de grootste (fenyl) substituent 3 keer hoger is in vergelijking met de membranen met de kleinste (cyano) substituent. Hieruit blijkt dat de sterische grootte van de LC-substituenten vooral de diffusie van gassen beïnvloedt in plaats van de oplosbaarheid. Het effect van de kinetische diameter van verschillende gassoorten op de gaspermeatie-eigenschappen van nematische LC-membranen wordt aangetoond door een 20 keer lagere diffusiecoëfficiënt voor het grotere Xe in vergelijking met het kleinere CO_2, wat resulteert in aanzienlijk lagere Xe-permeabiliteit.

Ten slotte wordt in **Hoofdstuk 6** teruggekeken op de verkregen resultaten en worden verschillende toekomstige onderzoeksrichtingen voor LC-membranen voor gasscheidingen voorgesteld.

Table of contents

Chapter 1

Introduction

This chapter has been partly reproduced from:

J. Kloos, N. Joosten, A. Schenning, K. Nijmeijer, Self-assembling liquid crystals as building blocks to design nanoporous membranes suitable for molecular separations, *J. Membr. Sci.* **2021**, 620, 118849.

1.1 General introduction

When the temperature of a material is raised, it generally changes its state from solid to liquid to gaseous. At least that was what the Austrian botanist and chemist Friedrich Reinitzer was expecting while making esters of cholesterol for his studies of plants in the late 19th century. Instead Reinitzer noted that cholesteryl benzoate, which is a cholesterol extracted from carrots, exhibits two distinct melting points and with that he discovered liquid crystals (LCs) [1]. At its first melting point, the material melted and became cloudy white and viscous, which later would be called a “mesophase”, while at its second melting point the material became clear and fully liquid. Unable to explain the phenomenon, Reinitzer went to the German physicist Otto Lehmann who studied the material and confirmed that the material at the mesophase shared characteristics of both liquid and crystals. Lehmann named the materials with these characteristics “fliessende krystalle” and with that the name “liquid crystals” was born [2,3].

After the discovery, liquid crystals (LCs) remained mostly a scientific curiosity for the next 75 years having no known applications. Although many materials were found to exhibit mesophases and their optical and electrical properties were already studied in the early 20th century [3–5], it was not until the 1950s that extensive efforts were made to develop applications for these materials and convert the previously scientific curiosity into a universal part of modern technology. In the 1950s, the invention of the first LC temperature indicator led to advances in medical diagnostics, electronic compound testing and aerodynamic structure analysis [6]. However, the most important technological invention is the development of the LC display (LCD) in the late 1960s followed by significant breakthroughs in LC technology between the 1980s and 1990s that have led to a profound impact on our modern society by introducing entirely new devices such as flat TV screens, computers, smartphones, digital projectors and countless other innovations [5–7]. The commercial success of LCDs stimulated research in both academia and industry to such an extent that for a long time this application strongly dominated international research efforts in the field. It was not until the mid-1990s that academic LC science start moving away from display research and start focusing on new topics by exploring other unique aspects of LCs, leading to new uses in optics, novel composites and biotechnology [8]. In the last two decades, LC research has advanced even more resulting in a wide range of new applications such as sensors [9–11], actuators [12–14], switching surfaces [15,16], shape memory [17], soft robotics [18–20], energy-saving reflection coatings [21,22] and membrane applications [23–31].

1.2 Liquid crystalline polymer materials

1.2.1 Liquid crystals and mesophases

Liquid crystals (LCs) are molecules that possess additional phases (mesophases) between the conventional isotropic liquid and anisotropic crystalline solid phase. In this so-called mesophase, LCs combine the mobility of liquids with a degree of long-range positional and orientational order like in solids, while maintaining liquid consistency. Different types of LCs have been identified, of which lyotropic and thermotropic are the most reported in the literature (Figure 1.1) [32,33].

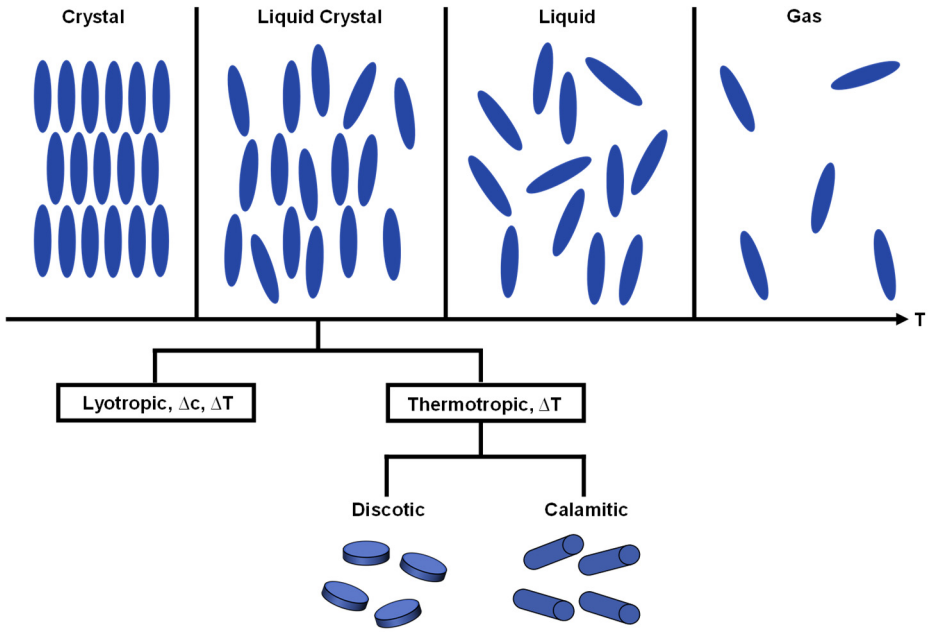

Figure 1.1: *Overview of the states of matter. The rods represent molecules that depending on the state of matter are ordered in a certain fashion. Liquid crystals have additional phases between conventional isotropic liquids and anisotropic crystalline solids. Two basic groups are lyotropic and thermotropic liquid crystals. Thermotropic phases can be further divided based on their molecular structure: discotic (disk-shaped) and calamitic (rod-shaped).*

Lyotropic mesophases are generally formed with amphiphilic molecules, which self-assemble in the presence of a solvent. Depending on the used conditions (temperature, amount of solvent and the structure of the molecule), various self-assembled phases can be achieved such as hexagonal phases, lamellar phases and bicontinuous cubic phases [34]. The self-assembled phases directly influence the morphology of the formed

nanostructures. In thermotropic LCs, the hexagonal, lamellar and bicontinuous cubic phases are formed only by heating or cooling the material. It is important to mention, that despite the differences between lyotropic and thermotropic LCs, LCs may exhibit both lyotropic and thermotropic behavior.

Thermotropic LCs are further distinguished based on the molecular shape of the molecules. The most common LCs are discotic (disk-shaped molecules) and calamitic (rod-shaped molecules) (Figure 1.1) [32,35]. Common chemical structures of discotic LCs contain a rigid disc-like core with multiple flexible end groups (Figure 1.2a). By cooling down from their isotropic liquid phase, the disk-shaped discotic LCs generally exhibit nematic (N) and various columnar mesophases (Figure 1.2b). In the nematic mesophase, LCs have an orientational order along the axis of the molecules (a common molecular director n), while the centers of mass of the LCs are still isotropically distributed in all directions. In the columnar phases, the mesogens self-assemble (stack) on top of each other, forming columns that can further self-organize into two-dimensional lattices such as columnar hexagonal and columnar rectangular phases [36].

A common chemical structure of calamitic LCs is a rigid core segment, existing of multiple linearly linked aromatic rings with one or two flexible end groups (often alkyl or alkoxy chains) (Figure 1.2a) [35]. These materials show similar behavior as discotic LCs when cooled down from their isotropic liquid phase but have different mesophases due to their molecular differences. The rod-shaped calamitic LCs can form various organizations like nematic (N) and smectic (Sm) mesophases (Figure 1.2c). The nematic mesophase is similar to the discotic LCs, only having orientational order whilst the centers of mass are isotropically distributed in all dimensions. Smectic A and smectic C mesophases are more ordered phases compared to the nematic phase and are generally observed at temperatures below the nematic phase. Smectic mesophases also show, next to orientational order, positional order of the centers of mass over the long axis, forming layers with a discrete layer spacing d (Figure 1.2c) [32]. In contrast to smectic A, the smectic C mesophase exhibits an additional tilt of the LCs in the smectic layer.

As in this thesis, only thermotropic calamitic LCs are used, the following sections will discuss this class of LCs.

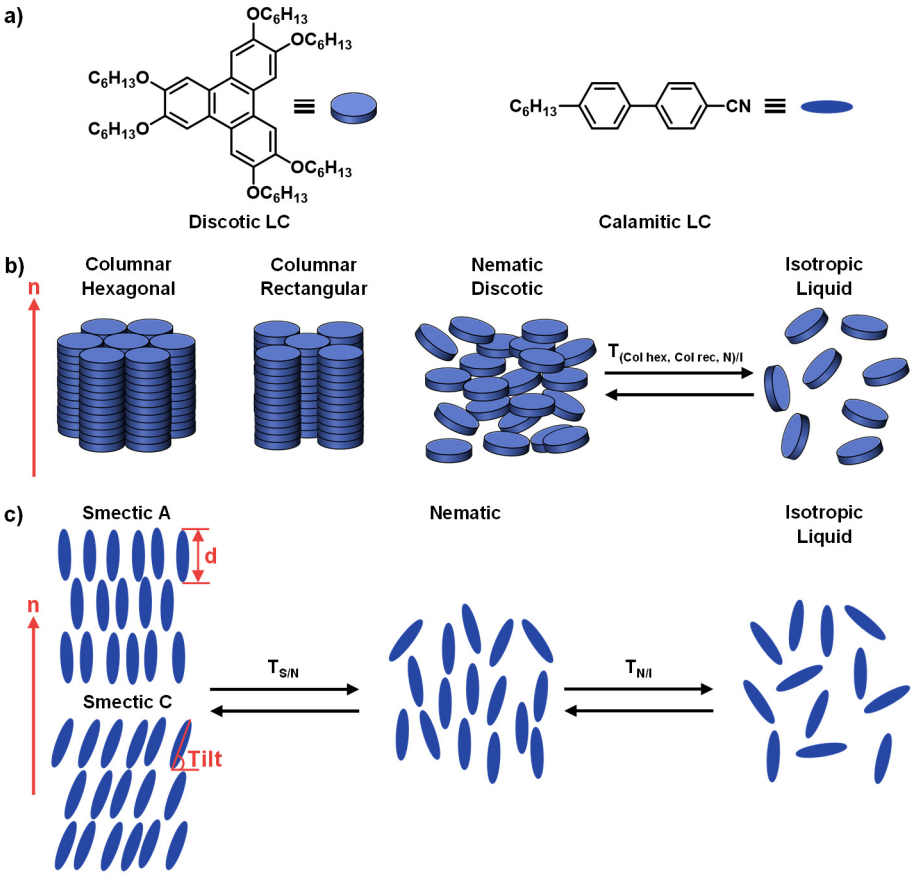

Figure 1.2: a) *Example of a discotic and calamitic LC structure.* ***b)*** *Possible mesophases of discotic and* ***c)*** *calamitic LCs.*

1.2.2 Alignment of liquid crystals

LCs are anisotropic, meaning that their physical properties are directionally dependent. Directional dependency occurs because LCs have a common molecular director (n), which results in different properties longitudinally or perpendicularly to this director [37,38]. Moreover, this director can be oriented in a certain direction, which is called the alignment of LCs. The alignment of self-assembled LCs is key for many applications. Without orientational control, LC phases do not form unidirectionally orientated monodomains at the macroscale. In most cases, self-assembly starts with nucleation and growth at different positions, resulting in the formation of randomly oriented polydomains of which larger individual domains grow 1 µm at most (Figure 1.3) [39].

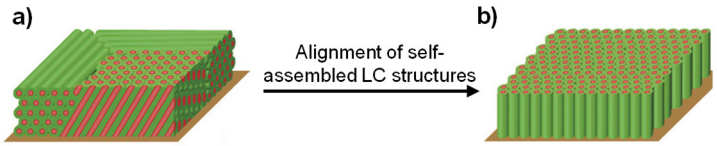

Figure 1.3: a) *LC polydomains with randomly oriented domains and* ***b)*** *unidirectionally oriented monodomains due to the alignment of the self-assembled LC structures. Adapted from Ref. [40] with permission of John Wiley and Sons, Inc.*

When the common molecular director (n) is parallel to the substrate, the LC molecules are aligned in a planar fashion. On the contrary, if the common molecular director (n) is perpendicular to the substrate, the molecules are aligned in a homeotropic fashion (Figure 1.4). The alignment of LCs can either be achieved by external forces, such as shear forces, magnetic fields and electric fields, or by surface-induced orientation [39].

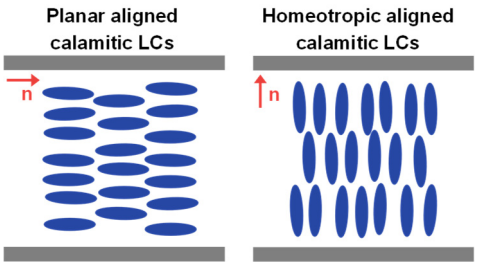

Figure 1.4: *Alignment of calamitic LCs between two substrates having planar or homeotropic alignment layers.*

One method to align LCs with an external force is by shearing a material parallel to a surface. An advantage of using shear forces is the easy application and the common tools required. LCs orient with their long axes parallel to the shear forces, which results in planar alignment for calamitic LCs. The viscosity of LCs has a big influence on the use of shear forces. If the viscosity is too low, there is not sufficient shear force to align the LCs. If the viscosity is too high, the shear force might not be high enough to align the LCs. However, even with an appropriate viscosity, it is difficult to apply shear forces homogenously over samples with thicker layers (micrometer-scale) [39]. The mechanism for the alignment of LCs by a magnetic- or an electric field is rather similar. Due to the anisotropic properties of LCs, the susceptibility towards magnetic- or electric fields is directionally dependent, which gives the possibility to use these external forces for the alignment of LCs. Although the alignment mechanism is similar, the methods have individual advantages and

disadvantages. Magnetic fields penetrate homogenously in a non-contact and non-destructive way into the bulk sample, resulting in alignment control over large areas [39]. A disadvantage of using magnetic fields is the need for superconducting magnets and strong magnetic fields (minimum of 3 T) are generally required to align LCs, limiting the scalability and ease of fabrication [41–43]. On the contrary, alignment with electric fields is already applied on an industrial scale in flat-panel applications [44]. However, electric fields can only be applied in contact with the substrate, which requires electrode contact.

Another method that is frequently used to align LCs is surface-induced orientation. Surface-induced orientation controls the alignment by changing the surface's anchoring conditions. If the surface of a substrate has a stronger interaction with the flexible sidechains of the LC, this results in homeotropic aligned LCs. If the surface of a substrate favors interactions with the rigid cores of the LCs, this results in the planar aligned LCs (Figure 1.4). The surface's anchoring conditions can be changed by using various types of molecular interactions tailored by e.g. hydrophobicity or chemical functional groups [45]. Additionally, these conditions can be further tailored by changing the physical interactions e.g. by rubbing the surface of the substrate. Alignment by surface treatment is therefore a versatile, simple and effective strategy to control the orientation of LCs, though limited to a certain LC layer thickness (micrometer-scale). In thicker LC films, the molecular interactions between the LC become more dominant over the LC-substrate interactions, which eventually results in randomly oriented polydomains [46].

1.2.3 Fabrication of liquid crystal polymer materials

For alignment, small LC molecules are attractive to use. Their low viscosity makes LC molecules easier to align compared to LC polymers. However, although anisotropic LC self-assemblies are formed, these structures will not provide the required mechanical strength to obtain robust materials. To increase the mechanical strength, LCs can be equipped with polymerizable functional groups to fixate the self-assembled morphology by photopolymerization. Functional groups that have been reported are vinyl(ethers), dienes, (meth)acrylates, thiols and epoxides and oxetanes [47–51]. Still, the acrylic reactive LCs are used the most often due to their straightforward synthesis, proper stability and robust polymerization [52,53]. After the in-situ polymerization of LCs in a mesophase, the order and alignment of the LCs are fixed and depending on the cross-link density the network can no longer undergo phase transitions. The formed LC networks are highly cross-linked and give strong robust films that can be used for all kinds of applications.

1.3 Liquid crystalline polymer membranes

1.3.1 Nanoporous membranes based on liquid crystals

The self-assembly properties of LCs can be used for preparing membranes with distinct and well-controlled morphologies for various membrane processes. Well-known research already studied the use of LCs for the fabrication of nanoporous membranes for water separation [23–30]. Water separations are used for water purification, desalination of saline water and selective recovery of valuable resources (e.g. minerals). In such separations, the size and charge of the retained species are important parameters. Depending on the size of the retained species, microfiltration (MF), ultrafiltration (UF), nanofiltration (NF) or reverse osmosis (RO) membranes are used to separate pollutants or recover valuable resources from waste streams [54–58]. MF and UF membranes are porous and separate only by size exclusion while RO membranes are non-porous (dense) and separate by differences in transmembrane mass transport rates of solutes due to differences in membrane/solute/solvent interactions [59]. NF membranes have properties in between UF and RO membranes due to their very small pore sizes varying between 0.5 – 2.0 nm [60]. Transport of neutral species takes place by mainly size exclusion, while transport of charged species takes place by molecular interactions between solute and membrane [57,61]. With these unique properties NF membranes can potentially be used to separate molecules and ions at a molecular level. However, molecular separations between similarly charged ions or separations of small valuable molecules and micropollutants are not yet possible because the current polymer materials and fabrication methods for water separation lack the design at a molecular level. Using the self-assembly properties of small reactive LC molecules is very appealing for the fabrication of nanoporous materials because it ensures control over the building blocks at a molecular level, which results in pore sizes that are determined by the size of the building blocks (varying between 0.5 and 2.0 nm) and leads to narrow pore size distributions [53,59,62].

1.3.2 Liquid crystalline polymer membranes for gas separation

Safeguarding a sustainable way of living for the future necessitates the transition from the current “linear” economy into a more sustainable “circular” economy. This means for example lower our greenhouse gas emissions (CO_2 and CH_4), which facilitates the global warming effect, are key in the coming decades. These major challenges drive the need to explore new polymer materials and more efficient separation methods such as e.g. membranes.

The performance of polymer membranes for gas separation is commonly expressed in permeabilities and selectivities. The permeability (P) is the rate, often expressed in Barrer, at which gases permeate through the membrane. Contrary to membranes for water separations, membranes used for gas separation are predominantly non-porous (dense). Gas transport through dense membranes is well described by the solution-diffusion model, which states that gas permeability is defined as the product of the diffusion coefficient (D_i) and the solubility coefficient (S_i) of a certain gas species (Equation 1.1) [63,64].

$$P_i = \frac{J_i \cdot L}{P_{i,feed} - P_{i,permeate}} = D_i \cdot S_i \qquad (1.1)$$

Here P_i is the permeability of gas species i (Barrer (10^{-10} $cm^3(STP)\cdot cm/(cm^2\cdot s\cdot cmHg)$)), J_i is the flux ($cm^3(STP)/cm^2\cdot s$), L is the thickness of the membrane (cm), $P_{i,\,feed}$ is the feed pressure (cmHg) and $P_{i,\,permeate}$ is the permeate pressure (cmHg). The ideal selectivity (α_i) is the ratio of permeabilities of different gases (gas species i and gas species j) and is calculated with Equation (1.2).

$$\alpha_{i/j} = \frac{P_i}{P_j} \qquad (1.2)$$

Non-porous polymer membranes separate gases via intrinsic differences in diffusivity and solubility for different gas species (Equation 1.1). However, the diffusion and solubility coefficients are greatly affected by many variables, such as the kinetic diameter and critical temperature of the measuring gas, and dictate the gas permeability and selectivity to a large extent. The solubility coefficient represents the uptake of the gaseous penetrant in the polymer membrane and mainly depends on the condensability of a gas [65]. The critical temperature of a gas is directly related to the condensability of a gas in a material and usually increases with increasing critical temperature. Other parameters that affect the condensability are molecular size and chemical affinity between gas and polymer matrix (via dipole/quadrupole moments) [66–68]. The diffusion coefficient represents the mobility of gas inside the membrane and mainly depends on the kinetic size of the gaseous penetrant and the available free volume in the membrane material. Smaller gases and high amounts of free volume usually result in higher diffusion coefficients compared to larger gases and low amounts of free volume [69]. The kinetic diameters, critical temperatures and quadrupole moments of gases relevant to this work are shown in Table 1.1 [70].

Table 1.1: *The kinetic diameter, critical temperature and quadrupole moment of relevant gases for this work [70].*

Gas species	Kinetic diameter [Å]	Critical temperature [K]	Quadrupole moment $[cm^2] \cdot 10^{40}$
He	2.60	5.19	0.00
CO_2	3.30	304.13	-13.71
Ar	3.43	151.00	0.00
N_2	3.64	126.20	-4.91
CH_4	3.80	190.55	0.00
Xe	3.96	289.77	0.00

Moreover, the diffusion coefficient is dependent on the available free volume and the size of the free volume elements in the polymer matrix, which greatly depends on the temperature and the glass transition temperature (T_g) of the polymer membrane [65,68,71]. Furthermore, the amount of free volume and the size of the free volume elements is highly influenced by the molecular morphology of the membranes.

Despite that polymeric membranes are often used for gas separations, most of the used polymers lack control over the morphology of the membrane on the molecular level which results in limitations such as poorly defined free volume. These limitations lead to a trade-off between gas permeability and selectivity which limits the performance of current membranes for gas separation [31,72–76]. Although the self-assembly of block copolymers has already been widely investigated for the removal of CO_2 from light gases [77,78], LCs have been rarely used for these applications. As small reactive LC molecules can be used to obtain a wide variety of ordered phases and orientations, which differ in molecular order, these materials are well-suited to provide control over the morphology of the membrane and thereby the transport properties of the membrane. For example, Bara et al. showed the importance of molecular order in LC membranes for gas separation [31], by measuring the performance of light gases, in cross-linked LC polymer membranes with and without a columnar morphology. The membranes with an ordered columnar morphology exhibit slightly lower CO_2 permeability but higher CO_2/N_2 and CO_2/CH_4 selectivity compared to the membranes without molecular order, showing the value of molecular order in LC membranes for gas separation.

Although the self-assembly properties of LCs show potential for gas separation processes, the effect of structure on membrane properties in LC membranes has not been

systematically investigated. Research on the effect of morphology, molecular orientation (alignment), chemistry and more subtle order differences such as layer spacing and tilt angle of the nanostructures is necessary to get a better understanding of the structure-property relationships in LC membranes for gas separations. Understanding these relationships can help to develop the next-generation membranes for gas separation.

1.4 Aim and outline of this thesis

This thesis aims to systematically explore the opportunities of using LCs for the fabrication of nanostructured membranes for gas separation, with a specific focus on the structure-property relationships. Since thermotropic calamitic LCs are already often used in other applications and have easy fabrication and alignment methods, these materials are used to prepare LC membranes with controlled molecular orders (morphologies), molecular orientations (alignments) and chemistries for gas separations. Also, more subtle order differences such as the effect of the layer spacing and tilt angle in smectic nanostructures are studied. The morphology and molecular orientation of the LC membranes are fully characterized after which the gas separation performances (permeability and selectivity) of different gases (He, CO_2, Ar, N_2, CH_4 and Xe) at 6 bar and temperatures up to 70 °C are evaluated. The gas transport properties (in terms of gas solubility and diffusion) of the membranes are investigated by comparing gas sorption and permeation performances.

Chapter 2 describes the effect of molecular order and orientation in LC polymer membranes on their gas separation performance. LC membranes are fabricated and characterized with various, distinct morphologies (isotropic, nematic cybotactic, and smectic C) and alignment (planar and homeotropic) while using the same chemical composition. The impact of molecular order and orientation is demonstrated in gas sorption and permeation performances.

In **Chapter 3**, the effect of chemical composition and temperature on gas permeability and solubility in smectic LC polymer membranes is investigated. Planar aligned smectic LC membranes with various compositions of an LC with a crown ether functionality to enhance CO_2 solubility and an LC cross-linker are fabricated and characterized. Gas sorption and permeation performances are measured below and above the glass transition temperature of the membranes to study the gas transport properties of the different membranes.

The effect of layer spacing and halogenation of the LC monomers on the gas separation performances of smectic LC polymer membranes is described in **Chapter 4**. Planar aligned

smectic LC membranes with various layer spacings and halogenated LCs are fabricated and characterized by using LCs with different alkyl spacer lengths, to tune the layer spacing of the smectic nanostructure, and LCs that contain various halogen substituents. All membranes are characterized by their sorption and permeation behavior to investigate the gas transport properties of the membranes.

Chapter 5 describes the gas separation performances of nematic LC polymer membranes with various substituents that differ in steric size. Planar aligned nematic LC membranes with respective nitrile, chlorine, methyl and phenyl substituents are fabricated and characterized by using LCs with a similar chemical backbone but different substituents. Gas sorption and performances of all membranes are measured to investigate the gas transport properties of the different membranes. In addition, the effect of the kinetic diameter of the measuring gas on the permeation performances of LC membranes is studied by comparing the gas sorption and permeation performances of different gases with similar critical temperatures but different kinetic diameters.

The last chapter, **Chapter 6**, reflects on the results obtained and provides challenges and opportunities for using LCs for gas separation applications.

References

[1] F. Reinitzer, *Monatshefte Für Chemie.* **1888**, 9, 421–441.

[2] O. Lehmann, *Zeitschrift Für Phys. Chemie.* **1889**, 4, 462–472.

[3] H. Kawamoto, *IEEE*. **2006**, 90, 460–500.

[4] T.J. Sluckin, D.A. Dunmur, H. Stegemeyer, *Crystals that flow: classic papers from the history of liquid crystals*, **2004**.

[5] G.A. Dilisi, *An Introduction to Liquid Crystals,* Institute of Physics, **2019**.

[6] B.T. Hogan, E. Kovalska, M.F. Craciun, A. Baldycheva, *J. Mater. Chem. C.* **2017**, 5, 11185–11195.

[7] J.P.F. Lagerwall, G. Scalia, *Curr. Appl. Phys.* **2012**, 12, 1387–1412.

[8] R. Stannarius, *Nat. Mater.* **2009**, 8, 617–618.

[9] D.J. Mulder, A.P.H.J. Schenning, C.W.M. Bastiaansen, *J. Mater.* Chem. C. **2014**, 2, 6695–6705.

[10] E.P.A. Van Heeswijk, A.J.J. Kragt, N. Grossiord, A.P.H.J. Schenning, *Chem. Commun.* **2019**, 55, 2880–2891.

[11] C. Ohm, M. Brehmer, R. Zentel, *Adv. Mater.* **2010**, 22, 3366–3387.

[12] M. Yamada, M. Kondo, J. Mamiya, Y. Yu, M. Kinoshita, C.J. Barrett, T. Ikeda, *Angew. Chemie*. **2008**, 120, 5064–5066.

[13] A.H. Gelebart, D.J. Mulder, M. Varga, A. Konya, G. Vantomme, E.W. Meijer, R.L.B. Selinger, D.J. Broer, *Nature.* **2017**, 546, 632–636.

[14] M. Pilz da Cunha, Y. Foelen, R.J.H. van Raak, J.N. Murphy, T.A.P. Engels, M.G. Debije, A.P.H.J. Schenning, *Adv. Opt. Mater.* **2019**, 7, 1801643.

[15] D. Liu, C.W.M. Bastiaansen, J.M.J. Den Toonder, D.J. Broer, *Macromolecules.* **2012**, 45, 8005–8012.

[16] F.L.L. Visschers, M. Hendrikx, Y. Zhan, D. Liu, *Soft Matter.* **2018**, 14, 4898–4912.

[17] K. Nickmans, D.A.C. van der Heijden, A.P.H.J. Schenning, *Adv. Opt. Mater.* **2019**, 7, 190059.

[18] O.M. Wani, H. Zeng, A. Priimagi, *Nat. Commun.* **2017**, 8, 1–7.

[19] M. Pilz da Cunha, S. Ambergen, M.G. Debije, E.F.G.A. Homburg, J.M.J. den Toonder, A.P.H.J. Schenning, *Adv. Sci.* **2020**, 7, 1–7.

[20] A. Buguin, M.H. Li, P. Silberzan, B. Ladoux, P. Keller, *J. Am. Chem. Soc.* **2006**, 128, 1088–1089.

[21] H. Khandelwal, A.P.H.J. Schenning, M.G. Debije, *Adv. Energy Mater.* **2017**, 7, 1602209.

[22] E.P.A. Van Heeswijk, J.J.H. Kloos, N. Grossiord, A.P.H.J. Schenning, *J. Mater. Chem. A.* **2019**, 7, 6113–6119.

[23] M. Zhou, T.J. Kidd, R.D. Noble, D.L. Gin, *Adv. Mater.* **2005**, 17, 1850–1853.

[24] G.M. Bögels, J.A.M. Lugger, O.J.G.M. Goor, R.P. Sijbesma, *Adv. Funct. Mater.* **2016**, 26, 8023–8030.

[25] M. Henmi, K. Nakatsuji, T. Ichikawa, H. Tomioka, T. Sakamoto, M. Yoshio, T. Kato, *Adv. Mater.* **2012**, 24, 2238–2241.

[26] M. Gupta, Y. Suzuki, T. Sakamoto, M. Yoshio, S. Torii, H. Katayama, T. Kato, *ACS Macro Lett.* **2019**, 8, 1303–1308.

[27] M. Zhou, P.R. Nemade, X. Lu, X. Zeng, E.S. Hatakeyama, R.D. Noble, D.L. Gin, *J. Am. Chem. Soc.* **2007**, 129, 9574–9575.

[28] S.M. Dischinger, J. Rosenblum, R.D. Noble, D.L. Gin, K.G. Linden, *J. Membr. Sci.* **2017**, 543, 319–327.

[29] J.A.M. Lugger, P.P. Marín San Román, C.C.E. Kroonen, R.P. Sijbesma, *ACS Appl. Mater. Interfaces.* **2021**, 13, 4385–4392.

[30] P. Marin San Roman, K. Nijmeijer, R.P. Sijbesma, *J. Membr. Sci.* **2022**, 644, 120097.

[31] J.E. Bara, A.K. Kaminski, R.D. Noble, D.L. Gin, *J. Membr. Sci.* **2007**, 288, 13–19.

[32] I. Dierking, *Textures of liquid crystals*, Wiley-Vch Verlag Gmbh, **2003**.

[33] M. Čepič, Eur. *J. Phys. Educ.* **2012**, 4, 27–33.
[34] G. Emrich, *Z. Phys. Chem.* **1996**, 193, 219–220.
[35] I. Dierking, Polymer-modified liquid crystals, *Royal Society of Chemistry*, **2019**.
[36] H.K. Bisoyi, Q. Li, *Prog. Mater. Sci.* **2019**, 104, 1–52.
[37] B. Outram, *Liquid Crystals*, IOP Publishing, **2018**.
[38] G. Vertogen, W.H. de Jeu, *J. Chem. Inf. Model.* **1988**, 45, 1689–1699.
[39] J. Cho, Y. Ishida, *Adv. Mater.* **2017**, 29, 1605974.
[40] T. Kato, J. Uchida, T. Ichikawa, T. Sakamoto, *Angew. Chemie - Int. Ed.* **2018**, 57, 4355–4371.
[41] X. Feng, M.E. Tousley, M.G. Cowan, B.R. Wiesenauer, S. Nejati, Y. Choo, R.D. Noble, M. Elimelech, D.L. Gin, C.O. Osuji, *ACS Nano.* **2014**, 8, 11977–11986.
[42] M.E. Tousley, X. Feng, M. Elimelech, C.O. Osuji, *ACS Appl. Mater. Interfaces.* **2014**, 6, 19710–19717.
[43] X. Feng, K. Kawabata, G. Kaufman, M. Elimelech, C.O. Osuji, *ACS Nano.* **2017**, 11, 3911–3921.
[44] M. Bremer, P. Kirsch, M. Klasen-Memmer, K. Tarumi, *Angew. Chemie.* **2013**, 125, 9048–9065.
[45] I.M. T. Rasing, *Surfaces and Interfaces of Liquid Crystals*, Springer-Verlag Berlin Heidelberg, **2013**.
[46] X. Feng, S. Nejati, M.G. Cowan, M.E. Tousley, B.R. Wiesenauer, R.D. Noble, M. Elimelech, D.L. Gin, C.O. Osuji, *ACS Nano.* **2016**, 10, 150–158.
[47] R.A.M. Hikmet, J. Lub, J.A. Higgins, *Polymer (Guildf).* **1993**, 34, 1736–1740.
[48] R.J. Baldwin, T. Kreouzis, M. Shkunov, M. Heeney, W. Zhang, I. McCulloch, *J. Appl. Phys.* **2007**, 101, 023713.
[49] H. Thiem, P. Strohriegl, M. Shkunov, I. McCulloch, *Macromol. Chem. Phys.* **2005**, 206, 2153–2159.
[50] H.T.A. Wilderbeek, M.G.M. Van der Meer, C.W.M. Bastiaansen, D.J. Broer, *J. Phys. Chem. B.* **2002**, 106, 12874–12883.
[51] D.J. Broer, J. Lub, G.N. *Mol, Macromolecules.* **1993**, 26, 1244–1247.
[52] D.J. Mulder, L.M.W. Scheres, J. Dong, G. Portale, D.J. Broer, A.P.H.J. Schenning, *Chem. Mater.* **2017**, 29, 6601–6605.
[53] J. Lugger, D.J. Mulder, R. Sijbesma, A. Schenning, *Materials (Basel).* **2018**, 11, 104.
[54] P.S. Goh, A.F. Ismail, *Desalination*. **2018**, 434, 60–80.
[55] Z. Yang, Y. Zhou, Z. Feng, X. Rui, T. Zhang, Z. Zhang, *Polymers (Basel)*. **2019**, 11, 1–22.
[56] N. Ghaffour, T.M. Missimer, G.L. Amy, *Desalination.* **2013**, 309, 197–207.
[57] S. Tul Muntha, A. Kausar, M. Siddiq, *Polym. - Plast. Technol. Eng.* **2017**, 56, 841–856.
[58] M.A. Shannon, P.W. Bohn, M. Elimelech, J.G. Georgiadis, B.J. Marĩas, A.M. Mayes, *Nature.* **2008**, 452, 301–310.
[59] D.M. Stevens, J.Y. Shu, M. Reichert, A. Roy, *Ind. Eng. Chem. Res.* **2017**, 56, 10526–10551.
[60] M. Mulder, *Basic principles of Membrane Technology*, Second ed, Kluwer Academic, **1996**.
[61] A.W. Mohammad, Y.H. Teow, W.L. Ang, Y.T. Chung, D.L. Oatley-Radcliffe, N. Hilal, *Desalination.* **2015**, 356, 226–254.
[62] J.R. Werber, C.O. Osuji, M. Elimelech, *Nat. Rev. Mater.* **2016**, 1, 16018.
[63] W.J. Koros, G.K. Fleming, S.M. Jordan, T.H. Kim, H.H. Hoehn, *Prog. Polym. Sci.* **1988**, 13, 339–401.
[64] R.W. Wijmans, J.G.; Baker, *J. Membr. Sci.* **1995**, 1–21.
[65] W.J. Koros, G.K. Fleming, *J. Membr. Sci.* **1993**, 83, 1–80.
[66] S. Sridhar, B. Smitha, T.M. Aminabhavi, *Sep. Purif. Rev.* **2007**, 36, 113–174.
[67] K. Ghosal, B.D. Freeman, *Polym. Adv. Technol.* **1994**, 5, 673–697.
[68] S.C. George, S. Thomas, *Prog. Polym. Sci.* **2001**, 26, 985–1017.
[69] R.W. Baker, *Membrane technologies and applications*, third ed., John Wiley & Sons, **2012**.

[70] P. Rallapalli, K.P. Prasanth, D. Patil, R.S. Somani, R. V. Jasra, H.C. Bajaj, *J. Porous Mater.* **2011**, 18, 205–210.

[71] L.M. Robeson, Q. Liu, B.D. Freeman, D.R. Paul, *J. Membr. Sci.* **2015**, 476, 421–431.

[72] P. Bernardo, E. Drioli, G. Golemme, *Ind. Eng. Chem. Res.* **2009**, 48, 4638–4663.

[73] M.R.A. Hamid, H.K. Jeong, Korean *J. Chem. Eng.* **2018**, 35, 1577–1600.

[74] B.D. Freeman, *Macromolecules*. **1999**, 32, 375–380.

[75] R.L. Burns, K.M. Steel, S.D. Burns, W.J. Koros, *Ind. Eng. Chem. Res.* **2004**, 43, 5942–5949.

[76] L.M. Robeson, *J. Membr. Sci.* **2008**, 320, 390–400.

[77] M.G. Buonomenna, W. Yave, G. Golemme, *RSC Adv.* **2012**, 2, 10745–10773.

[78] S.R. Reijerkerk, A. Arun, R.J. Gaymans, K. Nijmeijer, M. Wessling, *J. Membr. Sci.* **2010**, 359, 54–63.

Chapter 2

On the order and orientation in liquid crystalline polymer membranes for gas separation

Abstract

In this work, the effect of molecular order and orientation in liquid crystals (LCs) polymer membranes for gas permeation is demonstrated. Using the self-assembly of polymerizable LCs to prepare membranes ensures control over the supramolecular organization and alignment of the building blocks at a molecular level. Robust free-standing LC membranes were fabricated that have various, distinct morphologies (isotropic, nematic cybotactic and smectic C) and alignment (planar and homeotropic) while using the same chemical composition. Single gas permeation data show that the permeability decreases with increasing molecular order while the ideal gas selectivity of He and CO_2 over N_2 increases tremendously when going from randomly ordered to the highly ordered smectic C morphology. The diffusion coefficients showed a 10-fold decrease when going from randomly ordered membranes to ordered smectic C membranes. Comparison of gas sorption and permeation performances of planar and homeotropic aligned smectic C membranes show the effect of molecular orientation by a 3-fold decrease of the diffusion coefficient of homeotropic aligned smectic C membranes resulting in a diminished gas permeation and increased ideal gas selectivities.

This chapter has been published as:

J. Kloos, N. Jansen, M. Houben, A. Casimiro, J. Lub, Z. Borneman, A.P.H.J. Schenning, K. Nijmeijer, On the Order and Orientation in Liquid Crystalline Polymer Membranes for Gas Separation, *Chem. Mater.* **2021**, 33, 8323–8333.

2.1 Introduction

Over the past century, the average human welfare has increased tremendously due to technological advances resulting in the broad availability of electricity, healthcare, transportation and food and clean drinking water. However, these technological advances do not come without costs [1]. Besides the exploitation of earth's resources, large-scale energy production via incineration of fossil fuels resulted in increasing concentrations of greenhouse gases (CO_2 and CH_4) in the atmosphere, leading to global warming. The largest contributing greenhouse gases CO_2 and CH_4 are present in valuable gas sources such as natural gas, biogas or in waste streams like flue gases. To prevent emissions into the atmosphere, separations like CO_2/CH_4 and CO_2/N_2 are crucial to minimizing pollution [2-5]. Moreover, separations of rare gases such as helium from natural gas (He/CH_4 and He/N_2) are getting increasingly more important due to the higher global demand and costly production using conventional cryogenic processes [6,7].

Polymeric membrane technology decreases the operating and energy costs compared to other separation technologies and therefore gained a key role in gas separations over the past decades [8]. Other advantages of the use of polymeric membrane technology are milder operating conditions and a low ecological footprint compared to other separation technologies, making it a competitive separation technology [6,8,9]. Although polymeric membranes are successful and frequently used for gas separations, the used polymers are often not organized at a molecular level which results in limitations such as poorly defined free volume. These limitations lead to a trade-off between permeability and selectivity, described by Robeson's upper bound, which limits the performance of current membranes for gas separation [3,8,10–17]. The role of supramolecular organization and orientation in the polymer matrix on gas separation performance (permeability and selectivity) is relatively unknown. Understanding the effect of supramolecular organization and orientation could potentially lead to better membranes.

Self-assembly as a bottom-up method can be used to obtain a wide variety of ordered nanostructures and thereby gain control over the supramolecular organization and alignment of the building blocks at the molecular level [18–18]. There are two classes of materials that are of particular interest to obtaining nanostructured polymer membranes based on self-assembly. The first class is block copolymers that consist of two or more distinct homopolymers that are covalently bound to each other, thereby having the ability to self-assemble into various morphologies by micro-phase separation [18,22]. For gas

separations, block copolymers have been widely investigated for the removal of CO_2 from light gases [18,23]. Often one of the blocks in the copolymer is low molecular weight poly(ethyleneoxide) due to the favorable interactions of the quadrupole of CO_2 with the dipoles of the ether segments [14, 23–26].

The second class is liquid crystal (LCs) polymers that have sub-nm nanostructures by self-assembly of the LC molecular building blocks. The nanostructures are determined by the positional order of the LC monomers like nematic and smectic phases and can differ in orientation. A typical fabrication method to obtain robust, free-standing LC polymer membranes is to induce the self-assembly of reactive LC monomers inside an LC cell having alignment layers to control the molecular orientation. Subsequent cross-linking fixates the nanostructures. LC polymer membranes have already been investigated for water filtration [27–40]. However, these materials are rarely used for gas separations. Bara et al. [10] showed the importance of molecular order for gas separation, by testing the performance of light gases, of cross-linked LC polymer membranes with an ordered but not aligned columnar morphology. The nanostructured membranes exhibit a slightly lower CO_2 permeability but an increase in CO_2/N_2 and CO_2/CH_4 selectivity compared to the membranes without molecular order. As far as we know there is no additional work reported on this topic.

Here, we study the molecular order and orientation, of free-standing thermotropic LC polymer membranes with varies distinct morphologies for gas separations of He, Ar, N_2 and CO_2. Membranes are fabricated with various alignments and molecular order (isotropic, nematic, and smectic) while using the same chemical composition. An LC mixture consisting of a mono-methacrylate (M1) LC with a crown ether functionality and a smectic di-acrylate (M2) cross-linker is aligned and polymerized inside a glass cell with an alignment layer, resulting in robust, free-standing membranes (Figure 2.1). The single gas permeation performance (permeability, selectivity) of these films for various gases is studied and the effect of molecular orientation and order is shown.

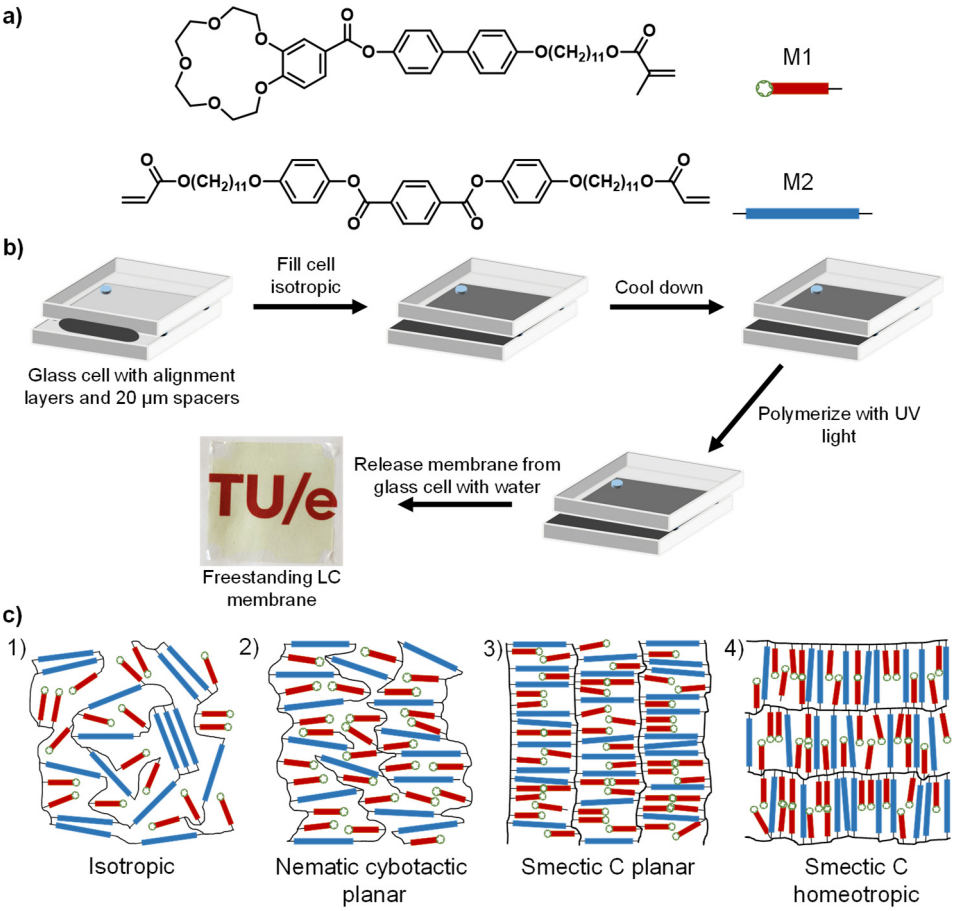

Figure 2.1: a) *Molecular structures of a mono-methacrylate crown ether LC (M1, red rods) and di-acrylate LC cross-linker (M2, blue rods) which are used in a 1:1 (wt%) ratio for all membranes.* ***b)*** *Schematic representation of the fabrication process of the LC membranes.* ***c)*** *Artist's impression of free-standing membranes with various morphologies that differ in degree of molecular order and orientation (cross-sectional area). Please note that only the cross-section of the free-standing membranes is shown and therefore the smectic C morphology looks similar to a smectic A morphology.*

2.2 Materials and methods

2.2.1 Chemicals

11-bromoundecyl methacrylate [34], and 11-(4-hydroxyphenoxy)undecyl acrylate [35], were kindly provided by Philips Research. 4,4'-biphenol, sodium iodide, anhydrous N, N-

dimethylformamide, anhydrous chloroform, thionyl chloride, anhydrous tetrahydrofuran, t-butyl-hydroquinone, 4-carboxybenzo-15-crown-5, terephthaloyl chloride, magnesium sulfate, hydrochloric acid (37%) and silica were purchased from Merck Life Science. Potassium carbonate and ethanol were obtained from VWR chemicals. Chloroform and triethylamine were purchased from Merck KgaA. Dichloromethane and ethyl acetate were obtained from Biosolve. Irgacure 819 was supplied by Ciba. For permeation and sorption measurements, the gases He (5.0 grade), CO_2 (4.5 grade), N_2 (5.0) grade and Ar (5.0 grade) were purchased from Linde gas (the Netherlands). All reagents were used as received, without further purification.

2.2.2 Synthesis of 4-((11-methacryloylundecan-1-yl)oxy)-4'-(4'-carboxybenzo-15-crown-5)biphenyl (M1) and intermediates

11-((4'-hydroxy-[1,1'-biphenyl]-4-yl)oxy)undecyl methacrylate

The synthesis of 11-((4'-hydroxy-[1,1'-biphenyl]-4-yl)oxy)undecyl methacrylate was based on the methods described before [36]. 11-bromoundecyl methacrylate (2.3 g, 7.2 mmol), 4',4-biphenol (2.5 g, 13.5 mmol), potassium carbonate (3.0 g, 22 mmol) and sodium iodide (0.2 g, 1.4 mmol) were added to a flask with a condenser. The system was dried with three cycles of vacuum/argon, after which the compounds were dissolved in 30 ml anhydrous N, N-dimethylformamide. The reaction mixture was stirred for 16.5 hours at 50 °C, followed by filtration and evaporation of the N, N-dimethylformamide by rotary evaporation. The resulting solid was dissolved in 100 ml chloroform and filtered. Subsequently, the chloroform of the collected filtrate was evaporated by rotary evaporation and the resulting solid was purified using column chromatography (dry loading, dichloromethane as eluent), yielding the final product as a white solid with a yield of 45%. ^{1}H NMR (400 MHz, Chloroform-*d*) δ 7.45 (d, *J* = 8.7 Hz, 2H), 7.42 (d, *J* = 8.6 Hz, 2H), 6.95 (d, *J* = 8.8 Hz, 2H), 6.89 (d, *J* = 8.6 Hz, 2H), 6.10 (s, *J* = 1.4 Hz, 1H), 5.55 (p, *J* = 1.6 Hz, 1H), 5.05 (s, 1H), 4.14 (t, *J* = 6.7 Hz, 2H), 4.00 (t, *J* = 6.6 Hz, 2H), 1.95 (t, *J* = 1.3 Hz, 3H), 1.79 (m, 2H), 1.69 (m, 2H), 1.48 (m, 2H), 1.41-1.27 (m, 12H). ^{13}C NMR (101 MHz, $CDCl_3$) δ 167.70, 158.26, 154.67, 136.53, 133.70, 133.23, 127.92, 127.66, 125.26, 115.59, 114.76, 68.11, 64.92, 29.55, 29.50 (2C), 29.40, 29.31, 29.25, 28.61, 26.07, 25.99, 18.35.

4'-Acylchloride-benzo-15-crown-5

The synthesis of 4'-acylchloride-benzo-15-crown-5 was based on the methods described before [41]. 4-carboxybenzo-15-crown-5 (0.766 g, 2.45 mmol) was added to a flask and dried with three cycles of vacuum/argon. Subsequently, 15 ml anhydrous chloroform was added and followed by slowly adding thionyl chloride (1.0 ml, 13.8 mmol). The resulting suspension was stirred for 3 hours at room temperature after which the solvent and excess thionyl chloride were removed under vacuum. The conversion of the resulting acyl chloride was checked with ATR FT-IR, showing good conversion. ATR FT-IR (cm^{-1}): 2895 (C-H stretch, Ar.), 1742 (C=O stretch acyl chloride), 1586 (C-C stretch Ar.), 1511, 1420, 1350, 1254 (C-O stretch ether), 1131, 747 (C-Cl stretch).

4-((11-methacryloylundecan-1-yl)oxy)-4'-(4'-carboxybenzo-15-crown-5)biphenyl (M1)

The synthesis of 4-((11-methacryloylundecan-1-yl)oxy)-4'-(4'-carboxybenzo-15-crown-5)biphenyl (M1) was based on the methods described before [41]. Triethylamine (0.34 ml, 2.35 mmol) was added dropwise over a period of 5 minutes to a solution of 4'-acylchloride-benzo-15-crown-5 (1.077 g, 2.35 mmol), 11-((4'-hydroxy-[1,1'-biphenyl]-4-yl)oxy)undecyl methacrylate (1.0 g, 2.35 mmol) in 5 ml anhydrous tetrahydrofuran cooled in an ice bath under argon atmosphere. After one hour the ice bath was removed and stirring was continued for 16 hours at room temperature after which the THF was evaporated. The remaining product was dissolved in 8 ml of chloroform and subsequently precipitated with 5 ml of ethanol. The precipitate was filtered and dried, yielding M1 as a white powder with a yield of 62%. ^{1}H NMR (400 MHz, Chloroform-*d*) δ 7.85 (dd, *J* = 8.4, 2.0 Hz, 1H), 7.68 (d, *J* = 2.1 Hz, 1H), 7.59 (d, *J* = 8.6 Hz, 2H), 7.50 (d, *J* = 8.7 Hz, 2H), 7.23 (d, *J* = 8.6 Hz, 2H), 6.96 (d, *J* = 8.7 Hz, 2H), 6.94 (d, *J* = 8.5 Hz, 1H), 6.10 (s, 1H), 5.55 (q, *J* = 1.7 Hz, 1H), 4.23 (m, 4H), 4.14 (t, *J* = 6.7 Hz, 2H), 4.00 (t, *J* = 6.6 Hz, 2H), 3.95 (m, 4H), 3.78 (d, *J* = 2.6 Hz, 8H), 1.94 (d, *J* = 1.2 Hz, 3H), 1.81 (m, 2H), 1.69 (m, 2H), 1.47 (p, *J* = 6.8 Hz, 2H), 1.42 – 1.25 (m, 12H). ^{13}C NMR (101 MHz, $CDCl_3$) δ 167.57, 165.01, 158.76, 153.78, 149.97, 148.62, 138.59, 136.57, 132.78, 128.10, 127.69, 125.14, 124.80, 122.07, 121.98, 114.96, 114.81, 112.09, 71.20 (2C) , 70.42, 70.32, 69.40, 69.26, 69.09, 68.65, 68.10, 64.85, 29.55, 29.50 (2C), 29.40, 29.30, 29.25, 28.62, 26.07, 25.99, 18.35. ATR FT-IR (cm^{-1}): 2900 (C-H stretch), 2345, 1725 (C=O ester), 1597 (C-C stretch Ar.), 1500, 1431, 1277 (C-O stretch), 1205 (C-O stretch), 1143, 1058, 961. HRMS (MALDI-TOF): $[M + Na]^+$ calcd. for $C_{42}H_{54}O_{10}Na$: 741.36; found: 741.30.

2.2.3 Synthesis of bis(4-((11-(acryloyloxy)undecyl)oxy)phenyl) terephthalate (M2)

Bis(4-((11-(acryloyloxy)undecyl)oxy)phenyl) terephthalate (M2)

Triethylamine (15.2 ml, 110 mmol) was added dropwise to a solution of 11-(4-hydroxyphenoxy)undecyl acrylate (33.1 g, 100 mmol) and terephthaloyl chloride (10.1 g, 50 mmol) in 200 ml of dichloromethane cooled in an ice bath under a nitrogen atmosphere. Stirring was continued for one night at room temperature after which the solution was extracted subsequently with 100 ml of an aqueous 1M HCl solution and 200 ml of brine and dried over magnesium sulfate. The crude product was obtained after filtration over a thin silica pad followed by evaporation. 29.1 g of M2 (73% yield) was obtained as white crystals after recrystallization from 300 ml of ethyl acetate. ^{1}H NMR (400 MHz, Chloroform-*d*) δ 8.31 (s, 4H), 7.14 (d, *J* = 9.0 Hz, 4H), 6.94 (d, *J* = 9.0 Hz, 4H), 6.40 (dd, *J* = 17.4, 1.5 Hz, 2H), 6.12 (dd, *J* = 17.3, 10.4 Hz, 2H), 5.81 (dd, *J* = 10.4, 1.5 Hz, 2H), 4.15 (t, *J* = 6.7 Hz, 4H), 3.97 (t, *J* = 6.5 Hz, 4H), 1.79 (m, 4H), 1.67 (m, 4H), 1.46 (m, 4H), 1.41 – 1.25 (m, 24H). ^{13}C NMR (101 MHz, $CDCl_3$) δ 166.35, 164.69, 157.10, 144.02, 133.96, 130.43, 130.21, 128.66, 122.25, 115.17, 68.44, 64.72, 29.54, 29.50 (2C), 29.38, 29.27, 29.25, 28.63, 26.05, 25.93. HRMS (MALDI-TOF): $[M + Na]^+$ calcd. for $C_{48}H_{62}O_{10}Na$: 821.42; found: 821.48.

2.2.4 Membrane preparation

An LC mixture consisting of 49.7 wt % M1, 49,7 wt % M2, 0.5 wt % photoinitiator (Irgacure 819) and 0.1 wt % inhibitor (TBHQ) was prepared by dissolving the compounds in a minimum amount of chloroform and subsequently evaporating the solvent. The membranes with a thickness of 20 µm were prepared by heating the LC mixture to the isotropic phase at 130 °C and using capillary suction between two glass plates equipped with 20 µm spacers to fill the glass cells. To obtain planar alignment, the glass plates were functionalized with a rubbed polyimide layer (Optimer AL 1254; JSR Corporation, Toyo Japan). After the glass cells were filled, the samples were placed inside a temperature-controlled N_2 box, in which the samples were cooled from 130 °C to the desired temperature (130 °C, 114 °C, 104 °C, for respectively isotropic, nematic and smectic morphologies) with a cooling rate of 1 °C/min. Subsequently, the samples were polymerized by exposing the samples for 10 min to an unfiltered spectrum of a collimated EXFO Omnicure S2000 UV lamp with a light intensity of 20 mW/cm^2 in the range of 320-390 nm. The glass cells were opened by immersing the samples in hot water (80 °C) for 10 minutes to obtain the free-standing membranes. For homeotropic alignment, Nissan

polyimide sunever (Nissan Chemical Industries ltd.) functionalized glass cells were used and the membranes were similarly processed as the planar aligned membranes described before.

2.2.5 Characterization

Nuclear magnetic resonance spectroscopy (NMR) spectra were recorded at room temperature on a Bruker, FT-NMR spectrometer AVANCE III HD-Nanobay (400 MHz, Bruker Ultrashield magnet, BBFO Probehead, BOSS1 shim assembly) in deuterated chloroform. Chemical shifts are given in ppm with respect to tetramethyl silane (TMS, 0 ppm) as the internal standard.

Matrix-assisted laser desorption/ionization time-of-flight mass spectrometry (MALDI-TOF MS) was performed on a Bruker Autoflex Speed MALDI-MS instrument using DCTB (2-[(2E)-3-(4-tert-butylphenyl)-2-methylprop-2-enylidene] malononitril) as matrix.

Attenuated total reflection fourier transform infrared spectroscopy (ATR FT-IR) spectra were recorded at room temperature on a Varian-cary 3100 FT-IR spectrometer equipped with a golden gate attenuated total reflectance (ATR) sampling accessory. Scans were taken over a range of 4000−650 cm^{-1}, with a spectral resolution of 4 cm^{-1} and 50 scans per spectrum.

Polarising optical microscopy (POM) was performed using a Leica DM 2700M optical microscope equipped with two polarizers that were operated either crossed or parallel with the sample in between, a Linkam hot-stage THMS600 with a Linkam TMS94 controller and a Leica DFC420 C camera.

Differential scanning calorimetry (DSC) measurements were recorded in hermetic T-zero aluminum sample pans using a TA Instruments Q2000 DSC equipped with a cooling accessory. The DSC measurements were performed with three cycles of heating and cooling at a rate of 1 °C/min with an isothermal equilibration of 3 minutes after each heating or cooling ramp. The transition temperatures were determined from the third heating and cooling cycle using TRIOS DSC software.

Medium- and wide-angle X-ray scattering (MAXS/WAXS) measurements were recorded on a GaneshaLab instrument equipped with a Genix-Cu ultralow divergence source producing X-ray photons of wavelength 1.54 Å and a flux of 108 photons per second.

Diffraction patterns were collected on a Pilatus 300 K silicon pixel detector with 487 × 619 pixels of 172 μm^2.

2.2.6 Gas sorption

Gas sorption of N_2 and CO_2 was performed at 6 bar and 20 °C for all membranes with a Rubotherm series IsoSORP® sorption instrument to determine the solubility coefficient (cm^3 STP/(cm^3·cmHg)) for both gases. The equipment uses a magnetically suspended balance to measure the sorbed weight of the gas. Before each sorption measurement, a buoyancy measurement with helium was performed to determine the initial sample weight and volume. Here the assumption was made that the solubility of helium is negligible. With the obtained sample weight and volume from the buoyancy measurement with helium, the measured sorbed weight is corrected using Equation (2.1).

$$m_{corrected} = m_{measured} + \rho_{gas} \cdot V_{sample} \qquad (2.1)$$

In Equation (2.1), $m_{corrected}$ is the corrected weight (g), $m_{measured}$ is the measured weight (g), ρ_{gas} is the density of the measuring gas (g/cm^3) and V_{sample} the sample volume (cm^3). With the corrected sorbed weight, the concentration of the measuring gas (N_2 or CO_2) was calculated at 6 bar and 20 °C using Equation (2.2).

$$C_i = \frac{m_i \cdot \rho_s}{m_0 \cdot \rho_i\,(STP)} \qquad (2.2)$$

In Equation (2.2), C_i (cm^3 (STP)/cm^3 polymer) is the concentration of gas in the membrane, m_i is the buoyancy corrected mass of gas in the polymer (g), ρ_s is the density of the membrane (g/cm^3), m_0 is the initial mass of the sample measured at vacuum (g) and ρ_i (STP) (g/cm^3) is the density of measuring gas at standard temperature and pressure (STP = 273.15 K and 1.013 bar). The solubility coefficient of N_2 and CO_2 in the membranes was calculated with Equation (2.3).

$$S = \frac{C_i}{P} \qquad (2.3)$$

In Equation (2.3), S is the gas solubility (cm^3 STP/(cm^3·cmHg)), C_i the concentration gas adsorbed (cm^3 (STP)/cm^3) and P the pressure (cmHg).

2.2.7 Single gas membrane performances

Gas permeation experiments using He, Ar, N_2 and CO_2 were performed in a stainless-steel cell with a permeation area of 2.1 cm^2. The flat sheet membranes were supported by a Whatman® filter paper (Grade 50 with a pore size of 2.7 µm) to provide additional mechanical support. The single gas permeability of the membranes was determined using Equation (2.4), at 20 °C in duplicate by measuring the permeate pressure increase over time in a calibrated volume with a feed pressure of 6 bar and vacuum at the permeate side.

$$P_i = \frac{\Delta P_{permeate} \cdot V_c \cdot V_m \cdot L \cdot 10^{10}}{\Delta t \cdot R \cdot T \cdot A \cdot \Delta P} \qquad (2.4)$$

In Equation (2.4), P_i is the permeability of gas species i (Barrer), $\Delta P_{permeate}$ is the increase in permeate pressure (Pa) per time interval Δt (s), V_c is the calibrated permeate volume (m^3), V_m is the molar volume at STP (cm^3/mol), L is the membrane thickness (cm), R is the gas constant (J/ K·mol), T is the permeate temperature (K), A is the membrane area (cm^2) and ΔP the transmembrane pressure (cmHg). Before each single gas permeation measurement, the membranes were conditioned for at least 1 hour with the gas to be measured. First, He permeation was measured followed by Ar and N_2. CO_2 permeation measurements were performed last since CO_2 could induce swelling of the membrane. The ideal selectivity of gas species i with respect to gas species j, $\alpha_{i/j}$ (-), was calculated with Equation (2.5).

$$\alpha_{i/j} = \frac{P_i}{P_j} \qquad (2.5)$$

The N_2 and CO_2 diffusion coefficients of the LC membranes were calculated by using Equation (2.6).

$$D = \frac{P}{S} \qquad (2.6)$$

In Equation (2.6), D is the diffusion coefficient (cm^2/s), P the permeability (Barrer) and S the solubility coefficient (cm^3 STP/(cm^3·cmHg)).

2.3 Results and discussion

2.3.1 Synthesis and characterization of M1 and 2

A photopolymerizable nematic mono-methacrylate (M1) and a smectic di-acrylate (M2) were selected and synthesized to fabricate membranes with various morphologies and alignments while using the same chemical composition (Figure 2.1a). M1 was selected for its crown ether moiety of which is known that the cyclic oligoethylene oxide segments have favorable interactions with CO_2. M2 was synthesized to improve the mechanical strength of the fabricated membranes and it was expected that undecyl side chains would enlarge and stabilize the smectic lamellar phase [42].

M1 was synthesized and characterized following a literature procedure (see Scheme 2.1 for reaction scheme) [1]. Intermediate product (4) and M1 were characterized by ^{1}H and ^{13}C nuclear magnetic resonance (NMR) and are in accordance with literature values [43]. Moreover, mass spectroscopy (MALDI-TOF) and attenuated total reflection Fourier transform infrared spectroscopy (ATR FT-IR) showed the successful synthesis of M1 [43]. The phase behavior of M1 was determined with differential scanning calorimetry (DSC) and polarizing optical microscopy (POM) [43]. DSC revealed upon cooling an isotropization temperature of 117 °C which is in accordance with the literature (114 °C respectively). Upon further cooling, M1 exhibits a nematic phase at 116 °C and crystallizes at 99 °C.

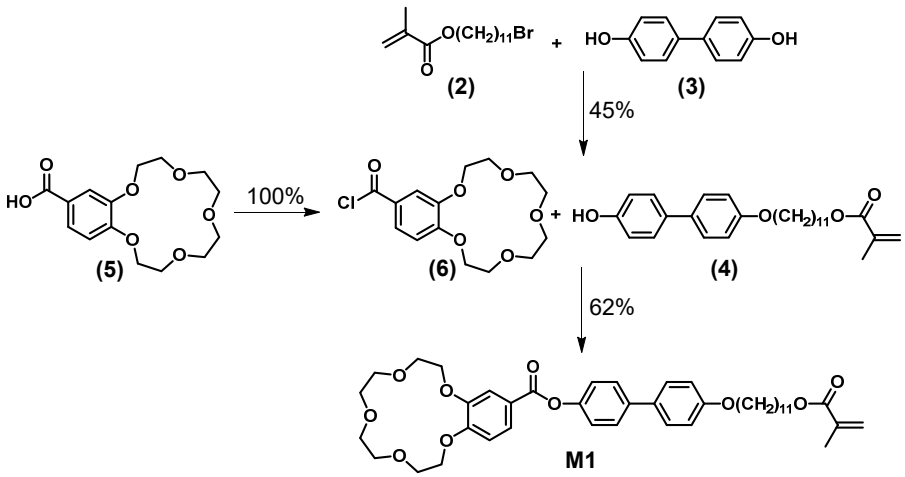

Scheme 2.1: *Reaction scheme of 4-((11-methacryloylundecan-1-yl)oxy)-4'-(4'-carboxybenzo-15-crown-5)biphenyl (M1).*

M2 was synthesized for the first time by the addition elimination reaction between intermediate terephthaloyl chloride (7) and 11-(4-hydroxyphenoxy)undecyl acrylate (8) (see Scheme 2.2 for reaction scheme). Characterization by ^{1}H NMR and ^{13}C NMR and MALDI-TOF confirmed the successful formation of M2 [43]. The phase transitions of M2 were determined with DSC and POM [43]. DSC revealed upon cooling an isotropization temperature of 132 °C. Further cooling shows a nematic phase between 132 °C and 131 °C, a smectic phase between 131 °C and 116 °C and crystallization at 115 °C.

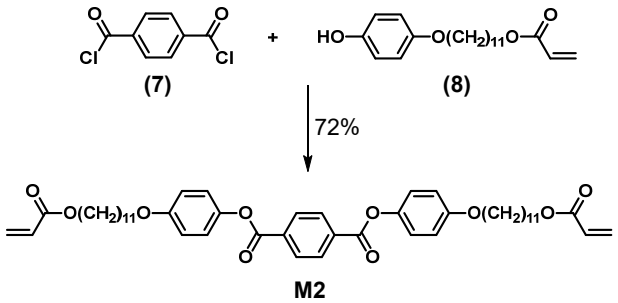

Scheme 2.2: *Reaction scheme of bis(4-((11-(acryloyloxy)undecyl)oxy)phenyl) terephthalate (M2).*

An LC mixture consisting of M1 and M2 (in a set ratio of 1:1 in wt%), a photoinitiator and an inhibitor was prepared and characterized with DSC and POM to determine the phase transitions [43]. DSC revealed an isotropization temperature of 118 °C. Upon cooling the LC mixture shows a nematic phase at 117 °C and a smectic phase at 108 °C and crystallizes at 100 °C, elucidating that this specific LC mixture can be used to prepare membranes with isotropic, nematic and smectic morphologies.

2.3.2 Preparation and characterization of liquid crystalline membranes

Membranes were prepared by incorporating the LC mixture in glass cells having different alignment layers to control the orientation (Figure 2.1b). The LC mixture was polymerized at 130 °C, 114 °C, and 104 °C, for respectively isotropic, nematic and smectic order and after opening of the cells, free-standing membranes were obtained (see Figure 2.1c for an artist's impression of the free-standing membranes with various morphologies that differ in molecular order and orientations). FTIR confirmed the full conversion of the acrylate moieties [43].

The alignment and organization of the polymerized membranes were investigated with POM [43]. Membranes with a planar alignment show dark images under parallel conditions

and bright images under 45° tilt, revealing birefringent polymer membranes. Homeotropically aligned membranes showed dark gray images for all angles. This indicates that the membranes are well aligned. Wide-angle X-ray scattering (WAXS) and medium-angle X-ray scattering (MAXS) were employed to further investigate the alignment and morphology of the membranes (Figure 2.2).

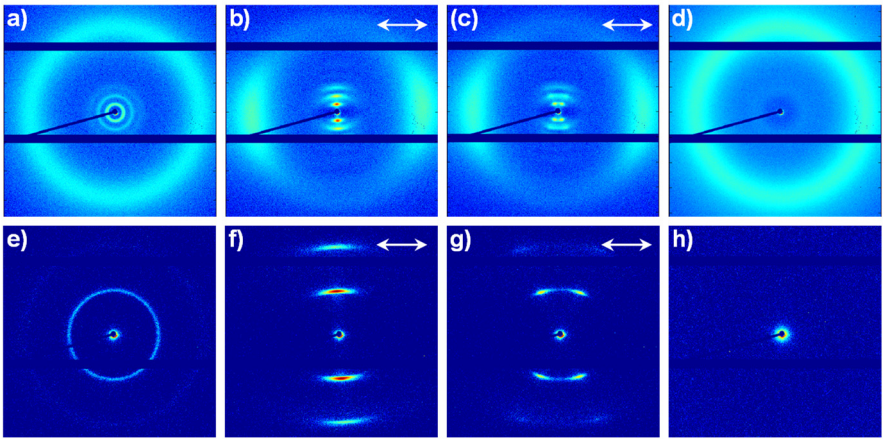

Figure 2.2: *WAXS (top row) and MAXS (bottom row) spectra of membranes with different molecular alignments and orientations.* ***a, e)*** *Membranes polymerized at 130 °C representing a random oriented (isotropic) morphology.* ***b, f)*** *Membranes polymerized at 114 °C representing a planar aligned nematic cybotactic morphology.* ***c, g)*** *Membranes polymerized at 104 °C representing a planar aligned smectic C morphology.* ***d, h)*** *Membranes polymerized at 104 °C representing a homeotropic aligned smectic C morphology. The single arrow shows the alignment direction.*

The 2D WAXS and MAXS spectra (Figure 2.2a,e) of the membranes that were polymerized at 130 °C show full diffuse circles in the wide and medium angle region. The full circle in the wide-angle region corresponds to randomly oriented LC molecules, which is characteristic for an isotropic morphology. However, the presence of two full circles in the MAXS (Figure 2.2e) indicates that the isotropic membranes contain randomly oriented layered structures, which corresponds to a smectic morphology. These randomly oriented layered structures were not expected because the membranes were fabricated well above the isotropization temperature. Moreover, POM images of the membranes fabricated at 130 °C show dark images at all angles, indicating an isotropic morphology. Combining the POM and XRD data makes it likely that the membranes fabricated at 130 °C have an isotropic morphology with randomly oriented smectic domains in the nm scale which are therefore not visible with POM (Figure 2.1c 1 illustrates the cross-section of an isotropic

bulk morphology with random oriented smectic domains). Figures 2.2b and 2.2f show the WAXS and MAXS spectra of membranes that were polymerized at 114 °C, respectively. Both WAXS and MAXS contain diffraction spots instead of full circles which indicates that all molecules are oriented in a common direction. In addition, the MAXS spectrum in Figure 2.2f shows two spots parallel to the alignment direction which would correspond to an ordered planar smectic A morphology. However, from the absence of smectic features in the POM it is concluded that these membranes have an ordered nematic morphology that contains localized, fluctuating regions of smectic domains in the nm scale (Figure 2.1c 2 illustrates the cross-section of a planar nematic bulk morphology with smectic domains). This so-called nematic cybotactic phase is known to appear close to the nematic-smectic transition [44,45]. Figure 2.2g shows the MAXS of membranes that were polymerized in a planar fashion at 104 °C. The MAXS shows splitting of the two centered spots, which corresponds to an ordered smectic C morphology that consists of a tilted layered structure with a tilt angle of 23° (Figure 2.1c 3 illustrates the cross-section of a planar smectic C morphology). Moreover, a layer spacing of 4.6 nm that corresponds to the distance between two smectic layers was determined. The determined layer spacing is in close approximation with the theoretical layer spacing of M2 (4.99 nm), which is expected to mainly determine the layer spacing as it is connecting the layered structures. The small discrepancy between the experimental determined and theoretical layer spacing can be explained by the fact that the flexible alkyl chain of M2 can be folded, leading to a slightly lower value. Contrary to the WAXS and MAXS spectra of planar aligned smectic C membranes, homeotropic aligned smectic C membranes in Figure 2.2d,h show no diffraction spots in the medium angle region because the X-ray beam is parallel to the LC molecules but only show a full diffuse circle in the wide-angle region (Figure 2.1c 4 illustrates the cross-section of a homeotropic smectic C morphology) [29]. The intermolecular spacing that corresponds to the intermolecular stacking of the LC building blocks was found to be 4.3 – 4.4 Å for all morphologies and orientations. The above confirms the formation of the different nanostructured membranes as presented in Figure 2.1c.

2.3.3 Effect of molecular order on single gas performances

The effect of molecular order on gas permeation performance was investigated by measuring single gas permeation of He, Ar, N_2 and CO_2 in membranes with isotropic, planar nematic cybotactic and planar smectic C morphologies. The permeation data are shown in Figure 2.3 (see reference [43] for permeation values).

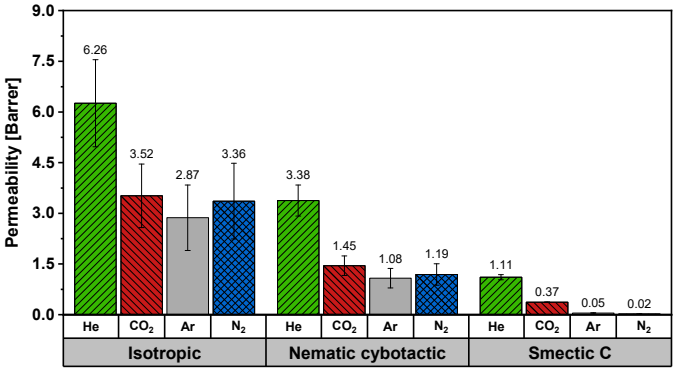

Figure 2.3: *Single gas permeability (He, Ar, N_2, and CO_2) of membranes with respectively isotropic, nematic cybotactic and smectic C morphologies at 20 °C and 6 bar feed pressure.*

Figure 2.3 shows that the permeability of all gases decreases when going from a randomly ordered (isotropic) to a highly ordered smectic C morphology. Helium has the highest permeability for all membranes, while the membranes with isotropic and nematic cybotactic morphologies have relatively similar permeabilities for CO_2, Ar and N_2. Oppositely, the permeability of membranes with the smectic C morphology decreases tremendously for Ar and N_2 (22-fold for Ar and 67-fold for N_2) compared to He and CO_2 (3-fold for He and 4-fold for CO_2). To visualize the effect of molecular order on the gas separation performance, the ideal gas selectivities were calculated from these permeation data, and the selectivities of the three most important gas pairs (He/N_2, CO_2/N_2 and He/CO_2) are shown in Figure 2.4 (see reference [43] for all gas pairs).

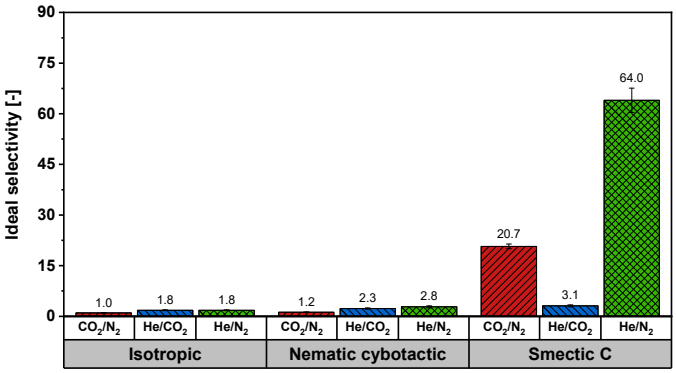

Figure 2.4: *Ideal gas selectivities (CO_2/N_2, He/CO_2, He/N_2) of membranes with respectively isotropic, nematic cybotactic and smectic C morphologies at 20 °C.*

Figure 2.4 shows that isotropic membranes exhibit almost no selectivity towards a specific gas species and only a slight selectivity increase for all gas pairs is observed for the nematic cybotactic morphology. However, selectivities towards He and CO_2 increase tremendously (24-fold for He/N_2 and 18-fold for CO_2/N_2) for the highly ordered smectic C morphology. The difference in gas permeability and selectivity between the nematic cybotactic and smectic C membranes is considerable and most likely originates from the difference in molecular order. As shown in section 2.3.2 the nematic cybotactic membranes have a less ordered nematic bulk that contains localized, more ordered smectic domains. For gas separation this means that permeation will mainly occur through the less ordered nematic bulk of these membranes. The smectic C membranes have an ordered smectic C bulk and permeation occurs through the smectic bulk, which results in lower gas permeabilities. These permeation results can be further explained by the effect of a combination of parameters being kinetic diameter, molecular weight, critical temperature, free volume and molecular interactions via the quadrupole moments of the gases. These parameters are presented in Table 2.1 [46].

Table 2.1: *The kinetic diameter, molecular weight, quadrupole moment and critical temperature of various gas species [46].*

Gas species	Kinetic diameter [Å]	Molecular weight [g/mol]	Quadrupole moment $[cm^2] \cdot 10^{40}$	Critical temperature [K]
He	2.60	4.00	0.00	5.19
CO_2	3.30	44.01	-13.71	304.13
Ar	3.43	39.94	0.00	151.00
N_2	3.64	28.01	-4.91	126.20

As the fabricated membranes can be considered dense, the mechanism of permeation is best described by the solution-diffusion model [47]. Dense membranes separate gases via their intrinsic differences in solubility and diffusivity. Irrespective of the molecular structure and orientation of the membrane, some general considerations can be given. Helium has the smallest kinetic diameter and lowest molecular weight of all measured gases, leading to a higher diffusion rate through the membrane, resulting in the highest permeability of all gases [48]. N_2 has a lower molecular weight than CO_2 and Ar but this is accompanied by the largest kinetic diameter of all measured gases. Combined with its low solubility in the polymer matrix due to its low critical temperature (see sorption section and Table 2.2), this results in a lower N_2 permeability than for He. CO_2 and Ar have similar kinetic diameters and molecular weights but CO_2 has a higher critical temperature which results in a higher solubility in the polymer matrix [49]. In addition, the CO_2 solubility is expected to be enhanced due to favorable interactions of the quadrupole of CO_2 with the dipole moments of the crown ethers [14,49].

For both the isotropic and nematic cybotactic LC membranes (Figure 2.1c 1,2), the permeabilities of CO_2, Ar and N_2 are relatively equal for the same membranes. This suggests that the differences in solubility and diffusivity between the gases cancel each other out while permeating the membrane. Based on the high critical temperature and quadrupole moment of CO_2 (high solubility and low diffusivity) and the large kinetic diameter of N_2 (low solubility and low diffusivity), one would expect a higher CO_2 permeability than N_2 permeability. Still, both have equal permeabilities which suggest that either the solubility of CO_2 or the effect of the kinetic diameter is lower than expected. By comparing the kinetic diameter and critical temperature (shown in Table 2.1) of CO_2, N_2

and Ar, one can hypothesize if the solubility or diffusivity is dominant for permeation through LC membranes with isotropic and nematic cybotactic morphologies. If the solubility would be the dominant effect, one would expect a higher Ar permeability than N_2 permeability because both gases have similar critical temperatures and therefore comparable solubilities but Ar has a smaller kinetic diameter than N_2. Since both Ar and N_2 have equal permeabilities this suggests that the diffusivity is dominant over the solubility and gas permeation through LC membranes with isotropic and nematic cybotactic morphologies mainly depends on diffusion. For membranes with an ordered smectic C morphology the permeability of Ar and N_2 is significantly lower than that of He and CO_2, resulting in an increase in He/N_2 and CO_2/N_2 selectivities. In line with the previous discussion this most probably originates from the increased molecular order. With that the total free volume within the membranes decreases, which affects the diffusion coefficient and increases the selectivity between gases with a larger kinetic diameter (Ar and N_2) and gases with a smaller kinetic diameter (He and CO_2). To further investigate the effect of molecular order on the gas permeability of these LC membranes the gas sorption of CO_2 was measured. Subsequently, the diffusion coefficient was calculated using Equation (2.6). Unfortunately, the N_2 sorption for all membranes was too low to obtain accurate values. Therefore, Table 2.2 only presents the permeabilities, solubility coefficients and diffusion coefficients of CO_2 in membranes with respectively isotropic, nematic cybotactic and smectic C morphologies.

Table 2.2: *CO_2 permeabilities, solubility coefficients measured at 6 bar and 20 ˚C and the associated calculated diffusion coefficients of LC membranes with respectively isotropic, nematic cybotactic and smectic C morphologies.*

Morphology	**P** $\left[\frac{cm^3(STP)\cdot cm}{cm^2\cdot s\cdot cmHg}\right]\cdot 10^{-10}$	**S** $\left[\frac{cm^3(STP)}{cm^3\cdot cmHg}\right]\cdot 10^{-3}$	**D** $\left[\frac{cm^2}{s}\right]\cdot 10^{-9}$
Isotropic	3.49	12.0	29.0
Nematic cybotactic	1.46	12.0	12.2
Smectic C	0.37	12.0	3.05

Sorption experiments (Table 2.2) show that the solubility coefficient of CO_2 is equal for all morphologies, meaning that the decrease in CO_2 permeability with increasing molecular order can be completely attributed to a decrease in the diffusion coefficient. Going from an

isotropic to a nematic cybotactic morphology the diffusion coefficient decreases 2 times while the smectic C morphology when compared to the isotropic morphology even shows a 10-fold decrease in the diffusion coefficient. A similar solubility coefficient for all morphologies indicates that the overall free volume in the membrane is equal for all morphologies [50]. It is therefore likely that with increasing molecular order not the total free volume within the LC membranes decreases, but the free volume elements within the membrane decrease in size. A decrease in the size of the free volume elements results in a larger reduction in diffusion coefficients for gases with larger kinetic diameters (Ar, N_2) than gases with smaller kinetic diameters (He, CO_2), inducing selectivity for the membranes with a smectic C morphology [51,52]. Contrary to membranes with a smectic C morphology, membranes with an isotropic or nematic cybotactic morphology exhibit far lower selectivities due to their larger free volume elements and therefore higher diffusion coefficients.

2.3.4 Effect of molecular orientation on single gas performances

The effect of molecular orientation was investigated by comparing the single gas performances of planar aligned smectic C membranes versus homeotropic aligned smectic C membranes. In the case of planar aligned membranes, the lamellar structures are oriented in the permeation direction, whereas in the homeotropic membranes, the lamellar structures are perpendicular to the permeation direction. Permeation data and ideal gas selectivities of planar and homeotropic aligned smectic C membranes are shown in Figure 2.5 (see reference [43] for permeability values and ideal selectivities of all gas pairs).

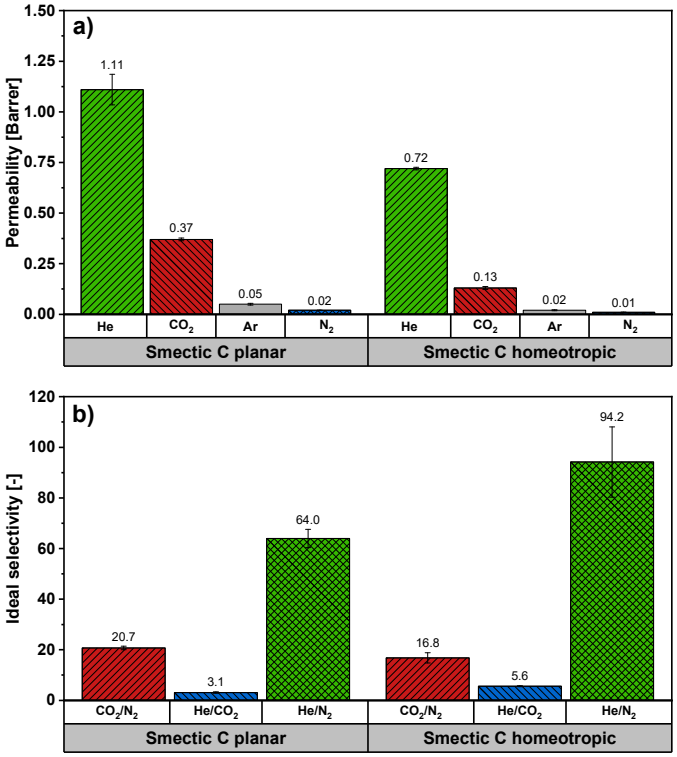

Figure 2.5: *Gas permeation data and ideal gas selectivities of different molecular orientations.* ***a)*** *Single gas permeability (He, Ar, N_2, and CO_2) of planar and homeotropic aligned smectic C membranes at 20 °C and 6 bar feed pressure.* ***b)*** *Ideal gas selectivities (CO_2/N_2, He/CO_2, He/N_2) of planar and homeotropic aligned smectic C membranes at 20 °C.*

Figure 2.5a shows that the permeability of all gases is diminished when going from a planar to a homeotropic orientation. This decrease in permeability can be attributed to a hindered gas transport. When the lamellar structures are oriented perpendicular to the permeation direction the gas molecules have to pass highly cross-linked acrylate areas of the membrane that inhibit diffusion and decrease the permeability. Contrary to the permeability, the ideal selectivities of homeotropic aligned membranes are higher compared to those of planar aligned membranes (Figure 2.5b). The highly cross-linked areas decrease the diffusion of gases with a larger kinetic diameter such as CO_2, Ar and N_2 more compared to the smaller He, resulting in enhanced He/N_2 and He/CO_2 selectivities. Surprisingly, the CO_2/N_2 selectivity of the homeotropic aligned membranes decreases by 20% compared to planar aligned membranes, indicating that CO_2 is more

retained by the cross-linked areas compared to N_2. To study this in more detail gas sorption of CO_2 was measured at 6 bar to determine the gas solubility and calculate the diffusion coefficients (Table 2.3).

Table 2.3: *CO_2 permeabilities and solubility coefficients measured at 6 bars and 20 °C and the associated calculated diffusion coefficients of planar and homeotropic aligned smectic C membranes.*

Morphology	P $\left[\frac{cm^3(STP)\cdot cm}{cm^2\cdot s\cdot cmHg}\right]\cdot 10^{-10}$	S $\left[\frac{cm^3(STP)}{cm^3\cdot cmHg}\right]\cdot 10^{-3}$	D $\left[\frac{cm^2}{s}\right]\cdot 10^{-9}$
Smectic C planar	0.37	12.0	3.05
Smectic C homeotropic	0.13	12.0	1.09

Sorption measurements (Table 2.3) show that the solubility coefficient of CO_2 is similar for both planar and homeotropic aligned smectic C membranes. This is expected because both orientations have the same chemistry and morphology but only differ in the direction in which the lamellar structures are aligned. Consequently, the decrease in permeability for homeotropic orientations can completely be attributed to a decrease in the diffusion coefficient. The 3-fold decrease of the diffusion coefficient of homeotropic aligned smectic C membranes compared to planar aligned smectic C membranes confirms that the lamellar structures perpendicular to the permeation direction result in increased resistance which decreases gas diffusion and permeation but favors the increase in selectivity for the smaller He gas.

2.4 Conclusions

The effect of molecular order and orientation in free-standing thermotropic liquid crystalline (LC) polymeric membranes on their gas separation performance for He, Ar, N_2 and CO_2 was studied. An LC mixture, consisting of a mono-methacrylate with a crown ether moiety and a smectic di-acrylate with a set chemical composition was aligned and polymerized, resulting in robust free-standing membranes with various, distinct morphologies that differ in type and degree of molecular order and orientation. A combination of POM, DSC and X-ray scattering measurements confirmed the isotropic, nematic cybotactic and smectic C morphologies of the LC membranes.

Gas sorption and single gas permeation of He, Ar, N_2 and CO_2 in membranes with isotropic, planar nematic cybotactic and planar smectic C morphologies demonstrated that the permeability of all gases decreases with increasing molecular order while the ideal gas selectivities towards He and CO_2 increased tremendously (36-fold for He/N_2 and 21-fold for CO_2/N_2) when going from randomly ordered to an ordered smectic C morphology. It was found that a decreasing diffusion coefficient with increasing molecular order is responsible for the decreasing permeability, showing that gas permeation through LC membranes mainly depends on diffusion rather than solubility. The effect of molecular orientation has been demonstrated by a 3-fold reduction of the diffusion coefficient of homeotropic aligned smectic C membranes due to hindered gas transport compared to planar aligned smectic C membranes. For homeotropic smectic C membranes yield that lamellar structures perpendicular to the permeation direction results in increased resistance which decreases gas diffusion and permeation. Contrary to the permeability, the ideal selectivities of homeotropic oriented membranes are higher compared to those of planar aligned membranes.

These results highlight the crucial role of molecular order and orientation in LC polymer membranes for gas separation. Further research towards LC chemistry for improved gas polymer matrix interactions and in-depth morphology performance experiments would be the next step to investigate the role of supramolecular organization on gas separation performance.

References

[1] A. Collins, A. Galli, T. Hipwood, A. Murthy, Environ. *Res. Lett.* **2020**, 15, 025008.

[2] S. Basu, A.L. Khan, A. Cano-Odena, C. Liu, I.F.J. Vankelecom, *Chem. Soc. Rev*. **2010**, 39, 750–768.

[3] P. Bernardo, E. Drioli, G. Golemme, *Ind. Eng. Chem. Res.* **2009**, 48, 4638–4663.

[4] D.F. Sanders, Z.P. Smith, R. Guo, L.M. Robeson, J.E. McGrath, D.R. Paul, B.D. Freeman, *Polymer (Guildf)*. **2013**, 54, 4729–4761.

[5] T.E. Rufford, S. Smart, G.C.Y. Watson, B.F. Graham, J. Boxall, J.C. Diniz da Costa, E.F. May, *J. Pet. Sci. Eng.* **2012**, 94–95, 123–154.

[6] C.A. Scholes, U.K. Ghosh, *Membranes (Basel)*. **2017**, 7, 1–13.

[7] A. Akbari, J. Karimi-Sabet, S.M. Ghoreishi, *Sep. Purif. Technol.* **2020**, 251, 117317.

[8] M.R.A. Hamid, H.K. Jeong, Korean *J. Chem. Eng.* **2018**, 35, 1577–1600.

[9] Y. Zhang, X. Feng, S. Yuan, J. Zhou, B. Wang, *Inorg. Chem. Front.* **2016**, 3, 896–909.

[10] J.E. Bara, A.K. Kaminski, R.D. Noble, D.L. Gin, *J. Membr. Sci.* **2007**, 288, 13–19.

[11] B.D. Freeman, *Macromolecules*. **1999**, 32, 375–380.

[12] R.L. Burns, K.M. Steel, S.D. Burns, W.J. Koros, *Ind. Eng. Chem. Res.* **2004**, 43, 5942–5949.

[13] L.M. Robeson, *J. Membr. Sci.* **2008**, 320, 390–400.

[14] M. Houben, Z. Borneman, K. Nijmeijer, *Sep. Purif. Technol.* **2021**, 255, 117307.

[15] Y. Xiao, B.T. Low, S.S. Hosseini, T.S. Chung, D.R. Paul, *Prog. Polym. Sci.* **2009**, 34, 561–580.

[16] S. Shahid, K. Nijmeijer, *J. Membr. Sci.* **2014**, 459, 33–44.

[17] M. Zhang, L. Deng, D. Xiang, B. Cao, S.S. Hosseini, P. Li, *Processes*. **2019**, 7, 51.

[18] M.G. Buonomenna, W. Yave, G. Golemme, *RSC Adv.* **2012**, 2, 10745–10773.

[19] T.P. Lodge, Macromol. *Chem. Phys*. **2003**, 204, 265–273.

[20] R.; Anne-Valerie, L. Ludwik, *Nat. Mater.* **2005**, 4, 19–31.

[21] S. Park, O. Yavuzcetin, B. Kim, M.T. Tuominen, T.P. Russell, *Small.* **2009**, 5, 1064–1069.

[22] S.B. Darling, *Prog. Polym. Sci.* **2007**, 32, 1152–1204.

[23] S.R. Reijerkerk, A. Arun, R.J. Gaymans, K. Nijmeijer, M. Wessling, *J. Membr. Sci.* **2010**, 359, 54–63.

[24] A. Car, C. Stropnik, W. Yave, K.V. Peinemann, *Sep. Purif. Technol.* **2008**, 62, 110–117.

[25] S.R. Reijerkerk, A.C. Ijzer, K. Nijmeijer, A. Arun, R.J. Gaymans, M. Wessling, *ACS Appl. Mater. Interfaces.* **2010**, 2, 551–560.

[26] A. Car, C. Stropnik, W. Yave, K.V. Peinemann, *Adv. Funct. Mater.* **2008**, 18, 2815–2823.

[27] M. Zhou, T.J. Kidd, R.D. Noble, D.L. Gin, *Adv. Mater.* **2005**, 17, 1850–1853.

[28] G.M. Bögels, J.A.M. Lugger, O.J.G.M. Goor, R.P. Sijbesma, *Adv. Funct. Mater.* **2016**, 26, 8023–8030.

[29] T. Liang, H.P.C. Van Kuringen, D.J. Mulder, S. Tan, Y. Wu, Z. Borneman, K. Nijmeijer, A.P.H.J. Schenning, *ACS Appl. Mater. Interfaces.* **2017**, 9, 35218–35225.

[30] M. Zhou, P.R. Nemade, X. Lu, X. Zeng, E.S. Hatakeyama, R.D. Noble, D.L. Gin, *J. Am. Chem. Soc.* **2007**, 129, 9574–9575.

[31] S.M. Dischinger, J. Rosenblum, R.D. Noble, D.L. Gin, K.G. Linden, *J. Membr. Sci.* **2017**, 543, 319–327.

[32] N. Marets, D. Kuo, J.R. Torrey, T. Sakamoto, M. Henmi, H. Katayama, T. Kato, *Adv. Healthc. Mater.* **2017**, 6, 1700252.

[33] M. Henmi, K. Nakatsuji, T. Ichikawa, H. Tomioka, T. Sakamoto, M. Yoshio, T. Kato, *Adv. Mater.* **2012**, 24, 2238–2241.

[34] K.D. Harris, R. Cuypers, P. Scheibe, G.N. Mol, J. Lub, C.W.M. Bastiaansen, D.J. Broer, *Smart Sensors, Actuators, MEMS II.* **2005**, 5836, 493–503.

[35] C.D. Braun, J. Lub, *Liq. Cryst.* **1999**, 26, 1501–1509.

[36] T. Sasaki, H. Hazato, A. Katsuragi, Y. Nakazawa, *Mol. Cryst. Liq. Cryst.* **2009**, 503, 81–98.

[37] C. Li, J. Cho, K. Yamada, D. Hashizume, F. Araoka, H. Takezoe, T. Aida, Y. Ishida*, Nat. Commun.* **2015**, 6, 6:8418.

[38] M. Gupta, Y. Suzuki, T. Sakamoto, M. Yoshio, S. Torii, H. Katayama, T. Kato, *ACS Macro Lett.* **2019**, 8, 1303–1308.

[39] T. Sakamoto, T. Ogawa, H. Nada, K. Nakatsuji, M. Mitani, B. Soberats, K. Kawata, M. Yoshio, H. Tomioka, T. Sasaki, M. Kimura, M. Henmi, T. Kato, *Adv. Sci.* **2018**, 5, 1700405.

[40] H.P.C. Van Kuringen, G.M. Eikelboom, I.K. Shishmanova, D.J. Broer, A.P.H.J. Schenning, *Adv. Funct. Mater*. **2014**, 24, 5045–5051.

[41] V. Percec, R. Rodenhouse, *Macromolecules.* **1989**, 22, 4408–4412.

[42] R.A.M. Hikmet, J. Lub, A.J.W. Tol, *Macromolecules.* **1995**, 28, 3313–3327.

[43] Figures and Tables of the characterizations of the synthesized compounds and fabricated polymer membranes are available in the supporting information of J. Kloos, N. Jansen, M. Houben, A. Casimiro, J. Lub, Z. Borneman, A.P.H.J. Schenning, K. Nijmeijer, *Chem. Mater.* **2021**, 33, 8323–8333.

[44] W.L. McMillan, *Phys. Rev. A.* **1972**, 6, 936–947.

[45] L. Nasrin, A.K. Nasir, A. Yoshizawa, S. Ghosh, M. Rahman, *Mater. Res. Express.* **2019**, 6, 115105.

[46] P. Rallapalli, K.P. Prasanth, D. Patil, R.S. Somani, R. V. Jasra, H.C. Bajaj, *J. Porous Mater.* **2011**, 18, 205–210.

[47] R.W. Wijmans, J.G.; Baker, *J. Membr. Sci.* **1995**, 1–21.

[48] S.C. George, S. Thomas, *Prog. Polym. Sci.* **2001**, 26, 985–1017.

[49] S. Wang, X. Li, H. Wu, Z. Tian, Q. Xin, G. He, D. Peng, S. Chen, Y. Yin, Z. Jiang, M.D. Guiver, *Energy Environ. Sci.* **2016**, 9, 1863–1890.

[50] C.C. Hu, C.S. Chang, R.C. Ruaan, J.Y. Lai, *J. Membr. Sci.* **2003**, 226, 51–61.

[51] K. Haraya, S.T. Hwang, *J. Membr. Sci*. **1992**, 71, 13–27.

[52] A.W. Thornton, K.M. Nairn, A.J. Hill, J.M. Hill, *J. Membr. Sci.* **2009**, 338, 29–37.

Chapter 3

Molecular order determines gas transport through smectic liquid crystalline polymer membranes with different chemical compositions

Abstract

In this work, the effect of chemical composition and temperature on gas permeability and solubility in well-ordered LC polymer membranes is investigated. Membranes with various compositions of a mono-methacrylate LC (M1) with a crown ether functionality to enhance CO_2 solubility and a smectic di-acrylate (M2) cross-linker were fabricated, while all having the same order (smectic C) and alignment (planar). Single gas sorption and permeation data show for the membranes with 30 wt% M1 a higher CO_2 solubility coefficient compared to membranes without M1, which results in a higher CO_2 permeability and selectivity. For membranes that contain more than 30 wt% M1 decreasing layer spacings leads to reduced gas solubilities that result in lower gas permeabilities without additional selectivity gain towards CO_2. The effect of temperature is demonstrated by comparing single gas sorption and permeation data below and above the T_g of the membranes. The diffusion coefficient increases above the T_g of the membranes with increasing M1 content leading to higher CO_2 permeabilities and selectivities.

This chapter has been published as:

J. Kloos, N. Jansen, M. Houben, K. Nijmeijer, A.P.H.J. Schenning, Zandrie Borneman, Molecular order determines gas transport through smectic liquid crystalline polymer membranes with different chemical composition, *ACS Appl. Polym. Mater.* **2022**, 4, 7426–7436.

3.1 Introduction

The tremendous increase of greenhouse gas emissions such as CO_2 and CH_4 from the incineration of fossil fuels for large-scale energy production and industrial activities results in great challenges for the sustainable development of our modern society [1]. Valuable gas sources such as natural gas and biogas, or waste streams like flue gases contain large amounts of greenhouse gases. Separations such as CO_2/CH_4 and CO_2/N_2 are therefore crucial to minimize or even prevent emissions into the atmosphere [2–5]. The most used methods to separate gases include cryogenic distillation, amine absorption, pressure swing adsorption and membrane separations [3,5,6]. Of these, polymeric membrane technology gained in the last decades a key role because of its low operating costs and high energy efficiency compared to the other separation technologies [1,6–8]. Despite that polymeric membranes are often used for gas separations, most of the used polymers are not highly ordered at a molecular level. This results in limitations such as poorly defined free volume and leads to a trade-off between gas permeability and selectivity, which limits the performance of current membranes for gas separation [3,8–13]. Controlling the membrane building blocks at a molecular level is a tool to improve membrane performance.

Self-assembly of liquid crystalline (LC) polymeric materials provides control over the supramolecular organization and alignment of the building blocks at the molecular level and can be used for membrane applications [9,14–16]. A variety of ordered nanostructures can be obtained, which, depending on the positional order of the LC monomers and the fabrication process, can differ in molecular order and orientation. Subsequent cross-linking of the LC monomers fixates the nanostructures and results in robust free-standing LC polymer membranes. Although LC polymer membranes have already been investigated for water separations [17–30], these materials are hardly investigated for gas separations. In chapter 2, we studied the role of supramolecular organization and orientation in free-standing thermotropic LC polymer membranes based on crown ether functionalized LCs for gas separation by using LC membranes with various distinct morphologies and alignment while using the same chemical composition (see Figure 3.1a for chemical structures) [2]. We found that control over the molecular order and orientation of the LC building blocks are important parameters that influence the gas separation performances to a great extent. Increasing the molecular order leads to lower gas permeabilities but higher gas selectivities. It was hypothesized that with increasing the molecular order in the membranes gas diffusion was reduced. The smaller free volume elements in the more ordered smectic C (lamellar structures) membranes hinder gases with larger kinetic

diameters (N_2) more than gases with smaller kinetic diameters (He and CO_2), resulting in lower gas permeabilities but higher selectivities. Furthermore, the orientation of the lamellar structures highly influences gas permeability and ideal gas selectivity. Membranes with the lamellar structures perpendicular to the permeation direction (homeotropic alignment) exhibit higher permeation resistances that result in reduced gas diffusion and lower gas permeabilities compared to membranes with the lamellar structures parallel to the permeation direction (planar alignment). Although the used LC polymers contained a crown ether functionality, the effect of the amount of this crown ether content on the gas separation performances was not studied, while it is known that polar ether segments have favorable interactions with CO_2 and can lead to enhanced CO_2 permeability and selectivity [31–35]. Moreover, the gas separation performances of polymeric membranes are greatly affected by temperature, especially when crossing the glass transition temperature (T_g) [6,36,37]. However, this effect was never investigated for LC-based polymer membranes.

Here we thus study the effect of chemical composition and temperature on gas permeability and solubility in free-standing thermotropic LC polymer membranes with planar aligned smectic morphologies for gas separations of He, CO_2, Ar and N_2 (Figure 3.1b). Well-aligned LC membranes with various compositions of a mono-methacrylate (M1) LC with a crown ether functionality and a smectic di-acrylate (M2) cross-linker are fabricated and characterized. The effect of chemical composition on the gas separation performances of LC membranes is investigated by measuring the single gas sorption and permeation of various gases. The effect of temperature on the membrane performance is shown by comparing single gas performances below and above the T_g of the membranes.

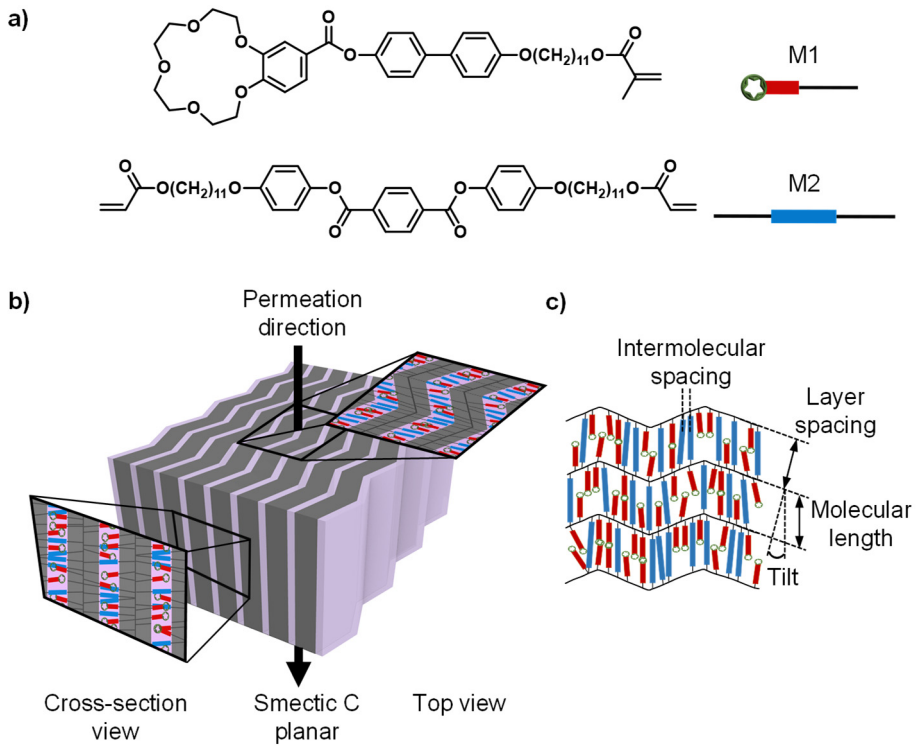

Figure 3.1: a) *Molecular structures of a mono-methacrylate LC with a crown ether functionality (M1, red rods) and a di-acrylate LC cross-linker (M2, blue rods).* ***b)*** *Artist impression of a top and cross-section view of a free-standing membrane with a planar aligned smectic C morphology.* ***c)*** *Artist impression of a top view of a planar aligned smectic C membrane which indicates the intermolecular spacing, layer spacing, molecular length and tilt angle of the smectic nanostructure.*

3.2 Background

3.2.1 Membrane gas separation

In gas separation non-porous (dense) membranes are predominantly used to separate different gases. Gas transport through dense membranes is best described by the solution-diffusion model, which states that gas transport occurs in three steps: (1) sorption of gases onto the membrane surface, (2) diffusion of the gases through the thickness of the membrane and lastly (3) desorption at the permeate side of the membrane [38,39]. The permeability (P_i), which is commonly used to express the membrane performance, is defined as the product of the diffusivity (D_i) and the solubility (S_i) of a certain gas species (Equation (3.1)).

$$P_i = \frac{J_i \cdot L}{P_{i,feed} - P_{i,permeate}} = D_i \cdot S_i \qquad (3.1)$$

In Equation (3.1) P_i is the permeability of gas species i (Barrer (10^{-10} $cm^3(STP)\cdot cm/(cm^2\cdot s\cdot cmHg)$)), J_i is the flux ($cm^3(STP)/cm^2\cdot s$), L is the thickness of the membrane (cm), $P_{i,\,feed}$ is the feed pressure (cmHg) and $P_{i,\,permeate}$ is the permeate pressure (cmHg). The ideal selectivity of gas species i with respect to gas species j, $\alpha_{i/j}$ (-), is calculated with the pure gas permeability of gas species i and j (Equation (3.2)).

$$\alpha_{i/j} = \frac{P_i}{P_j} \qquad (3.2)$$

It is important to note that gas permeability and selectivity under mixed-gas conditions can deviate significantly from the pure-gas values due to effects such as competitive sorption and plasticization [40–42]. According to the solution-diffusion model dense polymer membranes separate gases via their intrinsic differences in diffusivity and solubility. However, these parameters are bulk parameters and are affected by many variables. The diffusion coefficient mainly depends on the free volume in the polymers and the size of the gaseous penetrant, where high amounts of free volume and smaller gas molecules usually result in higher diffusion coefficients compared to low amounts of free volume and larger gases [43]. The solubility coefficient mainly depends on the condensability of the gas and the chemical affinity between the gas molecules and the membrane matrix. The condensability depends on the critical temperature of the gas and usually increases with increasing critical temperature [44]. Gas solubility can be enhanced when there is a chemical affinity between the penetrant and the polymer phase [6,36,37]. Gases such as CO_2, which has a quadrupole moment, have favorable interactions with polymers that contain polar functional groups leading to higher CO_2 solubility coefficients compared to solubility coefficients of inert gases [31–35].

Permeation is a thermally activated process and is therefore highly dependent on temperature. The temperature dependence of both gas diffusion and solubility follows an Arrhenius type of equation but the activation energy for these processes is affected differently [36,45]. Diffusion is generally a stronger function of temperature than solubility and diffusion typically increases considerably with increasing temperature, while solubility decreases with increasing temperature. As a result, gas permeability usually increases with temperature. Moreover, the diffusion coefficient is dependent on the free volume that is

available for diffusion, which greatly depends on temperature as well as the T_g of the polymer [37,44,46]. Above the T_g, where the polymer is in its rubbery state, the large-scale segmental motion of the polymer chains results in high amounts of free volume that lead to higher diffusion coefficients and gas permeabilities, but usually also in low selectivities. Below the T_g the polymer is in its glassy state and thermal motion of the polymer chains is restricted, which results in low diffusion coefficients and gas permeabilities but high selectivities. Therefore, the overall performance of a membrane can be tuned (i.e. the permeability) by changing the operating temperature to below or above the T_g of the polymer.

3.3. Materials and methods

3.3.1 Chemicals

The chemicals 11-bromoundecyl methacrylate [24] and 11-(4-hydroxyphenoxy)undecyl acrylate [25], were kindly provided by Philips Research. 4,4'-biphenol, sodium iodide, anhydrous chloroform, anhydrous N, N-dimethylformamide, t-butyl-hydroquinone, anhydrous tetrahydrofuran, thionyl chloride, 4-carboxybenzo-15-crown-5, magnesium sulfate, terephthaloyl chloride, hydrochloric acid (37%) and silica were obtained from Merck Life Science. Ethanol and potassium carbonate were purchased from VWR chemicals. Triethylamine and chloroform were purchased from Merck KGaA. Ethyl acetate and dichloromethane were purchased from Biosolve. Irgacure 819 was supplied by Ciba. For permeation and sorption measurements, the gases He (5.0 grade), CO_2 (4.5 grade), Ar (5.0 grade) and N_2 (5.0 grade) were obtained from Linde Gas (the Netherlands). All reagents were used as received without further purification.

3.3.2 Synthesis of M1 and M2

4-((11-methacryloylundecan-1-yl)oxy)-4'-(4'-carboxybenzo-15-crown-5)biphenyl (M1)

4-((11-methacryloylundecan-1-yl)oxy)-4'-(4'-carboxybenzo-15-crown-5)biphenyl (M1) was synthesized as described in Chapter 2. The characterization data are in accordance with Chapter 2 and other literature [47].

Bis(4-((11-(acryloyloxy)undecyl)oxy)phenyl) terephthalate (M2)

Bis(4-((11-(acryloyloxy)undecyl)oxy)phenyl) terephthalate (M2) was synthesized as described in Chapter 2. The characterization data are in accordance with Chapter 2.

3.3.3 Membrane preparation

LC mixtures consisting of various M1/M2 compositions (Figure 3.1a shows the chemical structures of M1 and M2, Table 1 presents the used ratios of M1 and M2), 0.5 wt % photoinitiator (Irgacure 819) and 0.1 wt % inhibitor (TBHQ) were prepared by dissolving the compounds in a minimum amount of chloroform and subsequently evaporating the solvent. Membranes with a thickness of 20 ± 0.4 µm were prepared by heating an LC mixture above its isotropic temperature (process temperature in Table 3.1) and using capillary suction between two glass plates with 20 µm spacers to fill the glass cells. To control the alignment of the samples and obtain planar alignment, the glass plates were functionalized with a rubbed polyimide layer (Optimer AL 1254; JSR Corporation, Toyo Japan). After the glass cells were filled, the samples were placed inside a temperature-controlled box with an N_2 flow at 140 °C for the 0/100 and 30/70 compositions and 130 °C for the 50/50, 60/40 and 70/30 compositions. The samples were left for 5 minutes at the above-mentioned temperature before they were cooled to the smectic phase using a cooling rate of 3 °C/min. Subsequently, the samples were photopolymerized by illuminating the samples for 10 min under an unfiltered spectrum of a collimated EXFO Omnicure S2000 UV lamp with a light intensity of 20 mW/cm^2 in the range of 320-390 nm. The samples were removed from the N_2 box and allowed to cool to room temperature. Free-standing membranes were obtained by immersing the samples for 10 minutes in water at 80 °C and subsequently opening the glass cells.

Table 3.1: *Fabrication conditions for LC membranes with various compositions of M1 and M2.*

M1/M2	Process temperature [°C]	Polymerization temperature [°C]	Cooling rate [°C/min]
0/100	140	122	3
30/70	140	115	3
50/50	130	104	3
60/40	130	99	3
70/30	130	96	3

3.3.4 Characterization

Attenuated total reflection fourier transform infrared spectroscopy (ATR FT-IR) spectra were recorded at room temperature on a Varian-Cary 3100 FT-IR spectrometer equipped with a golden gate attenuated total reflectance (ATR) sampling accessory. Scans were taken over a range of 4000−650 cm^{-1} with a spectral resolution of 4 cm^{-1} and 50 scans per spectrum.

Polarizing optical microscopy (POM) was performed using a Leica DM 2700M optical microscope equipped with two polarizers that were operated either crossed or parallel with the sample in between a Linkam hot-stage THMS600 with a Linkam TMS94 controller and a Leica DFC420 C camera.

Differential scanning calorimetry (DSC) measurements were recorded in hermetic T-zero aluminum sample pans using a TA Instruments Q2000 DSC equipped with a cooling accessory. The DSC measurements were performed with three cycles of heating and cooling at a rate of 3 °C/min with an isothermal equilibration of 3 minutes after each heating or cooling ramp. The transition temperatures were determined from the third heating and cooling cycle using TRIOS DSC software.

Medium- and wide-angle X-ray scattering (MAXS/WAXS) measurements were recorded on a GaneshaLab instrument equipped with a Genix-Cu ultralow divergence source producing X-ray photons of wavelength 1.54 Å and a flux of 108 photons per second. Diffraction patterns were collected on a Pilatus 300 K silicon pixel detector with 487 × 619 pixels of 172 μm^2.

3.3.5 Gas sorption

Gas sorption of CO_2 was measured with a Rubotherm series IsoSORP® sorption instrument to determine the solubility coefficient of all membranes. Before each measurement, the sample was degassed for 5 h by applying a vacuum to the measuring cell. Subsequently, a buoyancy measurement with helium was performed to determine the initial sample weight, volume and density of the sample. Here it was assumed that the solubility of helium is negligible. Gas sorption of CO_2 was measured at 6 bar and 20 °C, 40 °C and 70 °C respectively (equilibrium time of each measurement was 3 h). The equilibrium time was determined by monitoring the sorption over time. This showed that an equilibrium

time of 3 h for each measurement was sufficient for all membranes. The measured sorbed weight was corrected for the buoyancy effect according to Equation (3.3).

$$m_{corrected} = m_{measured} + \rho_{gas} \cdot V_{sample} \quad (3.3)$$

In Equation (3.3) $m_{corrected}$ is the corrected weight (g), $m_{measured}$ is the measured weight (g), ρ_{gas} is the density of the measuring gas (g/cm^3) and V_{sample} is the sample volume (cm^3). The concentration of CO_2 was calculated using Equation (3.4).

$$C_{CO_2} = \frac{m_{CO_2} \cdot \rho_s}{m_0 \cdot \rho_{CO_2}(STP)} \quad (3.4)$$

In Equation (3.4) C_{CO2} is the concentration of CO_2 in the membrane (cm^3 (STP)/cm^3 polymer), m_{CO2} is the buoyancy corrected mass of CO_2 in the polymer (g), ρ_s is the density of the membrane (g/cm^3), m_0 is the initial mass of the sample measured at vacuum (g) and ρ_{CO2} is the density of CO_2 gas at standard temperature and pressure (STP) (STP= 273.15 K and 1.013 bar) (g/cm^3). The solubility coefficient of CO_2 was calculated using Equation (3.5).

$$S_{CO_2} = \frac{C_{CO_2}}{P} \quad (3.5)$$

In Equation (3.5) S_{CO2} is the gas solubility of CO_2 (cm^3 STP/(cm^3·cmHg)), C_{CO2} is the concentration of CO_2 in the membrane (cm^3 (STP)/cm^3 polymer) and P is the pressure (cmHg).

3.6 Single gas membrane performances

Gas permeation experiments using He, CO_2, Ar or N_2 were performed in a stainless-steel cell with a permeation area of 2.1 cm^2. The flat sheet membranes were supported by a Whatman® filter paper (Grade 50 with a pore size of 2.7 µm) to prevent possible pressure-induced punctures. Single gas permeabilities were determined from the steady-state pressure increase in time in a calibrated volume at the permeate side of the membrane. The single gas permeabilities were determined using Equation (3.6) at 20 °C, 40 °C and 70 °C respectively in triplicate for two independently prepared membranes by measuring the permeate pressure increase over time in a calibrated volume with a feed pressure of 6 bar against a vacuum at the permeate side.

$$P_i = \frac{\Delta P_{permeate} \cdot V_c \cdot V_m \cdot L \cdot 10^{10}}{\Delta t \cdot R \cdot T \cdot A \cdot \Delta P} \quad (3.6)$$

In Equation (3.6) P_i is the permeability of gas species i (Barrer), $\Delta P_{permeate}$ is the increase in permeate pressure (Pa) per time interval Δt (s), V_c is the calibrated permeate volume (m^3), V_m is the molar volume at STP (cm^3/mol), L is the membrane thickness (cm), R is the gas constant (J/ K·mol), T is the permeate temperature (K), A is the membrane area (cm^2) and ΔP is the transmembrane pressure (cmHg). The membrane thickness in Equation (6) was determined by taking the average thickness of 7 spots that were measured over the entire membrane area with a micrometer. Before each permeation measurement, the membranes were conditioned overnight (12 h) at 6 bar with the gas to be measured. Subsequently, the permeation of each gas is measured in triplicate on the same membrane. The order of the measured gases was kept constant for all membranes (He, Ar, N_2 and CO_2) since CO_2 could induce swelling of the membrane. CO_2 diffusion coefficients of the membranes were calculated using Equation (3.1) in section 3.2. The ideal gas selectivities were calculated with Equation (3.2) in section 3.2.

3.4. Results and discussion

3.4.1 Preparation and characterization of liquid crystalline mixtures and membranes

A photopolymerizable nematic mono-methacrylate with a crown ether functionality (M1) and a smectic di-acrylate cross-linker (M2) were synthesized and characterized as described in Chapter 2 (Figure 3.1a). M1 was selected for its cyclic oligoethylene oxide segments, which are known for their favorable interactions with CO_2 leading to an enhanced CO_2 solubility [31-35], while M2 was selected for its stable smectic phase and to improve the mechanical strength of the fabricated membranes. The phase transitions of both M1 and M2 are in accordance with those from Chapter 2.

LC mixtures with various compositions of M1 and M2, a photoinitiator and an inhibitor were prepared and characterized with DSC and POM to determine the corresponding phase transitions [48]. Compositions containing more than 70 wt% M1 did not exhibit a stable smectic mesophase but only a broad nematic mesophase. Because Chapter 2 demonstrated that the gas separation performances of LC membranes are highly influenced by the membrane morphology, only mixtures that exhibit a smectic mesophase were used to prepare membranes to study the effect of chemical composition and temperature on the gas separation performances of LC membranes.

LC membranes were prepared by incorporating the LC mixtures in glass cells having an alignment layer to obtain planar alignment. The LC mixtures were polymerized in their smectic phase to fixate the lamellar morphology and, after opening of the cells, free-standing membranes were obtained (see Figure 3.1b,c for an artist's impression of the top and cross-section view of a free-standing membrane with a smectic C morphology). FTIR before and after polymerization confirmed the full conversion of the acrylate moieties [48].

The orientation (alignment) and organization (morphology) of the membranes were investigated with POM and XRD [48]. POM shows the planar alignment of the membranes with dark images under parallel conditions and bright images under 45° tilt, indicating that the membranes are well oriented. Wide-angle X-ray scattering (WAXS) and medium-angle X-ray scattering (MAXS) were measured to determine the morphology and alignment of the membranes at 20 °C and are shown in Figure 3.2.

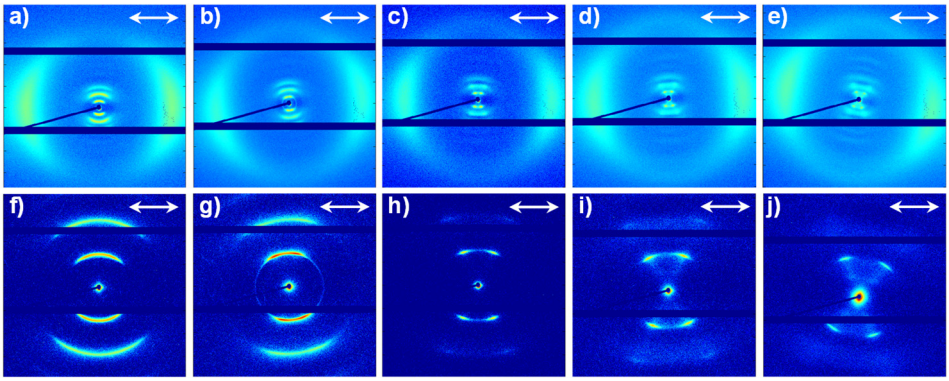

Figure 3.2: *WAXS (top row) and MAXS (bottom row) spectra of membranes consisting of an M1/M2 composition of respectively:* ***a, f)*** *0/100,* ***b, g)*** *30/70,* ***c, h)*** *50/50,* ***d, i)*** *60/40,* ***e, j)*** *70/30. The single arrow shows the alignment direction.*

The 2D WAXS and MAXS spectra of all membranes contain diffraction spots that indicate that all molecules are oriented in a common direction. All MAXS spectra show diffraction spots parallel to the alignment direction, which corresponds to an ordered smectic C morphology. The tilt angle of the tilted layered structures is found to be highly dependent on the chemical composition and varies between 18° for the membranes without M1 (0/100) and 32° for the membranes that contain 70 wt% M1 (70/30). Moreover, the layer spacing, which corresponds to the distance between two layers, was determined for all compositions and shown in Figure 3.3.

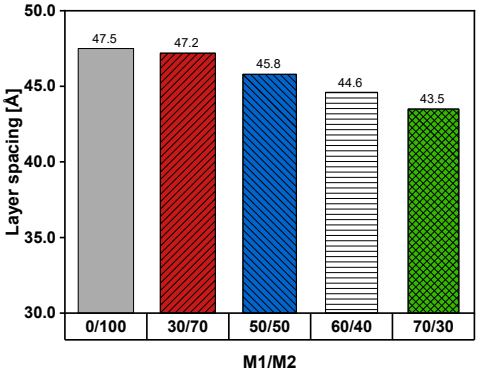

Figure 3.3: *The layer spacing of smectic C membranes with M1/M2 compositions of respectively 0/100, 30/70, 50/50, 60/40 and 70/30.*

Figure 3.3 shows that the layer spacings of membranes without M1 (0/100) and 30 wt% M1 (30/70) are in close agreement with the theoretical length of M2 (49.9 Å) that connects the lamellar structures and is therefore expected to mainly determine the layer spacing. However, for membranes that contain more than 30 wt% M1, the layer spacing starts to decrease. This can be explained because the length of M1 (theoretical length is 28.1 Å) is smaller than that of M2 making the layer spacings smaller with higher M1 contents. The intermolecular spacing that corresponds to the intermolecular stacking of the LC building blocks is not affected by the chemical composition and was similar for all compositions (varying between 4.5 – 4.8 Å). The above confirms the formation of a planar aligned smectic C morphology for all M1/M2 compositions at 20 °C.

To study the effect of temperature on membrane morphology, the thermal properties of the membranes with various M1/M2 compositions were measured with XRD and DSC. The membrane morphology was studied by measuring WAXS and MAXS spectra of membranes without M1 (0/100) and 70 wt% M1 (70/30) at 20 °C and 70 °C [48]. WAXS and MAXS spectra of membranes with both compositions (0/100 and 70/30) show similar morphologies, tilt angles, layer spacings and intermolecular spacing at 20 °C and 70 °C. This means that within this temperature range the membrane morphology is independent of temperature. Although membranes with 70 wt% M1 (70/30) are less cross-linked compared to membranes without M1 (0/100), these results show that 30 wt% cross-linker (M2) is sufficient to fixate the membrane morphology. DSC measurements show a weak signal between 46 °C and 55 °C that represents the glass transition temperature (T_g) of the membranes. The results are shown in Table 3.2.

Table 3.2: *Glass transition temperature of membranes with M1/M2 compositions of respectively 0/100, 30/70, 50/50, 60/40 and, 70/30.*

M1/M2	Glass transition temperature [°C]
0/100	55
30/70	47
50/50	46
60/40	46
70/30	46

Table 3.2 shows that the membranes without M1 (0/100) exhibit the highest T_g (55 °C) of all membranes. This is as expected because these membranes have the highest cross-link density of all membranes, which restricts the mobility of the polymer chains that leads to a higher T_g [49]. For the membranes with M1, the cross-link density decreases with increasing M1 content leading to higher polymer chain mobility and thereby lowering the T_g (46 °C for the membranes with 70 wt% M1). Remarkably, the T_g of the membranes with respectively 30 wt% (30/70) and 70 wt% M1 (70/30) only shows a difference of 1 °C, indicating that the cross-link density only has a slight effect on the T_g.

3.4.2 Effect of M1/M2 composition on single gas performances

The effect of the chemical composition on the gas permeation performances of the LC membranes was investigated by measuring single gas permeation of He, CO_2, Ar and N_2 at 20 °C for all membranes. To show the effect of M1 in more detail, the permeation data and ideal gas selectivities are normalized to the membranes without M1 (absolute permeability values of 0/100 are 1.21, 0.34, 0.05 and 0.02 Barrer for He, CO_2, Ar and N_2 respectively). The results are shown in Figure 3.4 (see reference [48] for all permeation and ideal selectivity values).

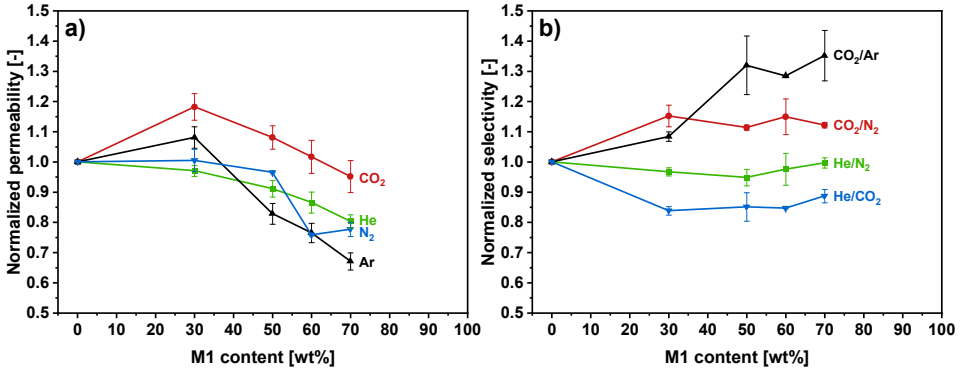

Figure 3.4: *Normalized gas permeation data and ideal gas selectivities of membranes with various M1/M2 compositions.* ***a)*** *Normalized single gas permeability (He, Ar, N_2 and CO_2) of membranes with M1/M2 compositions of respectively 0/100, 30/70, 50/50, 60/40 and 70/30 at 20 °C and 6 bar feed pressure.* ***b)*** *Normalized ideal gas selectivities (CO_2/Ar, CO_2/N_2, He/N_2, He/CO_2) of membranes with M1/M2 compositions of respectively 0/100, 30/70, 50/50, 60/40 and 70/30 at 20 °C.*

Figure 3.4a shows that the normalized permeability of CO_2 increases for membranes that contain 30 wt% M1. This increase in CO_2 permeability can be attributed to the favorable interactions of the quadrupole of CO_2 with the dipole moments of the crown ether moieties in M1 [1,31]. Surprisingly the normalized Ar permeability also slightly increases while it has no favorable interactions with the crown ether moieties. At higher M1 content, the CO_2 and Ar permeability decreases again. Similarly, the permeability of all other gases decreases over the full range. WAXS and MAXS measurements (section 3.4.1) show that the layer spacing for the membranes that contain 30 wt% M1 is equal to that of the membranes without M1 but starts to decrease with increasing M1 content. It is likely that a decreasing layer spacing also decreases the overall free volume within the membrane, which can affect solubility and therefore result in lower gas permeabilities [50]. The normalized ideal gas selectivities in Figure 3.4b show that the He/N_2 selectivity is independent of the composition, elucidating that the relative decrease in permeability is equal with increasing M1 content for He and N_2. However, the relative increase in CO_2 permeability with increasing M1 content results in enhanced CO_2/N_2 and CO_2/Ar selectivities for all membranes with increasing M1 content, while the corresponding He/CO_2 selectivity decreases for all membranes. Remarkably, all three selectivities (CO_2/N_2, CO_2/Ar and He/CO_2) show a nearly constant value after incorporating 30 wt% M1 (50 wt% M1 for CO_2/Ar), showing that incorporating more than 30 wt% M1 does not yield higher selectivities. Combining the permeation results with WAXS and MAXS measurements

shows that for the membranes with 30 wt% M1 both the CO_2 permeability and selectivity (CO_2/N_2 and CO_2/Ar) are enhanced, while a decreasing layer spacing for membranes that contain more than 30 wt% M1 results in lower gas permeabilities with no additional selectivity gain. Since dense membranes separate gases via their intrinsic differences in solubility and diffusivity, the mechanism of permeation and the effect of the layer spacing were studied by measuring gas sorption of CO_2 for all membranes. Subsequently, the diffusion coefficient of CO_2 was calculated using Equation (3.1). Unfortunately, N_2 and Ar sorption were too low to obtain accurate results. Therefore Table 3.3 only shows the permeabilities, solubility coefficients and diffusion coefficient of CO_2 in membranes with M1/M2 compositions of respectively 0/100, 30/70, 50/50, 60/40 and 70/30.

Table 3.3: *CO_2 permeabilities, solubility coefficients measured at 6 bar and 20 °C and the associated calculated diffusion coefficient of LC membranes with M1/M2 compositions of respectively 0/100, 30/70, 50/50, 60/40 and 70/30.*

M1/M2	P $\left[\frac{cm^3(STP)\cdot cm}{cm^2\cdot s\cdot cmHg}\right]\cdot 10^{-10}$	S $\left[\frac{cm^3(STP)}{cm^3\cdot cmHg}\right]\cdot 10^{-3}$	D $\left[\frac{cm^2}{s}\right]\cdot 10^{-9}$
0/100	0.34	10.6	3.22
30/70	0.41	13.1	3.09
50/50	0.37	12.0	3.05
60/40	0.35	11.7	2.99
70/30	0.33	10.6	3.07

Table 3 shows that the obtained diffusion coefficients are similar for all compositions, suggesting that the CO_2 permeability mainly depends on differences in solubility. Both CO_2 permeability and solubility increase by approximately 20% for membranes that contain 30 wt% M1 (3070) compared to membranes without M1 (0/100). This increase in CO_2 solubility most likely arises from the enhanced interaction between CO_2 and the LC-polymer matrix and shows the effect of the crown ether moieties in M1. However, the solubility decreases for the membranes that contain more than 30 wt% M1 and further decreases with increasing M1 content. Here, the decreasing layer spacing results in less overall free volume in the polymer matrix that lowers the gas solubility coefficients leading to reduced permeabilities for the membranes containing more than 30 wt% M1. These results show that incorporating crown ether functionalities in LC membranes influences

membrane performances by enhancing the chemical interactions between CO_2 and the polymer matrix affecting CO_2 solubility, while the layer spacing of the layered structures influences the membrane performance by affecting the overall free volume and thereby the gas solubility.

3.4.3 Effect of temperature on single gas performances

To study the effect of temperature on the single gas performances of LC membranes, He, CO_2, Ar and N_2 permeabilities at respectively 20 °C, 40 °C (below T_g) and 70 °C (above T_g) were measured for membranes with respectively M1/M2 compositions of 0/100, 30/70, 50/50 and 70/30. Due to the long measuring times, the membranes with a M1/M2 composition of 60/40 were not measured. The permeation data are shown in Figure 3.5.

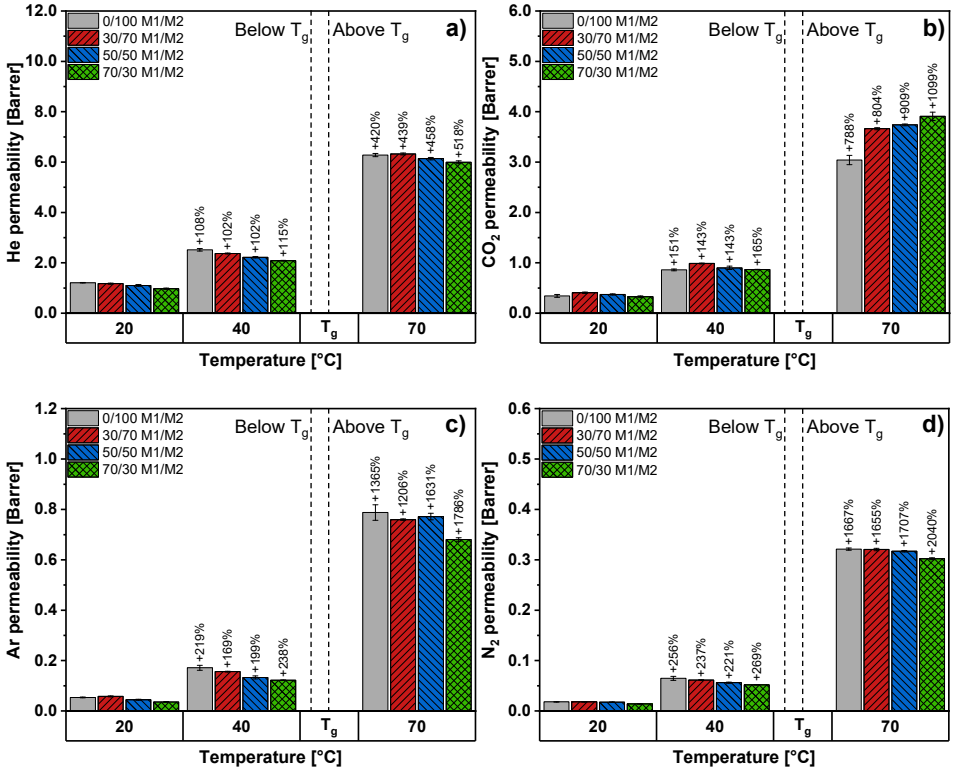

Figure 3.5: *The effect of temperature on the single gas permeability of:* ***a)*** *He,* ***b)*** *CO_2,* ***c)*** *Ar and* ***d)*** *N_2 of LC membranes with various M1/M2 compositions measured at respectively 20 °C, 40 °C, 70 °C and 6 bar feed pressure. The dotted lines between 40 °C and 70 °C represent the area where, depending on the M1/M2 composition, the glass transition temperature (T_g) of the membranes is located. The relative increase of permeability compared to the gas permeability at 20 °C is shown in*

percentage above the columns. The small error bars represent the spread of two independently prepared membranes, where each membrane is measured in triplicate.

Figure 3.5 shows that all gas permeabilities increase with increasing temperature. Especially above the T_g of the membranes (70 °C), the gas permeabilities show a large increase. Helium has the highest permeability at all temperatures, followed by CO_2, Ar and N_2. These results can be explained by the effect of a combination of parameters being kinetic diameter, critical temperature and molecular interactions via the quadrupole moments of the gases [51]. Helium has the smallest kinetic diameter of all measured gases, leading to a higher diffusion rate through the membranes and therefore the highest permeability of all gases. N_2 has the largest kinetic diameter of all measured gases resulting in a low diffusion rate through the membranes. Combined with a low critical temperature, which leads to low solubility in the polymer matrix, this results in the lowest permeability of all measured gases. CO_2 and Ar have similar kinetic diameters but have different critical temperatures resulting in a higher solubility and permeability for CO_2.

Contrary to the absolute increase of the permeabilities with increasing temperature, the relative increase of the permeabilities compared to the permeabilities at 20 °C (shown in percentages in Figure 3.5) shows the opposite behavior. Here, N_2 shows the largest permeability increase, followed by Ar, CO_2 and He. For dense membranes the gas permeability is the product of the solubility and the diffusivity of a certain gas species. Diffusion is generally a stronger function of temperature than the solubility coefficient and typically increases considerably with increasing temperature leading to higher permeabilities with increasing temperature. Less permeable gases, such as N_2, have higher diffusion activation energies than more permeable gases, such as He since the diffusion activation energy typically increases with increasing kinetic diameter [36]. Therefore, increasing the temperature can elevate the diffusion coefficient of the less permeable N_2 more than the diffusion coefficient of the more permeable He, leading to a relatively higher N_2 permeability increase compared to He. Moreover, the permeation data in Figure 3.5 show above the T_g of the membranes slight differences in gas permeability for the membranes with different M1/M2 compositions. The membranes that contain more M1 show for all gases a relatively higher increase in permeability. For He, Ar and N_2 this likely arises due to the lower cross-link density that decreases with increasing M1 content, resulting in more mobility for the polymer chains and thereby slightly higher permeabilities. However, for CO_2, increased chemical interactions with the crown ether functionalities above the T_g of the membranes can also play a role in the relatively higher increase in CO_2

permeability with increasing M1 content. This is because above the T_g of the membranes, the increased mobility of the crown ether moieties lead to improved interactions with CO_2, resulting in a larger increase in CO_2 permeability with increasing M1 content [52]. The gas separation performances at the different temperatures were further studied by determining the ideal gas selectivities from the permeation data. These are shown in Figure 3.6.

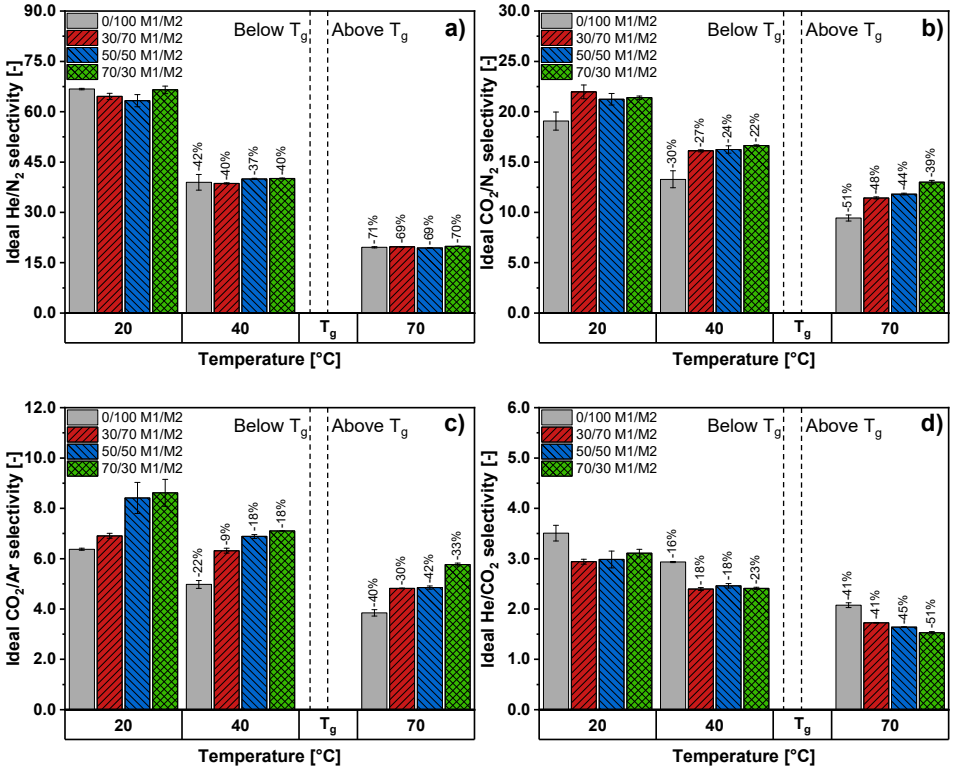

Figure 3.6: *The effect of temperature on the ideal gas selectivities of:* ***a)*** *He/N_2,* ***b)*** *CO_2/N_2,* ***c)*** *CO_2/Ar and* ***d)*** *He/CO_2 of LC membranes with various M1/M2 compositions measured at respectively 20 °C, 40 °C, 70 °C and 6 bar feed pressure. The dotted lines between 40 °C and 70 °C represent the area where, depending on the M1/M2 composition, the glass transition temperature (T_g) of the membranes is located. The relative increase of selectivity compared to the selectivity at 20 °C is shown in percentages above the columns. The small error bars represent the spread of two independently prepared membranes, where each membrane is measured in triplicate.*

Figure 3.6 shows that the selectivities towards He and CO_2 decrease with increasing temperature due to a relatively higher permeability increase of the lower permeable gases Ar and N_2 compared to the higher permeable gases He and CO_2. The He/N_2 selectivity

(Figure 3.6a) shows for all membranes a constant decrease with increasing temperature and is independent of the M1/M2 composition. This is as expected because the crown ether functionalities in M1 have no interactions with He and only slight interaction with the small quadrupole of N_2, resulting in similar He/N_2 selectivities for all compositions. The CO_2/Ar selectivity (Figure 3.6c) also decreases with increasing temperature. Although the M1/M2 composition of the membranes affects the CO_2/Ar selectivity at all temperatures, the relative decrease with increasing temperature is similar for all compositions. The He/CO_2 and CO_2/N_2 selectivities (Figure 3.6b,d) show rather different behavior. Above the T_g, the membranes with higher M1 contents have higher CO_2 permeabilities that result in lower He/CO_2 selectivities but higher CO_2/N_2 selectivities. To study the effect of temperature in more detail, CO_2 sorption was measured at 6 bar and 20 °C, 40 °C and 70 °C to determine the solubility and diffusion coefficients at these temperatures (Table 3.4).

Table 3.4: *CO_2 permeabilities, solubility coefficients measured at 6 bar and 20 °C, 40 °C and 70 °C and the associated calculated diffusion coefficient of LC membranes with various M1/M2 compositions.*

Temperature [°C]	M1/ M2	P $\left[\frac{cm^3(STP)\cdot cm}{cm^2\cdot s\cdot cmHg}\right]\cdot 10^{-10}$	S $\left[\frac{cm^3(STP)}{cm^3\cdot cmHg}\right]\cdot 10^{-3}$	D $\left[\frac{cm^2}{s}\right]\cdot 10^{-9}$
20	0/100	0.34	10.6	3.22
	30/70	0.41	13.1	3.09
	50/50	0.37	12.0	3.05
	70/30	0.33	10.6	3.07
40	0/100	0.86	6.89	12.5
	30/70	0.99	8.18	12.1
	50/50	0.90	7.55	11.9
	70/30	0.86	6.79	12.7
70	0/100	3.04	3.90	78.0
	30/70	3.66	5.55	66.0
	50/50	3.74	4.85	77.0
	70/30	3.91	3.98	98.3

Sorption measurements in Table 3.4 show that the solubility coefficient of CO_2 decreases with increasing temperature, confirming that the increase in CO_2 permeability with increasing temperature can be completely attributed to an increasing diffusion coefficient. Membranes that contain 30 wt% M1 (30/70) exhibit at all measured temperatures the highest solubility coefficients and membranes with more than 30 wt% M1 show a decreasing solubility coefficient with increasing M1 content. These results indicate that the decrease of the layer spacing with increasing M1 content leads to lower solubility coefficients at all measured temperatures. Below the T_g of the membranes (20 °C and 40 °C respectively), the diffusion coefficients are similar for all compositions, elucidating that for the different compositions the differences in CO_2 permeability mainly depend on the solubility coefficient at a specific temperature. However, above the T_g the difference in CO_2 permeability between the compositions is not only dependent on the solubility coefficient but also the diffusion coefficient. Upon the addition of M1, the diffusion coefficient decreases for the membranes with 30 wt% of M1 (30/70) compared to the membranes without M1 (0/100). Surprisingly, the diffusion coefficients of membranes that contain more than 30 wt% M1 increase with increasing M1 content, resulting in the highest diffusion coefficient for the membranes with 70 wt% M1 (70/30). This increase in the diffusion coefficient could be explained as follows. Above the T_g large-scale segmental motion in the polymer chains results in higher amounts of free volume leading to higher diffusion coefficients compared to below the T_g of the polymer. Increasing cross-link density usually results in decreased diffusion coefficients since cross-linking reduces the segmental motion in the polymer chains [36]. For the membranes with M1, the cross-link density decreases with increasing M1 content, leading to enhanced diffusion coefficients and thereby higher CO_2 permeabilities and selectivities for the membranes that contain more M1.

3.5. Conclusions

The effect of chemical composition and temperature on gas permeability and solubility in free-standing smectic liquid crystalline (LC) polymeric membranes for gas separations was studied. LC mixtures with various compositions of a mono-methacrylate with a crown ether functionality (M1) and a smectic di-acrylate (M2) cross-linker were aligned and polymerized, resulting in free-standing membranes with a smectic C morphology and planar alignment. The LC membranes were characterized with POM, DSC and X-ray scattering measurements that confirmed the smectic C morphology for all membranes with different M1/M2 compositions. The tilt angle and the layer spacing of the layered structures

are independent of temperature but are highly dependent on the chemical composition. By increasing the M1 content the tilt angle of the layered structures increases while the layer spacing decreases. Thermal characterization with DSC shows for all membranes a low heat capacity change for the glass transition temperature (T_g) that depending on the chemical composition varied between 46 °C and 55 °C.

Single gas sorption of CO_2 and permeation of He, CO_2, Ar and N_2 at 20 °C and 40 °C demonstrated that for all M1/M2 compositions the CO_2 permeability mainly depends on a difference in solubility. Both the CO_2 solubility and permeability increased for membranes that contain 30 wt% M1 compared to membranes without M1, leading to improved selectivities towards CO_2, demonstrating the favorable effect of the crown ether functionalities on the CO_2 gas separation performances. However, for membranes with more than 30 wt% M1, a decreasing layer spacing with increasing M1 content results in reduced gas solubilities that lead to lower gas permeabilities without additional selectivity gain towards CO_2. Single gas sorption and permeation data from 20 °C, 40 °C and 70 °C demonstrated that the permeability of all gases increases with increasing temperature, while ideal gas selectivities decrease. Above the T_g of the membranes, the CO_2 permeability and selectivity are not only dependent on the solubility coefficient but also on the diffusion coefficient resulting in higher CO_2 permeabilities and selectivities for the membranes with higher M1 contents. This suggests that above the T_g the differences in CO_2 permeability between the different M1/M2 compositions mainly depend on diffusivity rather than solubility. These results show that subtle order differences such as layer spacing in the layered structures also play a role in the gas separation performances of smectic LC polymer membranes.

References

[1] S. Wang, X. Li, H. Wu, Z. Tian, Q. Xin, G. He, D. Peng, S. Chen, Y. Yin, Z. Jiang, M.D. Guiver, *Energy Environ. Sci.* **2016**, 9, 1863–1890.

[2] S. Basu, A.L. Khan, A. Cano-Odena, C. Liu, I.F.J. Vankelecom, *Chem. Soc. Rev.* **2010**, 39, 750–768.

[3] P. Bernardo, E. Drioli, G. Golemme, *Ind. Eng. Chem. Res.* **2009**, 48, 4638–4663.

[4] D.F. Sanders, Z.P. Smith, R. Guo, L.M. Robeson, J.E. McGrath, D.R. Paul, B.D. Freeman, *Polymer (Guildf).* **2013**, 54, 4729–4761.

[5] T.E. Rufford, S. Smart, G.C.Y. Watson, B.F. Graham, J. Boxall, J.C. Diniz da Costa, E.F. May, *J. Pet. Sci. Eng.* **2012**, 94–95, 123–154.

[6] S. Sridhar, B. Smitha, T.M. Aminabhavi, *Sep. Purif. Rev.* **2007**, 36, 113–174.

[7] S. Kim, Y.M. Lee, Curr. Opin. *Chem. Eng.* **2013**, 2, 238–244.

[8] M.R.A. Hamid, H.K. Jeong, *Korean J. Chem. Eng.* **2018**, 35, 1577–1600.

[9] J.E. Bara, A.K. Kaminski, R.D. Noble, D.L. Gin, *J. Membr. Sci.* **2007**, 288, 13–19.

[10] B.D. Freeman, *Macromolecules.* **1999**, 32, 375–380.

[11] R.L. Burns, K.M. Steel, S.D. Burns, W.J. Koros, *Ind. Eng. Chem. Res.* **2004**, 43, 5942–5949.

[12] L.M. Robeson, *J. Membr. Sci.* **2008**, 320, 390–400.

[13] S. Shahid, K. Nijmeijer, *J. Membr. Sci.* **2014**, 459, 33–44.

[14] J. Kloos, N. Joosten, A. Schenning, K. Nijmeijer, *J. Membr. Sci.* **2021**, 620, 118849.

[15] J. Kloos, N. Jansen, M. Houben, A. Casimiro, J. Lub, Z. Borneman, A.P.H.J. Schenning, K. Nijmeijer, *Chem. Mater.* **2021**, 33, 8323–8333.

[16] D.L. Gin, J.E. Bara, R.D. Noble, B.J. Elliott, *Macromol. Rapid Commun.* **2008**, 29, 367–389.

[17] M. Zhou, T.J. Kidd, R.D. Noble, D.L. Gin, *Adv. Mater.* **2005**, 17, 1850–1853.

[18] G.M. Bögels, J.A.M. Lugger, O.J.G.M. Goor, R.P. Sijbesma, *Adv. Funct. Mater.* **2016**, 26, 8023–8030.

[19] M. Henmi, K. Nakatsuji, T. Ichikawa, H. Tomioka, T. Sakamoto, M. Yoshio, T. Kato, *Adv. Mater.* **2012**, 24, 2238–2241.

[20] K.D. Harris, R. Cuypers, P. Scheibe, G.N. Mol, J. Lub, C.W.M. Bastiaansen, D.J. Broer, *Smart Sensors, Actuators, MEMS II.* **2005**, 5836, 493–503.

[21] C.D. Braun, J. Lub, *Liq. Cryst.* **1999**, 26, 1501–1509.

[22] T. Sasaki, H. Hazato, A. Katsuragi, Y. Nakazawa, *Mol. Cryst. Liq. Cryst.* **2009**, 503, 81–98.

[23] C. Li, J. Cho, K. Yamada, D. Hashizume, F. Araoka, H. Takezoe, T. Aida, Y. Ishida, *Nat. Commun.* **2015**, 6, 6:8418.

[24] M. Gupta, Y. Suzuki, T. Sakamoto, M. Yoshio, S. Torii, H. Katayama, T. Kato, *ACS Macro Lett.* **2019**, 8, 1303–1308.

[25] T. Sakamoto, T. Ogawa, H. Nada, K. Nakatsuji, M. Mitani, B. Soberats, K. Kawata, M. Yoshio, H. Tomioka, T. Sasaki, M. Kimura, M. Henmi, T. Kato, *Adv. Sci.* **2018**, 5, 1700405.

[26] H.P.C. Van Kuringen, G.M. Eikelboom, I.K. Shishmanova, D.J. Broer, A.P.H.J. Schenning, *Adv. Funct. Mater.* **2014**, 24, 5045–5051.

[27] T. Liang, H.P.C. Van Kuringen, D.J. Mulder, S. Tan, Y. Wu, Z. Borneman, K. Nijmeijer, A.P.H.J. Schenning, *ACS Appl. Mater. Interfaces.* **2017**, 9, 35218–35225.

[28] M. Zhou, P.R. Nemade, X. Lu, X. Zeng, E.S. Hatakeyama, R.D. Noble, D.L. Gin, *J. Am. Chem. Soc.* **2007**, 129, 9574–9575.

[29] S.M. Dischinger, J. Rosenblum, R.D. Noble, D.L. Gin, K.G. Linden, *J. Membr. Sci.* **2017**, 543, 319–327.

[30] N. Marets, D. Kuo, J.R. Torrey, T. Sakamoto, M. Henmi, H. Katayama, T. Kato, *Adv. Healthc. Mater.* **2017**, 6, 1700252.

[31] M. Houben, Z. Borneman, K. Nijmeijer, *Sep. Purif. Technol.* **2021**, 255, 117307.
[32] S.R. Reijerkerk, A. Arun, R.J. Gaymans, K. Nijmeijer, M. Wessling, *J. Membr. Sci.* **2010**, 359, 54–63.
[33] A. Car, C. Stropnik, W. Yave, K.V. Peinemann, *Sep. Purif. Technol.* **2008**, 62, 110–117.
[34] S.R. Reijerkerk, A.C. Ijzer, K. Nijmeijer, A. Arun, R.J. Gaymans, M. Wessling, *ACS Appl. Mater. Interfaces.* **2010**, 2, 551–560.
[35] A. Car, C. Stropnik, W. Yave, K.V. Peinemann, *Adv. Funct. Mater.* **2008**, 18, 2815–2823.
[36] K. Ghosal, B.D. Freeman, Polym. *Adv. Technol.* **1994**, 5, 673–697.
[37] S.C. George, S. Thomas, *Prog. Polym. Sci.* **2001**, 26, 985–1017.
[38] W.J. Koros, G.K. Fleming, S.M. Jordan, T.H. Kim, H.H. Hoehn, *Prog. Polym. Sci.* **1988**, 13, 339–401.
[39] R.W. Wijmans, J.G.; Baker, *J. Membr. Sci.* **1995**, 1–21.
[40] G. Genduso, B.S. Ghanem, I. Pinnau, *Membranes (Basel).* **2019**, 9, 10.
[41] C.A. Scholes, J. Jin, G.W. Stevens, S.E. Kentish, *J. Polym. Sci. Part B Polym. Phys.* **2015**, 53, 719–728.
[42] R.W. Baker, *Ind. Eng. Chem. Res.* **2002**, 41, 1393–1411.
[43] R.W. Baker, *Membrane technologies and applications*, third ed., John Wiley & Sons, **2012**.
[44] W.J. Koros, G.K. Fleming, *J. Membr. Sci.* **1993**, 83, 1–80.
[45] V. Kulshrestha, K. Awasthi, N.K. Acharya, M. Singh, Y.K. Vijay, *Bull. Mater. Sci.* **2005**, 28, 643–646.
[46] L.M. Robeson, Q. Liu, B.D. Freeman, D.R. Paul, *J. Membr. Sci.* **2015**, 476, 421–431.
[47] V. Percec, R. Rodenhouse, *Macromolecules.* **1989**, 22, 4408–4412.
[48] Figures and Tables of the characterizations of the fabricated polymer membranes are available in the supporting information of J. Kloos, N. Jansen, M. Houben, K. Nijmeijer, A.P.H.J. Schenning, Zandrie Borneman, Molecular order determines gas transport through smectic liquid crystalline polymer membranes with different chemical composition, *ACS Appl. Polym. Mater.* (**2022**), 4, 7426–7436.
[49] S. Montserrat, *Polymer (Guildf).* **1995**, 36, 435–436.
[50] M.W. Hellums, W.J. Koros, G.R. Husk, D.R. Paul, *J. Membr. Sci.* **1989**, 46, 93–112.
[51] P. Rallapalli, K.P. Prasanth, D. Patil, R.S. Somani, R. V. Jasra, H.C. Bajaj, *J. Porous Mater.* **2011**, 18, 205–210.
[52] S.H. Jamali, M. Ramdin, T.M. Becker, S.K. Rinwa, W. Buijs, T.J.H. Vlugt, *J. Phys. Chem. B.* **2017**, 121, 8367–8376.

Chapter 4

Tuning the gas separation performances of smectic liquid crystalline polymer membranes by molecular engineering

Abstract

The effect of layer spacing and halogenation on the gas separation performances of free-standing smectic LC polymer membranes is investigated by molecular engineering. LC membranes with various layer spacings and halogenated LCs were fabricated while having a planar aligned smectic morphology. Single permeation and sorption data show a correlation between gas diffusion and layer spacing, which results in increasing gas permeabilities with increasing layer spacing while the ideal gas selectivity of He over CO_2 and He over N_2 decreases. The calculated diffusion coefficients show a 6-fold increase when going from membranes with a layer spacing of 31.9 Å to membranes with a layer spacing of 45.2 Å, demonstrating that the layer spacing in smectic LC membranes mainly affects the diffusion of gases rather than their solubility. A comparison of gas sorption and permeation performances of smectic LC membranes with and without halogenated LCs shows only a limited effect of LC halogenation by a slight increase in both solubility and diffusion coefficients for the membranes with halogenated LCs, resulting in a slightly higher gas permeation and increased ideal gas selectivities towards CO_2.

This chapter has been published as:

J. Kloos, M. Houben, J. Lub, Z. Borneman, K. Nijmeijer, A.P.H.J. Schenning, Tuning the gas separation performances of smectic liquid crystalline polymer membranes by molecular engineering, *Membranes (Basel)*. **2022**, 12, 805.

4.1 Introduction

The vast majority of our energy production is generated by the combustion of fossil fuels (e.g. coal and natural gas), which results in enormous amounts of greenhouse gases such as CO_2 and CH_4 being released into the atmosphere, leading to a rise in the average temperature of the Earth's atmosphere [1,2]. For a sustainable future, greenhouse gas emissions must be reduced, which makes separations such as CO_2/CH_4 and CO_2/N_2 crucial and relevant [3–6]. Polymeric membrane processes are, among other technologies, used for gas separation processes because of their low operating costs, high energy efficiency and easy scalability compared to other separation technologies [2,7–9]. However, most polymeric membranes used for gas separation are not ordered and aligned at the mesoscopic level, which affects the gas permeability and selectivity [4,8,10–12]. Using materials with self-assembly properties to obtain nanostructured polymer membranes provides additional parameters, such as control over the molecular order and alignment of the membrane building blocks, to tailor the gas separation properties. However, the effect of molecular order on the gas separation performance of such nanostructured materials has been rarely reported.

Liquid crystal (LC) molecules can self-assemble into various nanometer structures, which depending on the positional order of the LC monomers and the fabrication process can differ in molecular order and orientation. A frequently used fabrication method is to induce the self-assembly of reactive LC monomers inside a cell with spacer beads to tune the membrane thickness and alignment layers to control the molecular orientation. Subsequent cross-linking of the LC monomers to fixate the nanostructures is necessary to provide sufficient mechanical strength to obtain robust free-standing LC polymer membranes. So far LC polymer membranes have mainly been investigated for water separations [13-24], but hardly for gas separations [25-27]. Studies show the importance of molecular order and orientation in LC polymer membranes, see for example, Chapter 2. Here, highly ordered smectic C (lamellar nanostructured) membranes have lower gas permeabilities but selectivity towards He and CO_2 over N_2 increases tremendously compared to the membranes without molecular order (see Figure 4.1b for an artist's impression of a top view of an LC membrane with a smectic C morphology) [26]. Moreover, the highly ordered smectic C membranes with lamellar structures parallel to the permeation direction (planar alignment) exhibit higher gas permeations but lower selectivities compared to membranes with lamellar structures perpendicular to the permeation direction (homeotropic alignment). However, so far, the role of the dimensions of the nanostructures in the membranes on the

gas separation properties has hardly been reported [28]. Chapter 3 suggests that the layer spacing in smectic LC membranes plays an role on their gas separation performances. In this chapter, we change the layer spacing of smectic LC membranes by varying the length of the LC monomers. Moreover, incorporating halogen atoms such as chlorine or fluorine is known to enhance CO_2 permeability and selectivity by affecting both gas solubility and diffusion [29–32] and in addition, it also provides a more detailed insight into the gas transport in smectic LC polymer membranes.

Here, we investigate the effect of the layer spacing and halogenation on the gas separation performance of free-standing planar aligned smectic LC polymer membranes for gas separations of He, CO_2 and N_2. Various smectic LC membranes are fabricated and characterized consisting of either LCs with the same functional group but different alkyl spacer length or mixtures of two LCs with the same molecular length but containing different halogenated LCs (see Figure 4.1a for the LCs used in this research). The effect of layer spacing on the gas separation performances of smectic LC membranes is shown by measuring single gas sorption and permeation of various gases through membranes with various layer spacings. The effect of halogenation on the gas separation properties of smectic LC membranes is investigated by measuring the single gas sorption and permeation performances of membranes that contain different halogenated LCs.

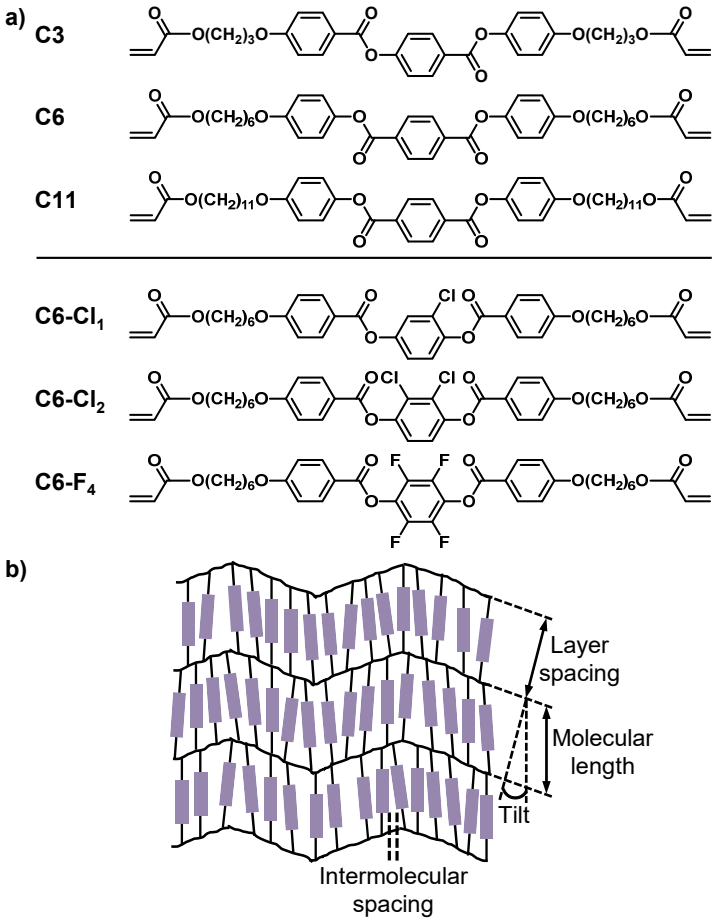

Figure 4.1: a) *Chemical structures of the LCs used in this research.* ***b)*** *Artist's impression of a top view of the planar aligned smectic C membranes which shows the layer spacing, molecular length, intermolecular spacing and tilt angle of the LC molecules. The purple rods represent the aromatic cores of the LCs.*

4.2 Materials and methods

4.2.1 Chemicals

The LC di-acrylate di-4-(11-acryloyloxyundecyloxy)phenyl terephthalate (C11) was prepared as described in Chapter 2 [26]. The 1,4-di-(4-(6-acryloyloxyhexyloxy)phenyl)terephthalate (C6) [33] and 2,3,5,6-tetrafluoro-4-(4-(6-acryloyloxyhexyloxy)benzoyloxy)phenyl 4-(6-acryloyloxyhexyloxy)benzoate (C6-F_4) [34] was prepared as described in the literature. The synthesis of 4-(3-

acryloyloxypropyloxy)phenyl 4-(4-(3- acryloyloxypropyloxy)benzoyloxy)benzoate (C3) is outlined in Scheme 4.1. (3-(acryloyloxy)propoxy)benzoic acid (9) was obtained from Synthon. The 4-((tetrahydro-2H-pyran-2-yl)oxy)phenol (1) and 4-((tetrahydro-2H-pyran-2-yl)oxy)benzoic acid (6) were both made according to a literature procedure [33]. The syntheses of 2,3-dichloro-1,4-phenylene bis(4-((6-(acryloyloxy)hexyl)oxy)benzoate) (C6-Cl_2) and 2-chloro-1,4-phenylene bis(4-((6-(acryloyloxy)hexyl)oxy)benzoate) (C6-Cl_1) are outlined in Scheme 4.2. The 4-(6-acryloyloxyhexyloxy)benzoic acid (10) was obtained from synthon and 2,3-dichlorohydroquinone (12a) was made according to the literature [35].

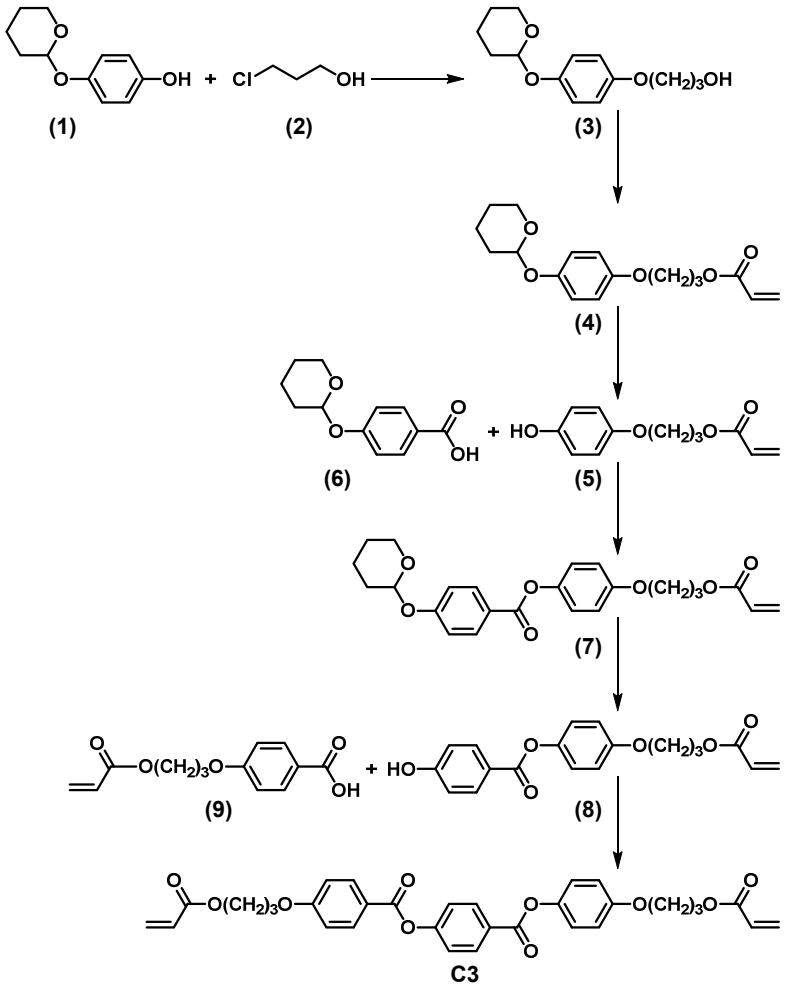

Scheme 4.1: *Synthetic route to 4-(3-acryloyloxypropyloxy)phenyl 4-(4-(3-acryloyloxypropyloxy)benzoyloxy) benzoate (C3).*

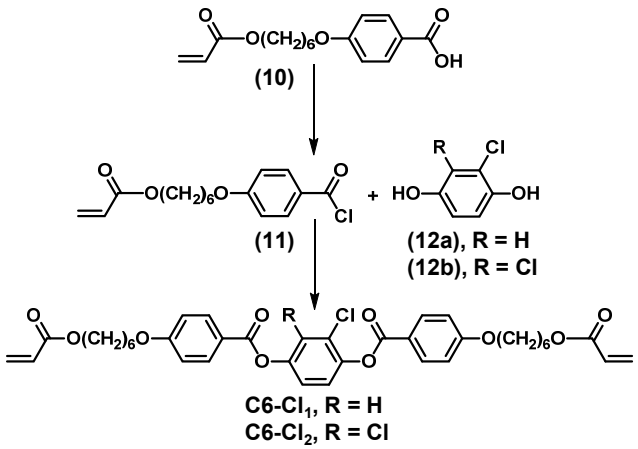

Scheme 4.2: *Synthetic routes to 2-chloro-1,4-phenylene bis(4-((6-(acryloyloxy)hexyl)oxy)benzoate) (C6-Cl$_1$) and 2,3-dichloro-1,4-phenylene bis(4-((6-(acryloyloxy)hexyl)oxy)benzoate) (C6-Cl$_2$).*

All other chemicals used for the synthesis of the LC monomers were obtained from Sigma-Aldrich. The synthetic preparations of the molecules in Schemes 4.1 and 4.2 are described in reference [36]. Irgacure 819 was supplied by Ciba. t-Butyl-hydroquinone was purchased from Merck Life Science. For permeation and sorption measurements, the gases He (5.0 grade), CO_2 (4.5 grade) and N_2 (5.0 grade) were obtained from Linde Gas (the Netherlands). All reagents were used as received without further purification.

4.2.2 Membrane preparation

LC mixtures with 0.5 wt% Irgacure 819 (photoinitiator) and 0.1 wt% t-butyl-hydroquinone (inhibitor) were prepared by dissolving the compounds in a minimum amount of chloroform and subsequently evaporating the solvent (LCs and fabrication conditions are displayed in Table 4.1, see Figure 4.1a for chemical structures). Planar aligned smectic C membranes were fabricated by processing the LC mixtures in the isotopic phase by capillary suction between two accurately 20 µm spaced glass plates. The glass plates were cleaned before use with isopropanol in an ultrasonic bath for 30 minutes, dried with N_2 and treated with UV ozone for 30 minutes. To obtain planar alignment, the glass plates were functionalized with a rubbed polyimide layer (Optimer AL 1254; JSR Corporation, Toyo Japan). Glass cells were prepared by gluing two functionalized glass plates together with glue that contained 20 µm glass spacer beads. The filled LC cells were placed inside a temperature-controlled N_2 box, in which the cells were cooled from the isotropic phase to the smectic phase using a cooling rate of 3 °C/min and subsequently polymerized by exposing the

samples for 10 min to an unfiltered spectrum of a collimated EXFO Omnicure S2000 UV lamp with a light intensity of 20 mW/cm^2 in the range of 320-390 nm. Free-standing membranes were obtained by opening the glass cells in hot water (80 °C).

Table 4.1: *Fabrication conditions for LC membranes with various layer spacings and LC membranes with various halogenated LCs.*

Compound/ Mixtures	Processing temperature [°C]	Polymerization temperature [°C]	Cooling rate [°C/min]
C3	180	100	3
C6	155	130	3
C11	140	122	3
C6 with 30 wt% C6-Cl$_1$	140	110	3
C6 with 30 wt% C6-Cl$_2$	145	115	3
C6 with 25 wt% C6-F$_4$	140	108	3

4.2.3 Characterization

Nuclear magnetic resonance (NMR) spectra were recorded on a 400 MHz Bruker Avance III HD spectrometer in deuterated chloroform with tetramethyl silane (TMS) as the internal standard.

Matrix-assisted laser desorption/ionization time-of-flight mass spectrometry (MALDI-TOF MS) was performed on a Bruker Autoflex Speed MALDI-MS instrument using DCTB (2-[(2E)-3-(4-tert-butylphenyl)-2-methylprop-2-enylidene] malononitril) as matrix.

Attenuated total reflection Fourier transform infrared spectroscopy (ATR FT-IR) spectra were recorded at room temperature on a Varian-Cary 3100 FT-IR spectrometer equipped with a golden gate attenuated total reflectance (ATR) sampling accessory. Scans were taken over a range of 4000−650 cm^{-1} with a spectral resolution of 4 cm^{-1} and 50 scans per spectrum.

Polarizing optical microscopy (POM) was performed using a Leica DM 2700M optical microscope equipped with two polarizers that were operated either crossed or parallel with

the sample in between a Linkam hot-stage THMS600 with a Linkam TMS94 controller and a Leica DFC420 C camera.

Differential scanning calorimetry (DSC) measurements were recorded in hermetic T-zero aluminum sample pans using a TA Instruments Q2000 DSC equipped with a cooling accessory. The DSC measurements were performed with three cycles of heating and cooling at a rate of 3 °C/min with an isothermal equilibration of 3 minutes after each heating or cooling ramp.

Medium- and wide-angle X-ray scattering (MAXS/WAXS) measurements were recorded on a GaneshaLab instrument equipped with a Genix-Cu ultralow divergence source producing X-ray photons of wavelength 1.54 Å and a flux of 108 photons per second. Diffraction patterns were collected on a Pilatus 300 K silicon pixel detector with 487 × 619 pixels of 172 μm^2.

4.2.4 Gas sorption

Gas sorption was measured with a Rubotherm series IsoSORP® sorption instrument to determine the CO_2 solubility coefficient of all membranes. Before each measurement, the sample was degassed for 5 h by applying a vacuum to the measuring cell followed by a buoyancy measurement with helium to determine the initial sample weight and volume of the sample. Here it was assumed that the solubility of helium is negligible. Gas sorption of CO_2 was measured at 6 bar and 40 °C (with an equilibrium time of 3 h). The measured sorbed weight was corrected for the buoyancy effect according to Equation (4.1).

$$m_{corrected} = m_{measured} + \rho_{gas} \cdot V_{sample} \qquad (4.1)$$

In Equation (4.1) $m_{corrected}$ is the corrected weight (g), $m_{measured}$ is the measured weight (g), ρ_{gas} is the density of the measuring gas (g/cm^3) and V_{sample} is the sample volume (cm^3). The concentration of CO_2 was calculated using Equation (4.2).

$$C_{CO_2} = \frac{m_{CO_2} \cdot \rho_s}{m_0 \cdot \rho_{CO_2\,(STP)}} \qquad (4.2)$$

In Equation (4.2) C_{CO2} is the concentration of CO_2 in the membrane (cm^3 (STP)/cm^3 polymer), m_{CO2} is the buoyancy corrected mass of CO_2 in the polymer (g), ρ_s is the density of the membrane (g/cm^3), m_0 is the initial mass of the sample measured

at vacuum (g) and ρ_{CO2} is the density of CO_2 gas at standard temperature and pressure (STP) (STP= 273.15 K and 1.013 bar) (g/cm^3). The CO_2 solubility coefficient was calculated using Equation (4.3).

$$S_{CO_2} = \frac{C_{CO_2}}{P} \qquad (4.3)$$

In Equation (4.3) S_{CO2} is the gas solubility of CO_2 (cm^3 STP/(cm^3·cmHg)), C_{CO2} is the concentration of CO_2 in the membrane (cm^3 (STP)/cm^3 polymer) and P is the pressure (cmHg).

4.2.5 Single gas membrane performances

Single gas permeation measurements of He, CO_2 and N_2 were performed in a custom-built permeation setup. The flat sheet membranes supported by a Whatman® filter paper (Grade 50 with a pore size of 2.7 µm), to prevent possible pressure-induced punctures, were placed in a stainless-steel cell with a permeation area of 2.1 cm^2 and the membrane cell was subsequently put in an oven (Convergence Inspector Hephaistos) to control the temperature. Single gas permeabilities were determined from the steady-state pressure increase in time in a calibrated volume at the permeate side of the membrane. The single gas permeabilities were calculated using Equation (4.4) at 40 °C for two different samples by measuring the permeate pressure increase over time in a calibrated volume with a feed pressure of 6 bar against a vacuum at the permeate side.

$$P_i = \frac{\Delta P_{permeate} \cdot V_c \cdot V_m \cdot L \cdot 10^{10}}{\Delta t \cdot R \cdot T \cdot A \cdot \Delta P} \qquad (4.4)$$

In Equation (4.4) P_i is the permeability of gas species i (Barrer), $\Delta P_{permeate}$ is the increase in permeate pressure (Pa) per time interval Δt (s), V_c is the calibrated permeate volume (m^3), V_m is the molar volume at STP (cm^3/mol), L is the membrane thickness (cm), R is the gas constant (J/ K·mol), T is the permeate temperature (K), A is the membrane area (cm^2) and ΔP is the transmembrane pressure (cmHg). The membrane thickness in Equation (4.4) was determined by taking the average thickness of 7 spots that were measured over the entire membrane area with a micrometer. Before the permeation measurements, the membranes were conditioned overnight (for 12 h) at 6 bar at the feed side with the gas to be measured and vacuum at the permeation side. Subsequently, the permeation of each gas was measured in triplicate on the same membrane. The order of the measured gases was kept constant for all membranes (He, N_2 and CO_2) since CO_2 could induce swelling of

the membrane. The ideal selectivity ($\alpha_{i/j}$) was calculated using the single gas permeabilities as shown in Equation (4.5), where P_i is the permeability of gas species i (Barrer) and P_j is the permeability of gas species j (Barrer).

$$\alpha_{i/j} = \frac{P_i}{P_j} \qquad (4.5)$$

The CO_2 diffusion coefficients of all membranes were calculated by using Equation (4.6).

$$D = \frac{P}{S} \qquad (4.6)$$

In Equation (4.6), D is the diffusion coefficient (cm^2/s), P the permeability (Barrer) and S the solubility coefficient (cm^3 STP/(cm^3·cmHg)).

4.3. Results and discussion

4.3.1 Preparation and characterization of the liquid crystalline molecules and mixtures

The effect of layer spacing on the gas separation performance of planar aligned smectic LC polymer membranes was studied by varying the length of the alkyl spacers in the LC monomers (C3, C6 and C11 in Figure 4.1a). The role of the chemical composition was investigated by incorporating bulky halogen groups such as chlorine or fluorine on the rigid LC core, which are known to enhance CO_2 permeability and selectivity (C6-Cl_1, C6-Cl_2 and C6-F_4 in Figure 4.1a) [29–32]. The LC monomers C6, C11 and C6-F_4 were synthesized and characterized as described in the literature [26,33,34], while C3, C6-Cl_1 and C6-Cl_2 were synthesized for the first time (see Scheme 4.1 and 4.2 for synthesis schemes). Characterization by ^1H and ^{13}C nuclear magnetic resonance (NMR) and mass spectroscopy (MALDI-TOF MS) confirmed the successful synthesis of all molecules. The phase transitions of all molecules were determined with differential scanning calorimetry (DSC) and polarizing optical microscopy (POM). These results are shown in Table 4.2 (see reference [36] for DSC and POM).

Table 4.2: *Phase transitions of the synthesized LCs.*

Compound	Isotropic [°C]	Nematic [°C]	Smectic [°C]
C3	>174	174-113	113-48
C6	>146	146-142	142-113
C11	>132	132-131	131-116
C6-Cl_1	>110	110-99	-
C6-Cl_2	>139	139-104	-
C6-F_4	>109	109-104	-

Table 4.2 shows that the C3, C6 and C11 monomers exhibit nematic and smectic mesophases but at different temperatures. C11 has the longest flexible alkyl spacer of all synthesized LCs, resulting in the lowest phase transitions. Contrary, C3 has the shortest alkyl spacer with less flexibility, which leads to the highest phase transitions of all LCs [37]. Only LC mixtures that exhibit a smectic mesophase were used to prepare membranes. Because the pure C6-Cl_1, C6-Cl_2 and C6-F_4 monomers only exhibit a nematic mesophase, LC mixtures consisting of C6 with C6-Cl_1, C6-Cl_2 and C6-F_4 were prepared and characterized with DSC and POM (see reference [36] for phase transition values). Compositions containing more than 30 wt% C6-Cl_1 or C6-Cl_2 and 25 wt% C6-F_4 did not exhibit a smectic mesophase and were therefore not used in this study. Hence, LC mixtures consisting of C6 with respectively 30 wt% C6-Cl_1 or C6-Cl_2 and 25 wt% C6-F_4 were used to prepare membranes to study the effect of halogenation on the gas separation performances of smectic LC membranes.

4.3.2 Preparation and characterization of liquid crystalline membranes

The LCs were mixed with a photoinitiator to fabricate LC membranes by photopolymerization. Planar aligned smectic LC membranes were prepared by incorporating the LC mixtures in glass cells with alignment layers to control the orientation of the LCs. After heat treatment, the LC mixtures were photopolymerized in the smectic mesophase to fixate the lamellar morphology. Free-standing LC membranes were obtained by opening the glass cells (see Figure 4.1b for an artist's impression of a top view

of a planar aligned smectic C membrane). FT-IR spectra before and after polymerization showed full conversion of the acrylate moieties [36].

The alignment and morphology of the membranes were investigated with POM [36] and showed the planar alignment of all membranes with dark images under parallel conditions and bright images under 45° tilt. Wide-angle X-ray scattering (WAXS) and medium-angle X-ray scattering (MAXS) were measured to further study the morphology and alignment of the membranes (Figure 4.2).

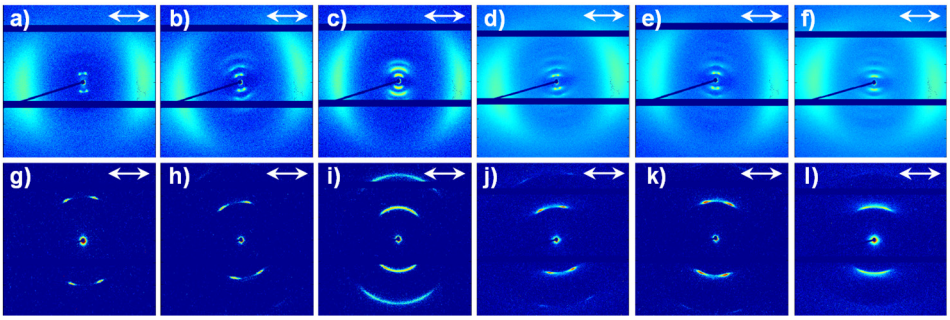

Figure 4.2: *WAXS (top row) and MAXS (bottom row) spectra of LC membranes consisting of LCs with various alkyl spacer lengths and various halogenated LCs.* ***a, g)*** *C3,* ***b, h)*** *C6,* ***c, i)*** *C11,* ***d, j)*** *C6 with 30 wt% C6-Cl*$_1$*,* ***e, k)*** *C6 with 30 wt% C6-Cl*$_2$*,* ***f, l)*** *C6 with 25 wt% C6-F*$_4$*. The single arrow shows the alignment direction.*

The 2D WAXS and MAXS spectra in Figure 4.2 show for all membranes diffraction lobes/spots, indicating that all molecules are aligned. The MAXS spectra of the C3 (Figure 4.2g), C6 (Figure 4.2h), C6 with 30 wt% C6-Cl$_1$ (Figure 4.2j) and C6 with 30 wt% C6-Cl$_2$ (Figure 4.2k) membranes show four diffraction spots parallel to the alignment direction, which corresponds to an ordered smectic C morphology. The MAXS spectra of the C11 membranes (Figure 4.2i) and the C6 membranes with 25 wt% C6-F$_4$ (Figure 4.2l) show diffraction lobes instead of spots, which is characteristic of a morphology between smectic A and smectic C [33]. The more smectic A character of the C11 membranes compared to the C6 and C3 membranes likely arises due to the increased flexibility of the longer alkyl spacer in the C11 membranes, leading to less stress in the lamellar layers and resulting in a more smectic A morphology. Besides the membrane morphology also the tilt angle, layer spacing and intermolecular spacing were determined from the WAXS and MAXS spectra (Table 4.3).

Table 4.3: *Morphology, tilt angle, layer spacing and intermolecular spacing of the fabricated LC membranes.*

Membranes	Morphology	Tilt angle [°]	Layer spacing [Å]	Intermolecular spacing [Å]
C3	SmC	21	31.9	4.6
C6	SmC	20	36.8	4.6
C11	SmA/C	18	45.2	4.6
C6 with 30 wt% C6-Cl_1	SmC	20	37.4	4.5
C6 with 30 wt% C6-Cl_2	SmC	22	37.5	4.6
C6 with 25 wt% C6-F_4	SmA/C	20	38.1	4.5

Table 4.3 shows that the tilt angle of the smectic structures is similar for all membranes (varying between 18° and 22°) and is not affected by either extending the alkyl spacer in the LC monomers or by incorporating halogen groups onto the LC core. However, the layer spacing, which corresponds to the distance between two layers, is found to be highly dependent on the length of the alkyl spacer in the LC membranes. The determined layer spacing is equal to 31.9 Å for the C3, 36.8 Å for the C6 and 45.2 Å for the C11 membranes which is in close agreement with the theoretical extended molecular length of the LC monomers (34.0 Å for C3, 40.0 Å for C6 and 49.9 Å for C11). The small difference between the experimentally measured and theoretical layer spacing can be explained by the fact that the flexible alkyl spacers in the molecules are likely folded, leading to slightly lower layer spacing values. Surprisingly, the C6 membranes that contain halogenated LCs show slightly higher layer spacing values compared to the C6 membranes without halogenated LCs. The layer spacing further increases with increasing halogen content, leading to the highest layer spacing for the C6 membranes with 25 wt% C6-F_4 (38.1 Å compared to 36.8 Å for the C6 membranes). Here, the bulky halogen groups can lead to more elongated alkyl chains, which results in slightly higher layer spacing values. The intermolecular spacing that corresponds to the intermolecular stacking of the LC molecules is not affected by the halogen groups and was found to be similar for all membranes (varying between 4.5 – 4.6 Å). The above confirms a planar alignment and smectic morphology for all fabricated LC membranes.

4.3.3 Effect of layer spacing on single gas performances

The effect of the layer spacing on the gas permeation properties of smectic LC membranes was investigated by measuring the single gas permeation of He, CO_2 and N_2 at 40 °C in smectic LC membranes with various layer spacings. Permeation data and ideal gas selectivities of He/N_2, CO_2/N_2 and He/CO_2 are shown in Figure 4.3 (see reference [36] for all permeation and ideal selectivity values). To show the effect of the layer spacing in more detail, the permeation data were also plotted against the layer spacing of the respective membranes (Figure 4.3c).

Figure 4.3a clearly shows that the gas permeability increases with increasing alkyl spacer length, resulting in the lowest gas permeabilities for the C3 membranes and the highest gas permeabilities for the C11 membranes. Obviously, He has the highest permeability of all membranes, followed by CO_2 and N_2. As the gas permeability through dense membranes depends on the kinetic diameter and critical temperature of the gas species [36,38]. Helium has the smallest kinetic diameter of all measured gases, which results in a higher diffusion rate through the membrane and the highest permeability of all gases. Contrary, N_2 has the largest kinetic diameter of all measured gases, leading to a lower diffusion rate through the membrane. Together with a low critical temperature, which affects the condensability of a gas and thereby the solubility in the polymer matrix, this results in the lowest permeability of all measured gases. CO_2 has a kinetic diameter between He and N_2 but has the highest critical temperature of all measured gases, resulting in a higher solubility and permeability between He and N_2. Figure 4.3c shows the relation between layer spacing and gas permeability of smectic LC membranes. The permeability of all gases decreases with decreasing layer spacing, resulting in the lowest permeabilities for the C3 membranes with a layer spacing of 31.9 Å, followed by the C6 and C11 membranes with layer spacings of, respectively, 36.8 Å and 45.2 Å. This correlation between layer spacing and gas permeability likely arises due to a change in the total free volume within the membrane or/and a change in the size of the free volume elements within the membrane upon a change in layer spacing [30]. A change in the total free volume or size of the free volume elements within dense membranes affects the solubility and diffusion of gases, which can lead to different gas permeabilities.

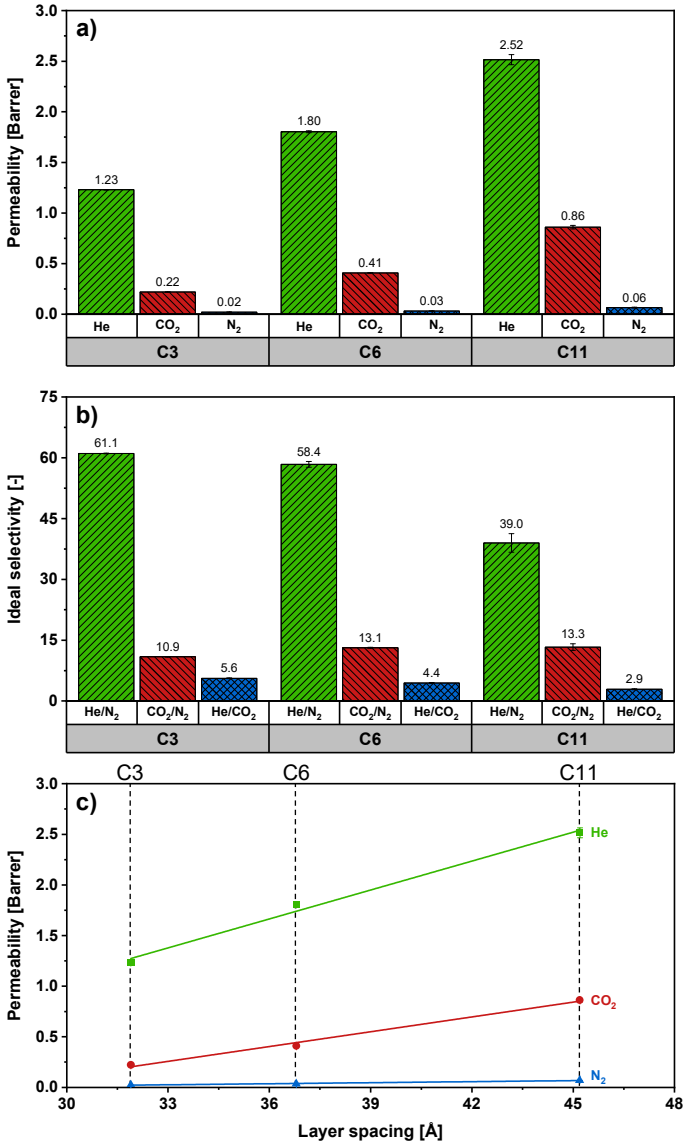

Figure 4.3: *Gas permeation data and ideal gas selectivities of smectic LC membranes with various layer spacings.* ***a)*** *Single gas permeability (He, CO_2 and N_2) of C3, C6 and C11 membranes measured at 40 °C and 6 bar feed pressure.* ***b)*** *Ideal gas selectivities (He/N_2, CO_2/N_2 and He/CO_2) of C3, C6 and C11 membranes measured at 40 °C and 6 bar feed pressure.* ***c)*** *Single gas permeability (He, CO_2 and N_2) versus the layer spacing of the C3, C6 and C11 membranes. The small error bars represent the spread of two independently prepared membranes, where each membrane is measured in triplicate.*

Contrary to the permeability, the ideal gas selectivity of He/N_2 and He/CO_2 decreases with increasing layer spacing (Figure 4.3b), resulting in the highest selectivities for the C3 membranes (respectively 61.1 for He/N_2 and 5.6 for He/CO_2) and the lowest selectivities for the C11 membranes (respectively 39.0 for He/N_2 and 2.9 for He/CO_2). The decrease in selectivity towards He probably originates from the increasing layer spacing of the lamellar structures, which results in larger free volume elements within the membrane. This affects the diffusion of gases with larger kinetic diameters such as CO_2 and N_2 more compared to the smaller He, resulting in a lower selectivity towards He. As the separation of He/N_2 and He/CO_2 gas pairs are mainly diffusion-controlled the selectivities decrease with increasing layer spacing of the lamellar structures. The CO_2/N_2 selectivity of the C6 and C11 membranes is similar but the CO_2/N_2 selectivity of the C3 membranes is surprisingly lower compared to the C6 and C11 membranes. Similar CO_2/N_2 selectivities were expected because the difference in kinetic diameter of CO_2 and N_2 (3.30 Å for CO_2 and 3.64 Å for N_2) is smaller compared to the difference in kinetic diameter of He and N_2 (2.60 Å for He and 3.64 Å for N_2), resulting in comparable diffusion rates of CO_2 and N_2 through the membrane. Moreover, the separation of the CO_2/N_2 gas pair is mainly sorption-controlled, meaning that these gases are mainly separated by their differences in gas solubility rather than differences in diffusion. This reduces the influence of the layer spacing on the permeability of CO_2 and N_2 and leads to very similar CO_2/N_2 selectivities for the C6 and C11 membranes.

4.3.4 Effect of halogenation on single gas performances

The effect of halogenation on the gas separation properties of smectic LC membranes was investigated by measuring the single gas permeation of He, CO_2 and N_2 at 40 °C for C6 membranes with various halogenated LCs (respectively 30 wt% C6-Cl_1, 30 wt% C6-Cl_2 and 25 wt% C6-F_4). The permeation data and ideal gas selectivities of He/N_2, CO_2/N_2 and He/CO_2 are shown in Figure 4.4 (see reference [36] for permeation and ideal selectivity values). For comparison, and to show the effect of halogenation in more detail, the permeation and ideal selectivity data of the C6 membranes without halogenated LCs are also included in Figure 4.4.

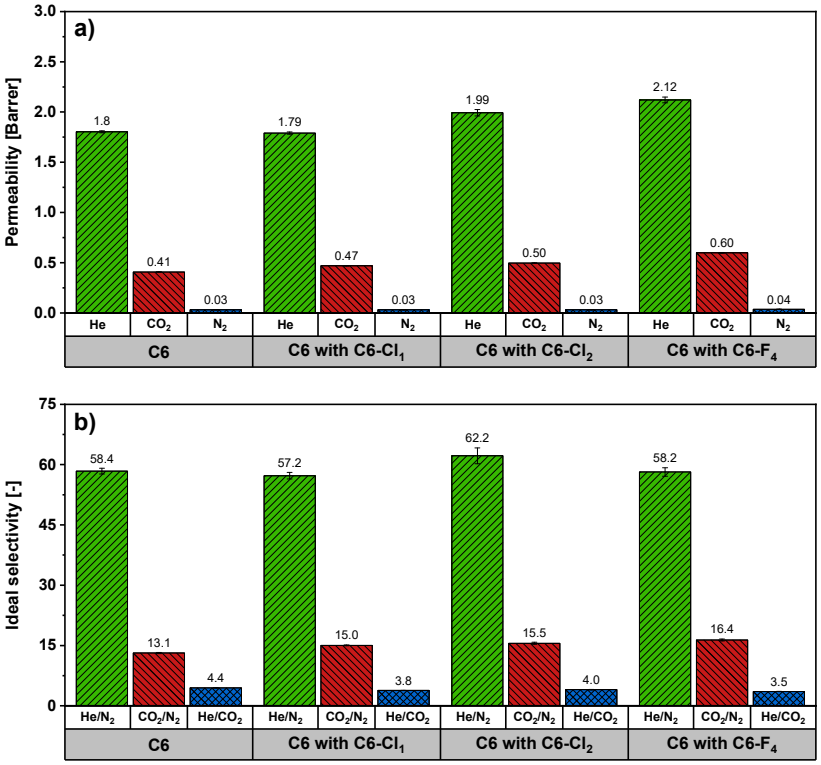

Figure 4.4: *Gas permeation data and ideal gas selectivities of smectic LC membranes with various halogenated LCs.* ***a)*** *Single gas permeability (He, CO_2 and N_2) of smectic C6 membranes with respectively 30 wt% C6-Cl_1, 30 wt% C6-Cl_2 and 25 wt% C6-F_4 measured at 40 °C and 6 bar feed pressure.* ***b)*** *Ideal gas selectivities (He/N_2, CO_2/N_2 and He/CO_2) of smectic C6 membranes with respectively 30 wt% C6-Cl_1, 30 wt% C6-Cl_2 and 25 wt% C6-F_4 at 40 °C. The small error bars represent the spread of two independently prepared membranes, where each membrane is measured in triplicate.*

Figure 4.4a shows that the C6 membranes with halogenated LCs only exhibit slightly higher permeabilities compared to the C6 membranes without halogenated LCs. These small differences likely arise from the relatively low halogen content in the halogenated C6 membranes (30 wt% for the membranes with C6-Cl_1 and C6-Cl_2 and 25 wt% for the membranes with C6-F_4), which is needed to obtain a smectic morphology. Despite the small permeability differences, the membranes show some subtle variations in permeation behavior. The permeability of all gases increases with increasing halogen content, resulting in the highest permeabilities for the membranes with 25 wt% C6-F_4. The membranes with 30 wt% C6-Cl_1 only show an increase in CO_2 permeability while the membranes with C6-

Cl_2 and C6-F_4 show increased permeabilities for all gases. The increased permeabilities for the membranes with halogenated LCs likely arises due to an increase in the total free volume and/or size of the free volume elements within the membranes with increasing halogen content. The bulky halogen substituents disrupt the chain packing of the molecules, which increases the diffusion coefficient of all gases, resulting in higher gas permeabilities for the membranes with halogenated LCs compared to the pristine C6 membranes. The CO_2 permeability of all membranes shows a relatively larger permeability increase compared to He and N_2. This can be explained 2-fold. Firstly, the quadrupole of CO_2 interacts favorably with the polar halogen groups, which leads to a higher solubility in the polymer matrix and therefore a higher CO_2 permeability [38]. Gases without these favorable interactions (He) or gases with only small interactions (N_2) are less affected by the polarity of the halogen groups, resulting in a lower permeability increase [29–31]. Secondly, C6 membranes that contain halogenated LCs show slightly higher layer spacings compared to the C6 membranes without halogenated LCs, which also affect the diffusion of gases through the membranes and lead to an increase in permeability (see sections 4.3.2 and 4.3.3). Contrary to the membranes with various alkyl spacer lengths, Figure 4.4b shows that the He/N_2 selectivity of the C6 membranes with halogenated LCs is similar for all membranes. Here, the small increase in layer spacing with increasing halogen content does not affect the selectivity towards He. The selectivity towards CO_2 increases with increasing halogen content due to improved CO_2-polymer matrix interactions, resulting in higher CO_2/N_2 selectivities and lower He/CO_2 selectivities for the C6 membranes with halogenated LCs compared to the C6 membranes. These permeation results show that the used halogen content, which is necessary to obtain smectic LC membranes, only has a limited effect on the gas separation performances (permeability/selectivity) of smectic LC membranes.

4.3.5 CO_2 sorption

Since the gas permeability of dense membranes is defined as the product of the solubility coefficient and the diffusion coefficient of a certain gas species, CO_2 sorption was measured to determine the CO_2 solubility coefficient and further investigate the effect of layer spacing and halogenation on gas solubility and diffusion in smectic LC membranes. The diffusion coefficient was subsequently calculated using Equation (4.6). Unfortunately, only CO_2 sorption could be measured because the N_2 sorption was for all membranes too low to obtain accurate values. The layer spacing, CO_2 permeabilities, CO_2 solubility coefficients and the associated calculated diffusion coefficients of all membranes are

shown in Table 4.4. To illustrate the effect of the layer spacing in more detail, the solubility coefficients and the diffusion coefficients were also plotted against the layer spacing of the membranes (Figure 4.5).

Table 4.4: *The layer spacing, CO_2 permeabilities, CO_2 solubility coefficients measured at 40 °C and 6 bar and the associated calculated diffusion coefficients of all membranes.*

Membrane	Layer spacing [Å]	P $\left[\frac{cm^3(STP)\cdot cm}{cm^2\cdot s\cdot cmHg}\right]\cdot 10^{-10}$	S $\left[\frac{cm^3(STP)}{cm^3\cdot cmHg}\right]\cdot 10^{-3}$	D $\left[\frac{cm^2}{s}\right]\cdot 10^{-9}$
C3	31.9	0.22	6.94	3.16
C6	36.8	0.41	5.95	6.85
C11	45.2	0.86	4.68	18.4
C6 with 30 wt% C6-Cl_1	37.4	0.47	5.86	8.01
C6 with 30 wt% C6-Cl_2	37.5	0.50	6.05	8.22
C6 with 25 wt% C6-F_4	38.1	0.60	6.74	8.88

Sorption experiments in Table 4.4 show that the layer spacing affects both the CO_2 solubility coefficients and the diffusion coefficients of smectic LC membranes. The solubility coefficients slightly decrease with increasing layer spacing (Figure 4.5a), resulting in the highest solubility coefficient for the C3 membranes and the lowest solubility coefficient for the C11 membranes. This decrease in solubility coefficient with increasing layer spacing can be explained as follows. Varying the alkyl spacer length of the LC monomers not only affects the layer spacing but also the amount of ether/ester groups present in the membrane. The polar ether/ester oxygen groups interact favorably with the quadrupole of CO_2, which usually leads to higher CO_2 solubility coefficients for the membranes with more ether/ester groups [39–43]. The ether/ester content of the membranes decreases with increasing alkyl spacer length, resulting in the highest CO_2 solubility coefficient for the C3 membranes and lower CO_2 solubility coefficients for the C6 and C11 membranes (C3 > C6 > C11).

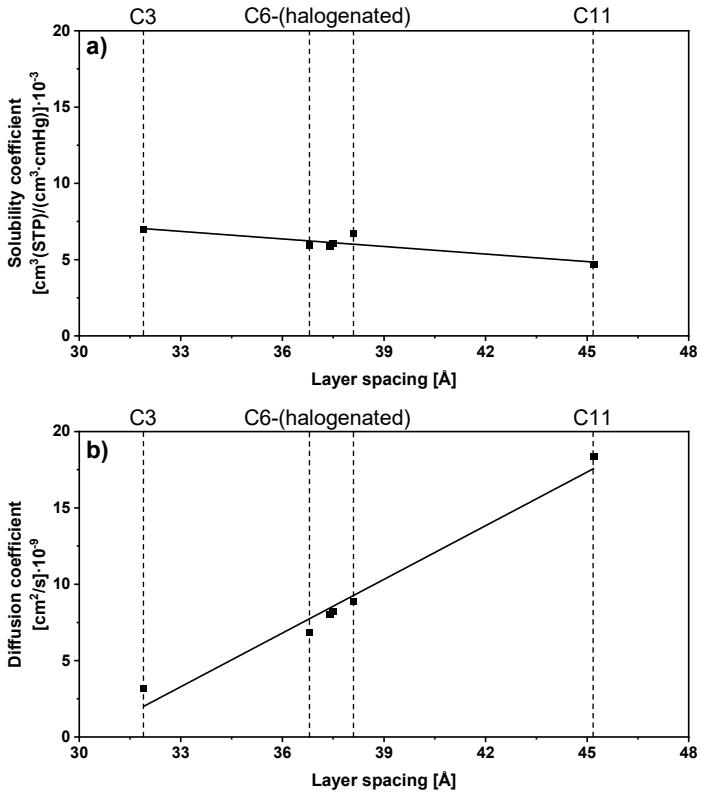

Figure 4.5: *Effect of layer spacing on the CO_2* ***a)*** *solubility coefficient* ***b)*** *and diffusion coefficient in smectic LC membranes.*

Furthermore, the C6 membranes with halogenated LCs show slightly higher solubility coefficients compared to the C6 membranes, showing the highest solubility coefficient for the C6 membranes with 25 wt% C6-F_4. Here, additional favorable interactions between CO_2 and the polar halogen groups lead to improved CO_2-polymer matrix interactions, which results in a higher solubility coefficient with increasing halogen content. Contrary to the solubility coefficient, the diffusion coefficient increases tremendously with increasing layer spacing (Figure 4.5b). The diffusion coefficient of the C6 membranes is 2 times higher compared to the C3 membranes, while the C11 membranes even show a 6-fold increase in the diffusion coefficient compared to the C3 membranes. This indicates that the increasing gas permeability with increasing layer spacing for the C3, C6 and C11 membranes can be attributed to an increasing diffusion coefficient. However, the aromatic-aliphatic ratio, which is increasing when going from C11 to C3, might also affect the

diffusion coefficient. For the C6 membranes with halogenated LCs, the slight increase in CO_2 permeability and selectivity can be attributed to an increase in both solubility and diffusion coefficients. The bulky polar halogen groups in the halogenated C6 membranes lead to improved CO_2-polymer matrix interactions and slightly higher layer spacing values, resulting in increased solubility and diffusion coefficients for the C6 membranes with halogenated LCs compared to the C6 membranes without halogenated LCs.

The solubility and diffusion coefficients of gases are highly affected by the available free volume and the size of the free volume elements within the membrane. Usually, the solubility coefficient increases with increasing free volume within a membrane because higher amounts of free volume provides more sorption sites for gases. The diffusion coefficient is highly affected by the size of the free volume elements. The activation energy of diffusion is lower for larger free volume elements leading to a higher diffusion coefficient. The very similar solubility coefficients for all membranes indicate that the overall free volume is equal and is not much affected by either the layer spacing or the bulky polar halogen groups in the smectic structures [44]. It is therefore expected that with increasing layer spacing, not the total free volume within the smectic LC membrane increases, but the free volume elements within the membrane increase in size. This increases the diffusion coefficients for all gases, leading to higher permeabilities with increasing layer spacing values. However, the diffusion coefficient of gases with larger kinetic diameters (CO_2 and N_2) is more affected by the size of the free volume elements compared to gases with a smaller kinetic diameter (He), resulting in lower selectivities towards He for the C11 membranes [45,46].

4.4. Conclusions

The effect of the layer spacing and halogenation on the gas separation performance of free-standing planar aligned smectic LC polymer membranes for gas separations of He, CO_2 and N_2 was investigated. All LC membranes consisting of LCs with similar chemical compositions but different alkyl spacer lengths and membranes containing halogenated LCs have a planar alignment and smectic morphology. The tilt angle of the smectic structures was similar for all membranes but the layer spacing was found to be highly dependent on the length of the alkyl spacer, resulting in smectic LC membranes with various layer spacing values.

Gas sorption of CO_2 and single gas permeation of He, CO_2 and N_2 demonstrated that the permeability increases with increasing layer spacing, while the ideal gas selectivity towards He decreases with increasing layer spacing. It was found that an increasing diffusion coefficient with increasing layer spacing is responsible for the increased permeability, showing that the layer spacing in smectic LC membranes mainly affects the diffusion of gases rather than their solubility. The effect of incorporating bulky halogens onto the LC cores has been shown to only have a limited effect on the gas permeability and ideal gas selectivity due to the relatively low halogen content in the used membranes, which was needed to maintain a smectic morphology. The CO_2 permeability of all membranes with halogenated LCs slightly increases with increasing halogen content due to an increase in CO_2 solubility and diffusion coefficients, resulting in slightly improved selectivities towards CO_2.

These results show that especially layer spacing is a crucial parameter that directly controls the diffusion coefficient of gases in smectic LC membranes and can be used to tune their gas separation performances (permeability/selectivity). Future work should focus on improving the separation performances by reducing the membrane thickness. This research provides insights into the structure-performance relations with single gas measurements, but future research should study the performances under mixed-gas conditions and investigate plasticization and physical aging of the membranes.

References

[1] L. Huang, J. Liu, H. Lin, *J. Membr. Sci.* **2020**, 610, 118253.

[2] S. Wang, X. Li, H. Wu, Z. Tian, Q. Xin, G. He, D. Peng, S. Chen, Y. Yin, Z. Jiang, M.D. Guiver, *Energy Environ. Sci.* **2016**, 9, 1863–1890.

[3] S. Basu, A.L. Khan, A. Cano-Odena, C. Liu, I.F.J. Vankelecom, *Chem. Soc. Rev.* **2010**, 39, 750–768.

[4] P. Bernardo, E. Drioli, G. Golemme, *Ind. Eng. Chem. Res.* **2009**, 48, 4638–4663.

[5] D.F. Sanders, Z.P. Smith, R. Guo, L.M. Robeson, J.E. McGrath, D.R. Paul, B.D. Freeman, *Polymer (Guildf).* **2013**, 54, 4729–4761.

[6] T.E. Rufford, S. Smart, G.C.Y. Watson, B.F. Graham, J. Boxall, J.C. Diniz da Costa, E.F. May, *J. Pet. Sci. Eng.* **2012**, 94–95, 123–154.

[7] S. Kim, Y.M. Lee, *Curr. Opin. Chem. Eng.* **2013**, 2, 238–244.

[8] M.R.A. Hamid, H.K. Jeong, *Korean J. Chem. Eng.* **2018**, 35, 1577–1600.

[9] S. Sridhar, B. Smitha, T.M. Aminabhavi, *Sep. Purif. Rev.* **2007**, 36, 113–174.

[10] B.D. Freeman, *Macromolecules.* **1999**, 32, 375–380.

[11] R.L. Burns, K.M. Steel, S.D. Burns, W.J. Koros*, Ind. Eng. Chem. Res.* **2004**, 43, 5942–5949.

[12] L.M. Robeson, *J. Membr. Sci.* **2008**, 320, 390–400.

[13] M. Zhou, T.J. Kidd, R.D. Noble, D.L. Gin, *Adv. Mater.* **2005**, 17, 1850–1853.

[14] G.M. Bögels, J.A.M. Lugger, O.J.G.M. Goor, R.P. Sijbesma, *Adv. Funct. Mater.* **2016**, 26, 8023–8030.

[15] S.M. Dischinger, J. Rosenblum, R.D. Noble, D.L. Gin, K.G. Linden, *J. Membr. Sci.* **2017**, 543, 319–327.

[16] N. Marets, D. Kuo, J.R. Torrey, T. Sakamoto, M. Henmi, H. Katayama, T. Kato, *Adv. Healthc. Mater.* **2017**, 6, 1700252.

[17] M. Henmi, K. Nakatsuji, T. Ichikawa, H. Tomioka, T. Sakamoto, M. Yoshio, T. Kato, *Adv. Mater.* **2012**, 24, 2238–2241.

[18] T. Sasaki, H. Hazato, A. Katsuragi, Y. Nakazawa, *Mol. Cryst. Liq. Cryst.* **2009**, 503, 81–98.

[19] C. Li, J. Cho, K. Yamada, D. Hashizume, F. Araoka, H. Takezoe, T. Aida, Y. Ishida, *Nat. Commun.* **2015**, 6, 6:8418.

[20] M. Gupta, Y. Suzuki, T. Sakamoto, M. Yoshio, S. Torii, H. Katayama, T. Kato, *ACS Macro Lett.* **2019**, 8, 1303–1308.

[21] T. Sakamoto, T. Ogawa, H. Nada, K. Nakatsuji, M. Mitani, B. Soberats, K. Kawata, M. Yoshio, H. Tomioka, T. Sasaki, M. Kimura, M. Henmi, T. Kato, *Adv. Sci.* **2018**, 5, 1700405.

[22] H.P.C. Van Kuringen, G.M. Eikelboom, I.K. Shishmanova, D.J. Broer, A.P.H.J. Schenning, *Adv. Funct. Mater.* **2014**, 24, 5045–5051.

[23] T. Liang, H.P.C. Van Kuringen, D.J. Mulder, S. Tan, Y. Wu, Z. Borneman, K. Nijmeijer, A.P.H.J. Schenning, *ACS Appl. Mater. Interfaces.* **2017**, 9, 35218–35225.

[24] M. Zhou, P.R. Nemade, X. Lu, X. Zeng, E.S. Hatakeyama, R.D. Noble, D.L. Gin, *J. Am. Chem. Soc.* **2007**, 129, 9574–9575.

[25] J.E. Bara, A.K. Kaminski, R.D. Noble, D.L. Gin, *J. Membr. Sci.* **2007**, 288, 13–19.

[26] J. Kloos, N. Jansen, M. Houben, A. Casimiro, J. Lub, Z. Borneman, A.P.H.J. Schenning, K. Nijmeijer, *Chem. Mater.* **2021**, 33, 8323–8333.

[27] S.J.A. Houben, J. Kloos, Z. Borneman, A.P.H.J. Schenning, *J. Polym. Sci.* **2022**, 60, 803–811.

[28] J. Kloos, N. Jansen, M. Houben, K. Nijmeijer, A.P.H.J. Schenning, Z. Borneman, *ACS Appl. Polym. Mater.* (**2022**), 4, 7426–7426.

[29] K. Ghosal, B.D. Freeman, *Polym. Adv. Technol.* **1994**, 5, 673–697.

[30] M.W. Hellums, W.J. Koros, G.R. Husk, D.R. Paul, *J. Membr. Sci.* **1989**, 46, 93–112.

[31] X. Wang, T.J. Wilson, C.R. Maroon, J.A. Laub, S.E. Rheingold, K.D. Vogiatzis, B.K. Long, *ACS Appl. Polym. Mater.* **2022**.

[32] F. Kadirkhan, P.S. Goh, A.F. Ismail, W.N.F. Wan Mustapa, M.H.M. Halim, W.K. Soh, S.Y. Yeo, *Membranes (Basel).* **2022**, 12, 71.

[33] R.A.M. Hikmet, J. Lub, A.J.W. Tol, *Macromolecules.* **1995**, 28, 3313–3327.

[34] M. Ikenaga, D. Kubota, T. Yamamoto, Liquid Crystal Composition, Liquid Crystal Element, and Liquid Crystals Display Device. U.S. Patent 2013/0256595 A1, 3 October 2013.

[35] F. Dallacker, J. van Wersch, *Chem. Ber.* **1972**, 105, 3301–3305.

[36] Figures and Tables of the characterizations of the synthesized compounds and fabricated polymer membranes are available in the supporting information of J. Kloos, M. Houben, J. Lub, Z. Borneman, K. Nijmeijer, A.P.H.J. Schenning, *Membranes (Basel).* **2022**, 805.

[37] M. Sikirić, I. Primožič, Y. Talmon, N. Filipović-Vinceković, *J. Colloid Interface Sci.* **2005**, 281, 473–481.

[38] P. Rallapalli, K.P. Prasanth, D. Patil, R.S. Somani, R. V. Jasra, H.C. Bajaj, *J. Porous Mater.* **2011**, 18, 205–210.

[39] M. Houben, Z. Borneman, K. Nijmeijer, *Sep. Purif. Technol.* **2021**, 255, 117307.

[40] S.R. Reijerkerk, A. Arun, R.J. Gaymans, K. Nijmeijer, M. Wessling, *J. Membr. Sci.* **2010**, 359, 54–63.

[41] A. Car, C. Stropnik, W. Yave, K.V. Peinemann, *Sep. Purif. Technol.* **2008**, 62, 110–117.

[42] H.Z. Chen, T.S. Chung, *Int. J. Hydrogen Energy.* **2012**, 37, 6001–6011.

[43] J. Liu, G. Zhang, K. Clark, H. Lin, *ACS Appl. Mater. Interfaces.* **2019**, 11, 10933–10940.

[44] C.C. Hu, C.S. Chang, R.C. Ruaan, J.Y. Lai, *J. Membr. Sci.* **2003**, 226, 51–61.

[45] K. Haraya, S.T. Hwang, *J. Membr. Sci.* **1992**, 71, 13–27.

[46] A.W. Thornton, K.M. Nairn, A.J. Hill, J.M. Hill, *J. Membr. Sci.* **2009**, 338, 29–37.

Chapter 5

Nematic liquid crystalline polymer membranes for gas separation

Abstract

The gas separation performances of free-standing planar aligned nematic LC polymer membranes are investigated for gas separations of He, CO_2, CH_4 and Xe. The membranes consist of derivatives of 1,4-phenylene bis(4-((6-(acryloyloxy)hexyl)oxy)benzoate)s with respective cyano, chloro, methyl and phenyl substituents on the central aromatic cores. Single gas permeation and sorption data show increasing gas permeabilities with increasing steric size of the substituents while the ideal gas selectivity of He over CH_4 and He over CO_2 decreases. The sorption coefficient of all membranes is independent of the LC substituents while the subsequently extracted diffusion coefficient for the membranes with a phenyl substituent is 3 times higher compared to the membranes with a cyano substituent, demonstrating that the steric size of the LC substituents mainly affects the diffusion of gases rather than the solubility of the gases. Irrespective of a methyl or a phenyl substituent a larger kinetic diameter of Xe gives a 20 times lower diffusion coefficient compared to the smaller species (CO_2).

This chapter has been adapted from:

J. Kloos, J. Lub, M. Houben, Zandrie Borneman, K. Nijmeijer, A.P.H.J. Schenning, Nematic liquid crystalline polymer films for gas separation, *Liq. Cryst.* **2022**, 1–9.

5.1 Introduction

Thermotropic liquid crystal (LC) molecules are small molecules that can self-assemble into various nanostructures and provide excellent control over the molecular order and orientation of the molecules [1–5]. Nanostructures like nematic and smectic morphologies can be obtained, which differ in positional order of the LC monomers, by varying the temperature in the fabrication process (Figure 5.1b). Subsequent cross-linking of the LC monomers is necessary to obtain free-standing LC polymer membranes [2,3].

Safeguarding a sustainable future results in the necessity to lower our greenhouse gas emissions (CO_2 and CH_4) and makes separations such as CO_2/CH_4 and CO_2/N_2 crucial and relevant [6–9]. Polymeric membrane processes are often used in gas separation processes due to their high energy efficiency, low operating costs and easy scalability compared to other separation technologies [10–13]. Using LC materials that can self-assemble into nanostructured polymer membranes provides control over the molecular order and alignment of the membrane building blocks and can be used to tune the gas separation properties. However, the gas separation performances of such nanostructured materials have been hardly reported in literature.

In Chapters 3 and 4 we investigated smectic LC polymer membranes for gas separation. Now, we investigate the effect of several substituents on the gas separation properties of free-standing planar aligned nematic LC polymer membranes with respective cyano, chloro, methyl and phenyl substituents (C6-CN, C6-Cl, C6-CH_3 and C6-C_6H_5 in Figure 5.1a) for gas separations of He, CO_2, CH_4 and Xe. Several nematic LC membranes are fabricated and characterized consisting of LCs with different substituents, which differ in steric size, on the central aromatic cores of the di-acrylate monomers. The gas separation properties of the prepared membranes are characterized by single gas sorption and permeation measurements to study the effect of the substituents on gas permeability and ideal gas selectivity. Moreover, the effect of the kinetic diameter of different gas species (CO_2 and Xe) on the gas separation properties of nematic LC membranes was studied by comparing single gas permeation and sorption data of nematic LC membranes with different substituents.

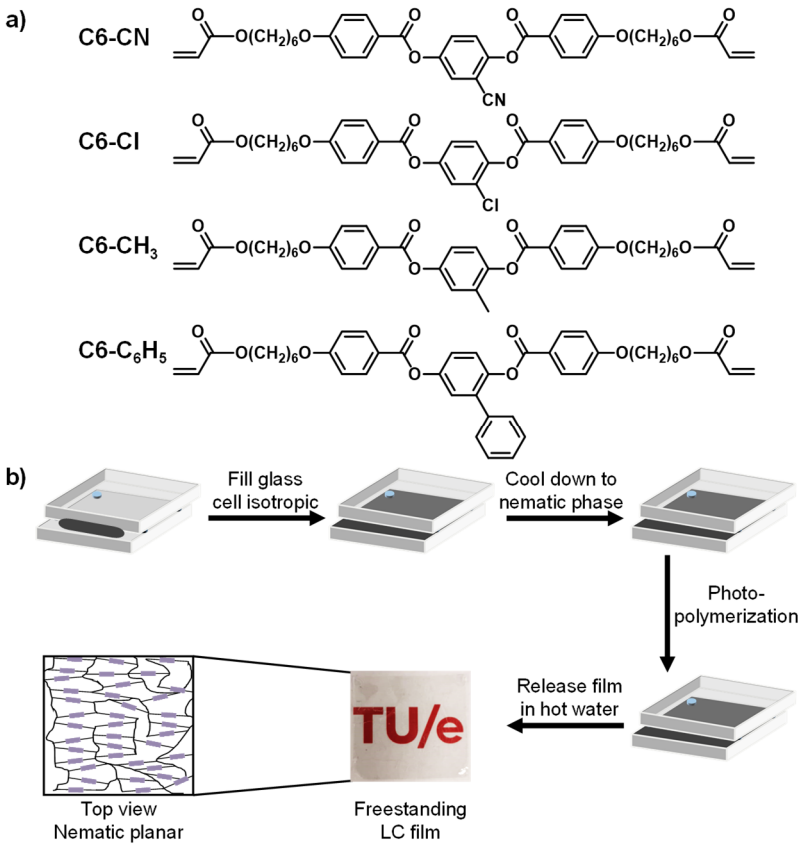

Figure 5.1: a) *The molecular structures of the nematic LCs under investigation.* ***b)*** *Schematic representation of the fabrication process of nematic LC membranes. The purple rods represent the aromatic cores of the LCs.*

5.2 Materials and methods

5.2.1 Chemicals

2-chloro-1,4-phenylene bis(4-((6-(acryloyloxy)hexyl)oxy)benzoate) (C6-Cl) was prepared as described in Chapter 4. 2-methyl-1,4-phenylene bis(4-((6-(acryloyloxy)hexyl)oxy)benzoate) (C6-CH_3) was obtained from Merck Life Science. The synthesis of 2-cyano-1,4-phenylene bis(4-((6-(acryloyloxy)hexyl)oxy)benzoate) (C6-CN) and [1,1'-biphenyl]-2,5-diyl bis(4-((6-(acryloyloxy)hexyl)oxy)benzoate) (C6-C_6H_5) is outlined in Scheme 5.1 (section 5.3.1). 4-(6-acryloyloxyhexyloxy)benzoic acid (1) was obtained from Synthon and [1,1'-biphenyl]-2,5-diol (3b) from TCI. 2-cyanohydroquinone (3a) was made according to a literature procedure [14].

All other chemicals that were used for the synthesis of the LC monomers were obtained from Sigma-Aldrich. Irgacure 819 was supplied by Ciba. t-Butyl-hydroquinone was purchased from Merck Life Science. For permeation and sorption measurements, the gases He (5.0 grade), CO_2 (4.5 grade) and CH_4 (4.5 grade) were obtained from Linde Gas (the Netherlands). Xe (5.0 grade) was supplied by Westfalen BV (the Netherlands). All reagents were used as received without further purification.

5.2.2 Membrane preparation

LC mixtures with 0.5 wt% photoinitiator (Irgacure 819) and 0.1 wt% inhibitor (t-Butyl-hydroquinone) were prepared by dissolving the compounds in a minimum amount of dichloromethane and subsequently removing the solvent after mixing (see Figure 5.1 for the chemical structures of the LCs and fabrication process). Planar aligned nematic membranes were fabricated by processing the LC mixtures in the isotropic phase by capillary suction between two 20 µm spaced glass plates. The glass plates were cleaned before use with isopropanol in an ultrasonic bath for 30 minutes, dried with N_2 and treated with UV ozone for 20 minutes. To obtain planar alignment, the glass plates were functionalized with a rubbed polyimide layer (Optimer AL 1254; JSR Corporation, Toyo Japan). Glass cells were prepared by gluing two glass plates together with glue that contained 20 µm glass spacer beads. The glass cells were filled with the LC mixture and placed inside a temperature-controlled N_2 box, in which the glass cells were cooled from the isotropic phase to the nematic phase using a cooling rate between 1-2 °C/min. The planar aligned LC monomers were polymerized by exposing the samples for 10 min to an unfiltered spectrum of a collimated EXFO Omnicure S2000 UV lamp with a light intensity of 20 mW/cm^2 in the range of 320-390 nm. Free-standing membranes were obtained by carefully opening the glass cells in water at 80 °C.

5.2.3 Characterization

Nuclear magnetic resonance (NMR) spectra were recorded on a 400 MHz Bruker Avance III HD spectrometer in deuterated chloroform with tetramethyl silane (TMS) used as an internal standard.

Matrix-assisted laser desorption/ionization time-of-flight mass spectrometry (MALDI-TOF MS) was performed on a Bruker Autoflex Speed MALDI-MS instrument using CHCA (α-cyano-4-hydroxycinnamic acid) as matrix.

Attenuated total reflection fourier transform infrared spectroscopy (ATR FT-IR) spectra were recorded at room temperature on a Varian-Cary 3100 FT-IR spectrometer equipped with a golden gate attenuated total reflectance (ATR) sampling accessory. Scans were taken over a range of 4000−650 cm^{-1} with a spectral resolution of 4 cm^{-1} and 50 scans per spectrum.

Polarizing optical microscopy (POM) was performed using a Leica DM 2700M optical microscope equipped with two polarizers that were operated either crossed or parallel with the sample in between a Linkam hot-stage THMS600 with a Linkam TMS94 controller and a Leica DFC420 C camera.

Differential scanning calorimetry (DSC) measurements were recorded in hermetic T-zero aluminum sample pans using a TA Instruments Q2000 DSC equipped with a cooling accessory. The DSC measurements were performed with three cycles of heating and cooling at a rate of 2 °C/min with an isothermal equilibration of 3 minutes after each heating or cooling ramp.

Medium- and wide-angle X-ray scattering (MAXS/WAXS) measurements were recorded on a GaneshaLab instrument equipped with a Genix-Cu ultralow divergence source producing X-ray photons of wavelength 1.54 Å and a flux of 108 photons per second. Diffraction patterns were collected on a Pilatus 300 K silicon pixel detector with 487 × 619 pixels of 172 μm^2.

5.2.4 Single gas performances

Single gas permeation measurements of He, CO_2, CH_4 and Xe were performed in a custom-built permeation setup and have been carried out according to the same procedure described in the previous Chapters. The single gas permeabilities were determined from the steady-state pressure increase in time in a calibrated volume at the permeate side of the membrane at a temperature of 40 °C and a feed pressure of 6 bar. The order of the measured gases was kept constant for all membranes (He, CH_4, Xe and CO_2) because CO_2 could induce swelling of the membranes. The ideal gas selectivity ($\alpha_{i/j}$) was calculated from the single gas permeabilities by using Equation (5.1).

$$\alpha_{i/j} = \frac{P_i}{P_j} \qquad (5.1)$$

In Equation (5.1) P_i is the permeability of gas species i (Barrer) and P_j is the permeability of gas species j (Barrer).

5.2.5 Gas sorption

The gas permeability through dense polymer membranes is well described by the solution diffusion model, which states that the gas permeability (P_i) is defined as the product of the diffusion coefficient (D_i) and the solubility coefficient (S_i) of a certain gas species [15,16]. The diffusion coefficient and the solubility coefficient highly depend on a combination of parameters such as the kinetic diameter, critical temperature and interactions via the quadrupole moments of the gas species. These parameters are shown in Table 5.1 [17].

Table 5.1: *The kinetic diameter, critical temperature and quadrupole moment of the measured gases (He, CO_2, CH_4 and Xe) [17].*

Gas species	Kinetic diameter [Å]	Critical temperature [K]	Quadrupole moment $[cm^2] \cdot 10^{40}$
He	2.60	5.19	0.00
CO_2	3.30	304.13	-13.71
CH_4	3.80	190.55	0.00
Xe	3.96	289.77	0.00

Gas sorption of CO_2 and Xe was measured at 6 bar and 40 °C with a magnetic suspension balance, using a Rubotherm series IsoSORP® sorption instrument, to investigate the effect of the different substituents and the effect of the kinetic diameter of the measured gases on the gas separation properties of nematic LC membranes. The measurements and the solubility coefficient of the gases were determined as described in the previous Chapters. The CO_2 and Xe diffusion coefficients were calculated by filling in the obtained sorption and permeability data in Equation (5.2).

$$D_i = \frac{P_i}{S_i} \qquad (5.2)$$

In Equation (5.2), D_i is the diffusion coefficient (cm^2/s), P_i the permeability (Barrer) and S_i the solubility coefficient (cm^3 STP/($cm^3 \cdot$cmHg)) of a certain gas species.

5.3 Results and discussion

5.3.1 Synthesis and characterization of the liquid crystalline molecules and mixtures

The effect of several substituents on the gas separation properties of planar aligned nematic LC membranes was investigated by preparing LC monomers with respective cyano, chloro, methyl and phenyl substituents (C6-CN, C6-Cl, C6-CH_3 and C6-C_6H_5 in Figure 5.1a). These substituents were selected for their difference in steric size (cyano < chloro < methyl < phenyl). However, it must be noted that the polar cyano and chloro groups in C6-CN and C6-Cl can lead to improved interactions with CO_2, which can lead to enhanced CO_2 permeability and selectivity for these membranes [18–23]. LC monomer C6-CH_3 is commercially available and often used in LC applications. The LC monomer C6-Cl was synthesized and characterized following the procedure described in Chapter 4, while C6-CN and C6-C_6H_5 were synthesized according to Scheme 5.1. The synthetic preparations are described in reference [24]. Characterization by ^1H and ^{13}C nuclear magnetic resonance (NMR) and mass spectroscopy (MALDI-TOF MS) confirmed the successful formation of all synthesized molecules.

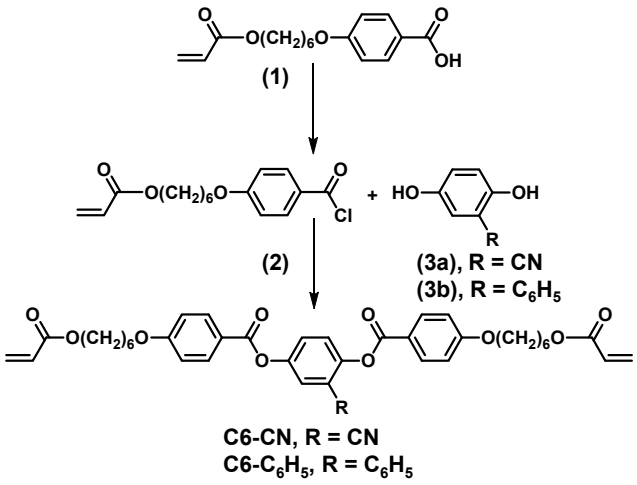

Scheme 5.1: *Synthetic routes to 2-cyano-1,4-phenylene bis(4-((6-(acryloyloxy)hexyl)oxy)benzoate) (C6-CN) and [1,1'-biphenyl]-2,5-diyl bis(4-((6-(acryloyloxy)hexyl)oxy)benzoate) (C6-C_6H_5).*

The LC behavior of the molecules was studied by determining the phase transition temperatures with differential scanning calorimetry (DSC) and polarizing optical

microscopy (POM). The results are shown in Table 5.2 (see reference [24] for DSC graphs and POM images).

Table 5.2: *Phase transitions and fabrication conditions of all LCs used in this study.*

Compound/ Mixture	Isotropic [°C]	Nematic [°C]	Polymerization temperature [°C]	Cooling rate [°C/min]
C6-CN	>104	104-96	100	2
C6-Cl	>110	110-99	100	2
C6-CH_3	>113	113-86	100	2
C6-C_6H_5	>30	30-20	-	-
C6-C_6H_5 with 20 wt% C6-CH_3	>39	39-30	32	1

All LC monomers exhibit a nematic phase but at different temperature ranges. The compounds C6-CN, C6-Cl and C6-CH_3 have similar isotropic-nematic phase transitions but C6-C_6H_5, which has the largest substituent of all LCs used in this study, has the lowest isotropic-nematic phase transition [25,26]. Because the viscosity of the pure C6-C_6H_5 monomer was too high to prepare well-aligned membranes, LC mixtures consisting of C6-C_6H_5 with C6-CH_3 were prepared and characterized with DSC and POM. Compositions of C6-C_6H_5 with 20 wt% C6-CH_3 and more could be used to fabricate aligned membranes, hence an LC mixture consisting of C6-C_6H_5 with 20 wt% C6-CH_3 was used.

5.3.2 Preparation and characterization of liquid crystalline membranes

Planar aligned nematic LC membranes were prepared by mixing the LCs with a photoinitiator and inhibitor and subsequently incorporating the LC mixtures in glass cells with alignment layers. After heat treatment, the LC mixtures were photopolymerized to fixate the aligned nematic morphology. Subsequent opening of the glass cells in hot water yielded free-standing nematic LC membranes. FT-IR spectra of the LC membranes showed full conversion of the acrylate moieties after photopolymerization [24].

POM shows the planar alignment of all membranes with dark images under parallel conditions and bright images under 45° tilt [24]. Wide-angle X-ray scattering (WAXS) and

medium-angle X-ray scattering (MAXS) were measured to further confirm the morphology and alignment of the prepared membranes (Figure 5.2).

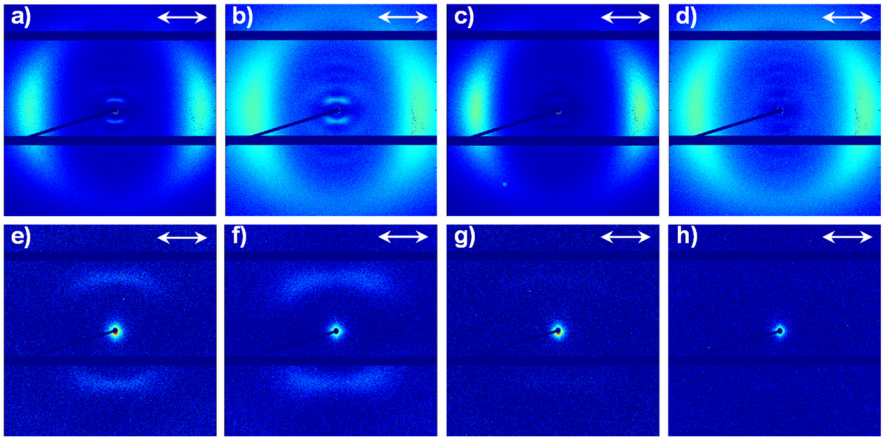

Figure 5.2: *WAXS (top row) and MAXS (bottom row) spectra of the prepared nematic LC membranes with different substituents.* ***a, e)*** *C6-CN,* ***b, f)*** *C6-Cl,* ***c, g)*** *C6-CH_3,* ***d, h)*** *C6-C_6H_5 with 20 wt% C6-CH_3. The single arrow shows the alignment direction.*

The two-dimensional (2D) WAXS spectra in Figure 5.2 show for all membranes diffraction spots, indicating aligned LCs. The C6-CH_3 and C6-C_6H_5 membranes show only diffraction spots in the wide-angle region (Figure 5.2c,d), which is characteristic for a nematic molecular organization. Additionally, the C6-CN and C6-Cl membranes show weak diffused diffraction spots in the medium-angle region (Figure 5.2e,f), which is characteristic for a nematic cybotactic morphology having localized nanometer-sized smectic domains [27,28]. The intermolecular spacing that corresponds to the intermolecular stacking of the molecules is not affected by the different substituents and was found to be similar for all membranes, varying between 4.6 – 4.7 Å. The above results show the successful fabrication of the planar aligned nematic LC membranes.

5.3.3 Single gas permeation and selectivity of nematic LC membranes

The effect of various substituents in nematic LC membranes on the gas permeation data (He, CO_2 and CH_4) and ideal gas selectivities (He/CH_4, CO_2/CH_4 and He/CO_2) are presented in Figure 5.3 (see reference [24] for all permeation and ideal selectivity values).

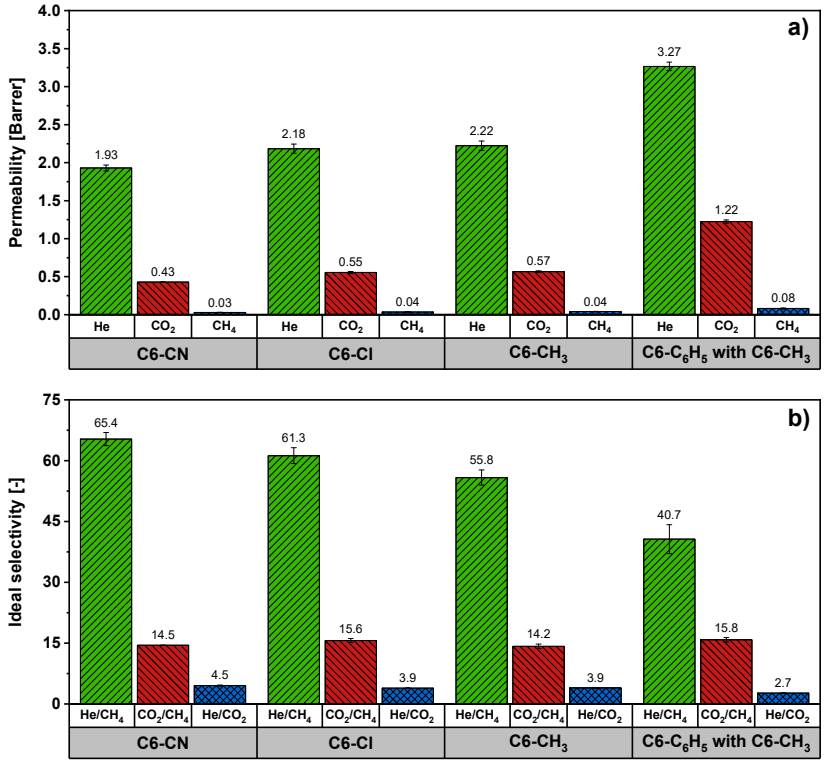

Figure 5.3: *Gas permeation data and ideal gas selectivities of nematic LC membranes with cyano, chloro, methyl and phenyl substituents.* ***a)*** *Single gas permeability (He, CO_2 and CH_4) of C6-CN, C6-Cl, C6-CH_3 and C6-C_6H_5 with 20 wt% C6-CH_3 membranes measured at 40 °C and 6 bar feed pressure.* ***b)*** *Ideal gas selectivities (He/CH_4, CO_2/CH_4 and He/CO_2) of C6-CN, C6-Cl, C6-CH_3 and C6-C_6H_5 with 20 wt% C6-CH_3 membranes at 40 °C. The small error bars represent the spread of two independently prepared membranes, where each membrane is measured in triplicate.*

Figure 5.3a shows that the permeability of all gases is affected by the substituents on the LC monomers, showing the lowest permeabilities for the C6-CN membranes and the highest permeabilities for the C6-C_6H_5 membranes (C6-CN < C6-Cl < C6-CH_3 < C6-C_6H_5). This most likely originates from the different steric sizes of the substituents on the central aromatic cores of the LC monomers that affect the packing density of the polymer chains. A frequently used system for evaluation of the relative steric size of functional groups is the Winstein-Holness A-value system [29–32], which states that the relative steric size of the substituents used in this study is CN < Cl < CH_3 < C_6H_5. Comparing the relative steric sizes of the substituents with the measured gas permeabilities of the C6-CN, C6-Cl, C6-

CH_3 and C6-C_6H_5 membranes reveals a relationship between the increasing steric size of the substituents and increasing gas permeabilities. Here, a larger steric size of the substituent leads to a larger overall free volume and/or size of the free volume elements in the membrane, resulting in higher diffusion rates through the membranes and therefore higher gas permeabilities for membranes with larger substituents. However, next to the steric size of the substituents also the small difference in molecular organization between the membranes might affect the gas permeabilities [33,34].

Contrary to the gas permeability, the ideal gas selectivity of He/CH_4 and He/CO_2 decreases with increasing steric size of the substituents (Figure 5.3b). This results in the highest selectivities for the C6-CN membranes (respectively 65.4 for He/CH_4 and 4.5 for He/CO_2) and the lowest selectivities for the C6-C_6H_5 membranes (respectively 40.7 for He/CH_4 and 2.7 for He/CO_2). This decrease in selectivity towards He can be attributed to the increase of the total free volume and/or size of the free volume elements with increasing steric size of the substituents. This effect also affects the diffusion of CO_2 and CH_4, which have larger kinetic diameters than He, resulting in lower selectivities towards He. Counterintuitively, the CO_2/CH_4 selectivity is similar for all membranes. Although one would expect that the CO_2/CH_4 selectivity decreases with the increasing steric size of the substituents (C6-CN > C6-Cl > C6-CH_3 > C6-C_6H_5), the difference in kinetic diameter between CO_2 and CH_4 (respectively 3.30 Å and 3.80 Å) is smaller compared to the difference between the kinetic diameter of He and CH_4 (respectively 2.60 Å and 3.80 Å), resulting in more comparable diffusion rates of CO_2 and CH_4 through the membrane. This diminishes the effect of steric size of the substituents and leads to very similar CO_2/CH_4 selectivities for all membranes. Secondly, the relatively low cyano and chloro content in the C6-CN and C6-Cl membranes does not give a significant improvement in CO_2 permeability and selectivity compared to the C6-CH_3 and C6-C_6H_5 membranes and therefore results in comparable CO_2/CH_4 selectivities for all membranes.

5.3.4 Gas sorption and diffusion of nematic LC membranes

The effect of the different substituents on the gas separation properties of nematic LC membranes was further studied to identify the underlying mechanism for the observed differences. CO_2 sorption in the membranes was measured to determine the solubility coefficient and subsequently extract the diffusion coefficient using Equation (5.2). Unfortunately, only CO_2 sorption could be measured because He was used for the buoyancy measurements and the CH_4 sorption was for all membranes too low to obtain

accurate values. The CO_2 permeabilities, CO_2 solubility coefficients and associated diffusion coefficients of all membranes are shown in Table 5.3.

Table 5.3: *CO_2 permeabilities, CO_2 solubility coefficients measured at 6 bar and 40 °C and the associated calculated diffusion coefficients of all membranes.*

Membrane	P $\left[\frac{cm^3(STP)\cdot cm}{cm^2\cdot s\cdot cmHg}\right]\cdot 10^{-10}$	S $\left[\frac{cm^3(STP)}{cm^3\cdot cmHg}\right]\cdot 10^{-3}$	D $\left[\frac{cm^2}{s}\right]\cdot 10^{-9}$
C6-CN	0.43	8.05	5.33
C6-Cl	0.55	8.83	6.28
C6-CH_3	0.57	8.38	6.76
C6-C_6H_5 with 20 wt% C6-CH_3	1.22	7.37	16.6

Table 5.3 shows that the solubility coefficient of CO_2 is similar for all membranes, meaning that the increase in CO_2 permeability with increasing steric size of the substituents can be completely attributed to an increase in the diffusion coefficient. All membranes exhibit similar CO_2 solubility coefficients, elucidating that the polar cyano and chloro groups in the C6-CN and C6-Cl membranes do not lead to improved CO_2-polymer matrix interactions. This explains the similar CO_2/CH_4 selectivities (as depicted in Figure 5.3). Consequently, the polarity of the cyano and chloro groups in the C6-CN and C6-Cl membranes does not affect the gas separation performance of these membranes and the difference in performance solely depends on steric effects of the substituents. Contrary to the solubility coefficient, the diffusion coefficient increases with increasing steric size of the substituents, resulting in a 3 times higher diffusion coefficient for the C6-C_6H_5 membranes compared to the C6-CN membranes. The similar solubility coefficients of the membranes indicate that not the total free volume [35], but the size of the free volume elements in the membranes increase with increasing size of the substituents. This finding is in accordance with the intermolecular spacing of the molecules (section 5.3.2), which is similar for all membranes, indicating that the overall free volume in the membranes is similar regardless of the size of the substituents. However, although the intermolecular spacing is similar for all membranes, the size of the free volume pockets in the membranes likely increase with increasing size of the substituents. These increased free volume pockets increase the

diffusion coefficients of all gases and result in higher permeabilities for the membranes containing larger substituents. The diffusion coefficient of the larger CO_2 and CH_4 gases is more affected by the size of the free volume elements compared to the smaller He, resulting in lower selectivities towards He with increasing steric size of the substituents [36,37].

5.3.5 The effect of the kinetic diameter of different gas species on the gas separation properties

The effect of the kinetic diameter on the gas separation properties of the LC membranes was studied in more detail by comparing single gas permeation and sorption data of CO_2 and Xe because both have similar critical temperatures but Xe has a larger kinetic diameter. Due to the scarcity of Xe, its permeation and sorption were only measured for the C6-CH_3 and C6-C_6H_5 membranes. For comparison, the permeation data of He and CH_4 are also plotted in Figure 5.4.

Figure 5.4a shows that irrespective of the LC substituent He has the highest permeability followed by CO_2, CH_4 and Xe, following the order of kinetic diameter and critical temperature of the measured gases. As discussed in section 5.3.3, the larger steric size of the phenyl substituent in the C6-C_6H_5 membranes results in larger free volume pockets in the membranes and therefore higher permeabilities for all gases (including Xe) but lower ideal gas selectivities towards He when compared to the C6-CH_3 membranes with the smaller sized methyl substituent. Figure 5.4b shows that the selectivity towards Xe for both the C6-CH_3 and C6-C_6H_5 membranes decreases for gas pairs with more similar kinetic diameters, resulting in the highest selectivity for He/Xe > CO_2/Xe > CH_4/Xe. The CO_2 and Xe permeabilities, solubility coefficients and the associated calculated diffusion coefficients for the C6-CH_3 and C6-C_6H_5 with 20 wt% C6-CH_3 membranes are shown in Table 5.4.

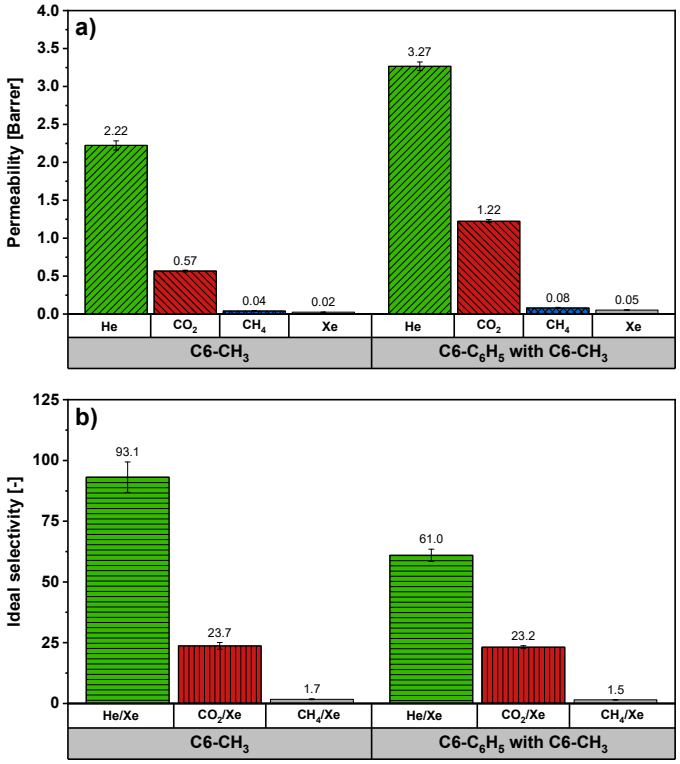

Figure 5.4: *Gas permeation data and ideal gas selectivities of nematic LC membranes with methyl and phenyl substituents.* ***a)*** *Single gas permeability (He, CO_2, CH_4 and Xe) of C6-CH_3 and C6-C_6H_5 with 20 wt% C6-CH_3 membranes measured at 40 °C and 6 bar feed pressure.* ***b)*** *Ideal gas selectivities (He/Xe, CO_2/Xe and CH_4/Xe) of C6-CH_3 and C6-C_6H_5 with 20 wt% C6-CH_3 membranes at 40 °C.*

Table 5.4: *CO_2 and Xe permeabilities and solubility coefficients measured at 40 °C and 6 bar and the associated calculated diffusion coefficients of the C6-CH_3 and C6-C_6H_5 membranes.*

Membrane	Gas species	P $\left[\frac{cm^3(STP)\cdot cm}{cm^2\cdot s\cdot cmHg}\right]\cdot 10^{-10}$	S $\left[\frac{cm^3(STP)}{cm^3\cdot cmHg}\right]\cdot 10^{-3}$	D $\left[\frac{cm^2}{s}\right]\cdot 10^{-9}$
C6-CH_3	CO_2	0.57	8.38	6.76
	Xe	0.02	6.89	0.349
C6-C_6H_5 with 20 wt% C6-CH_3	CO_2	1.22	7.37	16.6
	Xe	0.05	6.38	0.847

Table 5.4 shows that for both membranes the slightly lower critical temperature of Xe compared to CO_2 (289.77 versus 304.13 K) leads to a 1.2 times lower solubility coefficient for Xe compared to CO_2. However, due to its larger size, the diffusion coefficient of Xe is approximately 20 times lower than the diffusion coefficient of CO_2, which means that the low Xe permeability mainly originates from the low diffusion rate of Xe through the membrane.

5.4 Conclusions

New LC 1,4-phenylene bis(4-((6-(acryloyloxy)hexyl)oxy)benzoate)s derivatives were successfully synthesized and fully characterized. The gas permeation performance for He, CO_2, CH_4 and Xe of well-aligned free-standing planar aligned nematic LC polymer membranes with respective cyano, chloro, methyl and phenyl substituents was investigated.

Single gas permeation of He, CO_2 and CH_4 and gas sorption of CO_2 demonstrated that the gas permeability of the nematic LC membranes increases with increasing steric size of the substituents, while the ideal gas selectivities towards He decrease with increasing steric size of the substituents. An increasing diffusion coefficient with increasing substituent steric size was responsible for these effects and not the solubility of the gases in the polymer matrix. The effect of kinetic diameter is most obvious from a 20-fold reduction of the diffusion coefficient of the larger Xe compared to the smaller CO_2, resulting in considerably lower Xe permeabilities.

References

[1] I. Dierking, *Textures of liquid crystals*, Wiley-Vch Verlag Gmbh, **2003**.

[2] J. Kloos, N. Joosten, A. Schenning, K. Nijmeijer, *J. Membr. Sci.* **2021**, 620, 118849.

[3] J. Lugger, D.J. Mulder, R. Sijbesma, A. Schenning, *Materials (Basel).* **2018**, 11, 104.

[4] D. Andrienko, *J. Mol. Liq.* **2018**, 267, 520–541.

[5] G.W. Taylor, *Ferroelectrics.* **1987**, 73, 265.

[6] S. Basu, A.L. Khan, A. Cano-Odena, C. Liu, I.F.J. Vankelecom, *Chem. Soc. Rev.* **2010**, 39, 750–768.

[7] P. Bernardo, E. Drioli, G. Golemme, *Ind. Eng. Chem. Res.* **2009**, 48, 4638–4663.

[8] D.F. Sanders, Z.P. Smith, R. Guo, L.M. Robeson, J.E. McGrath, D.R. Paul, B.D. Freeman, *Polymer (Guildf).* **2013**, 54, 4729–4761.

[9] T.E. Rufford, S. Smart, G.C.Y. Watson, B.F. Graham, J. Boxall, J.C. Diniz da Costa, E.F. May, *J. Pet. Sci. Eng.* **2012**, 94–95, 123–154.

[10] S. Kim, Y.M. Lee, *Curr. Opin. Chem. Eng.* **2013**, 2, 238–244.

[11] S. Wang, X. Li, H. Wu, Z. Tian, Q. Xin, G. He, D. Peng, S. Chen, Y. Yin, Z. Jiang, M.D. Guiver, *Energy Environ. Sci.* **2016**, 9, 1863–1890.

[12] M.R.A. Hamid, H.K. Jeong, *Korean J. Chem. Eng.* **2018**, 35, 1577–1600.

[13] S. Sridhar, B. Smitha, T.M. Aminabhavi, *Sep. Purif. Rev.* **2007**, 36, 113–174.

[14] R.J. Bergeron, J. Wiegand, J.S. McManis, N. Bharti, *J. Med. Chem.* **2006**, 49, 7032–7043.

[15] W.J. Koros, G.K. Fleming, S.M. Jordan, T.H. Kim, H.H. Hoehn, *Prog. Polym. Sci.* **1988**, 13, 339–401.

[16] R.W. Wijmans, J.G.; Baker, *J. Membr. Sci.* **1995**, 1–21.

[17] P. Rallapalli, K.P. Prasanth, D. Patil, R.S. Somani, R. V. Jasra, H.C. Bajaj, *J. Porous Mater.* **2011**, 18, 205–210.

[18] K. Ghosal, B.D. Freeman, *Polym. Adv. Technol.* **1994**, 5, 673–697.

[19] X. Wang, T.J. Wilson, C.R. Maroon, J.A. Laub, S.E. Rheingold, K.D. Vogiatzis, B.K. Long, *ACS Appl. Polym. Mater.* **2022**.

[20] M.W. Hellums, W.J. Koros, G.R. Husk, D.R. Paul, *J. Membr. Sci.* **1989**, 46, 93–112.

[21] F. Kadirkhan, P.S. Goh, A.F. Ismail, W.N.F. Wan Mustapa, M.H.M. Halim, W.K. Soh, S.Y. Yeo, *Membranes (Basel).* **2022**, 12, 71.

[22] S.M. Mahurin, J.S. Yeary, S.N. Baker, D. en Jiang, S. Dai, G.A. Baker, *J. Membr. Sci.* **2012**, 401–402, 61–67.

[23] J.E. Bara, C.J. Gabriel, E.S. Hatakeyama, T.K. Carlisle, S. Lessmann, R.D. Noble, D.L. Gin, *J. Membr. Sci.* **2008**, 321, 3–7.

[24] Figures and Tables of the characterizations of the synthesized compounds and fabricated polymer membranes are available in the supporting information of J. Kloos, J. Lub, M. Houben, Z. Borneman, K. Nijmeijer, A.P.H.J. Schenning, J. Kloos, J. Lub, M. Houben, Z. Borneman, K. Nijmeijer, *Liq. Cryst.* **2022**, 1–9.

[25] E.M. Averyanov, *Liq. Cryst.* **1987**, 2, 491–504.

[26] M.A. Osman, *Zeitschrift Fur Naturforsch. - Sect. A J. Phys. Sci.* **1983**, 38, 693–697.

[27] W.L. McMillan, *Phys. Rev. A.* **1972**, 6, 936–947.

[28] L. Nasrin, A.K. Nasir, A. Yoshizawa, S. Ghosh, M. Rahman, *Mater. Res. Express.* **2019**, 6, 115105.

[29] S. Winstein, N.J. Holness, *J. Am. Chem. Soc.* **1955**, 77, 5562–5578.

[30] E. V. Anslyn, D.A. Dougherty, *Modern Physical Organic Chemistry*, Univ. Sci. Books, **2005**.

[31] H. Förster, F. Vögtle, *Angew. Chemie Int. Ed. English.* **1977**, 16, 429–441.

[32] E. Solel, M. Ruth, P.R. Schreiner, *J. Am. Chem. Soc.* **2021**, 143, 20837–20848.

[33] J. Kloos, N. Jansen, M. Houben, A. Casimiro, J. Lub, Z. Borneman, A.P.H.J. Schenning, K. Nijmeijer, *Chem. Mater.* **2021**, 33, 8323–8333.

[34] J.E. Bara, A.K. Kaminski, R.D. Noble, D.L. Gin, *J. Membr. Sci.* **2007**, 288, 13–19.

[35] C.C. Hu, C.S. Chang, R.C. Ruaan, J.Y. Lai, *J. Membr. Sci.* **2003**, 226, 51–61.

[36] K. Haraya, S.T. Hwang, *J. Membr. Sci.* **1992**, 71, 13–27.

[37] A.W. Thornton, K.M. Nairn, A.J. Hill, J.M. Hill, *J. Membr. Sci.* **2009**, 338, 29–37.

Chapter 6

Epilogue

This chapter has been partly reproduced from:

J. Kloos, N. Joosten, A. Schenning, K. Nijmeijer, Self-assembling liquid crystals as building blocks to design nanoporous membranes suitable for molecular separations, *J. Membr. Sci.* **2021**, 620, 118849.

6.1 Introduction

This thesis aimed to explore the opportunities of using liquid crystalline (LC) materials for the fabrication of nanostructured membranes for gas separations by systematically investigating the structure-property relationships. The aspects under study were the influence of the molecular order and orientation of the LC nanostructures (**Chapter 2**), the layer spacing and tilt angle of the nanostructures (**Chapter 3** and **Chapter 4**), the operating temperature and chemical composition of the LC monomers (**Chapter 3**, **Chapter 4** and **Chapter 5**) and the steric size of the substituents in the LC monomers (**Chapter 5**) on the gas separation performance.

An important finding in this PhD work is that the self-assembly properties of thermotropic calamitic LCs can be used to tune/control the gas separation performances of LC membranes. The easiest way to achieve this is by changing the molecular order and/or orientation of the LC nanostructures. However, more subtle order differences, such as layer spacing and tilt angle of the smectic morphology and different substituents on the LC cores for the nematic morphology, can also be used to tune the gas separation performances of LC membranes. The presented aspects offer the opportunity to tune the diffusion of gases, which provides control over the permeation behavior (gas permeability and selectivity) of the membranes. Incorporating functional groups that have a chemical affinity (via dipole/quadrupole moments) with certain gas species only leads to a slight improvement of the performances of the LC membranes studied in this thesis. Following this, the next section reflects on the results obtained and provides challenges and opportunities for using LCs for gas separation applications.

6.2 Challenges

6.2.1 Characterization and stability of liquid crystalline polymer membranes for gas separation

Although the membranes presented in this thesis show potential for using LCs for gas separations, there is still a long way to go before these materials could be considered of being used on a commercial scale for gas separation applications. For example, although it is common for new materials to first characterize the gas separation performance using pure gas permeability measurements under relatively mild conditions, these measurements do not represent the membrane separation performances under industrial conditions. When gas permeation is performed under mixed-gas conditions, permeability

and selectivity can deviate significantly from the pure-gas values [1]. The presence of other gases and vapors in the feed stream can lead to competitive sorption, which reduces the gas solubility, and also possibly plasticizes the membrane, which increases the diffusivity of gases. This usually leads to lower selectivities compared to the ideal selectivities that are computed from the pure-gas values [1–3]. Mixed gas permeation measurements are therefore much more useful to evaluate the membrane performance under real-world conditions and should therefore be the next step to evaluate the performances of these LC materials.

Another important issue that needs to be addressed is the stability of the membranes regarding physical aging and plasticization, which can greatly affect the performance of the membranes. These two phenomena are especially relevant regarding the industrial application of glassy polymers. Physical aging arises in glassy polymers where ineffectively packed polymer chains reorganize into a denser state, which leads to a reduction in the excess free volume [4,5]. As a consequence, the permeability can decrease significantly over time. Contrary to physical aging, plasticization is a phenomenon where the permeability increases over time when exposed to plasticizing penetrants such as CO_2, C_3H_6, C_3H_8 and water vapor [6]. The sorption of plasticizing penetrants swells the membrane, which increases the chain mobility and consequently increases the free volume in the membrane, leading to increased permeabilities [7]. Investigating these phenomena is crucial to determine the viability of LC membranes during longer operating times.

6.2.2 Improving the performances of liquid crystalline polymer membranes for gas separation

The largest challenge of using LC membranes for gas separations will be improving their performances in terms of permeability and selectivity. Even under ideal conditions the permeabilities of the LC membranes presented in this thesis are low compared to commercially available membranes and the selectivities are at best moderate. For example, cellulose acetate, which is industrially used to separate CO_2 from natural gas, has an approximately 10 times higher CO_2 permeability compared to the best performing LC membrane in this thesis (Chapter 5) and a twice as high CO_2/CH_4 selectivity (pure-gas values) [3,8,9]. Although cellulose acetate outperforms the LC membranes, cellulose acetate itself is now being replaced by polyimide and polyaramide membranes because those polymers are less susceptible to plasticization and have even higher CO_2/CH_4

selectivities under industrial conditions. In fact, to make LC membranes attractive for commercial use, the CO_2/CH_4 selectivity needs to be above 40 in industrial conditions [3].

In this thesis we tried to improve the CO_2 permeability and selectivity of LC membranes by incorporating functional groups such as polar cyclic ether and halogen groups for their favorable interactions with CO_2, which are known to enhance CO_2 solubility and usually increase the CO_2 permeability and selectivity [10–14]. However, this only increased the CO_2 permeability and CO_2/N_2 selectivity by approximately 10 – 15%, which is only a small improvement. Moreover, incorporating these groups into the membranes exposed one major drawback of using LCs to fabricate nanostructured membranes: The mesophases of LCs are easily disrupted/affected by molecular interactions and steric effects of the substituents used on the LC monomers, reducing the possibilities of using different chemistries to improve the separation performances of LC membranes. This became clear from the results in Chapter 3 and Chapter 4, where higher cyclic ether and halogen contents in the LC mixtures resulted in the loss of the more ordered smectic morphology. Therefore only membranes with relatively low cyclic ether and halogen content could be fabricated, which resulted in only small improvements in the CO_2 permeability and selectivity.

Recently another method was reported to increase the gas permeability in smectic LC membranes. Houben et al. [15] fabricated a composite membrane of a microporous polypropylene (PP) scaffold with a smectic LC network, consisting of a mixture of dimerized benzoic acid derivative mono-acrylate and di-acrylate cross-linker LCs, that can reversibly switch its gas permeability upon pH changes. In the hydrogen-bonded state the composite membrane has a low He, N_2 and CO_2 permeability while by pH switching from the hydrogen-bonded state to the salt form the gas permeabilities increase by one order of magnitude. However, this increase in permeability goes at expense of the selectivity, which decreases tremendously when the composite membrane is switched to its salt form. So although the gas permeability of smectic LC membranes can be increased using this method, the membranes ability to separate gases is compromised which is not desired for membrane applications.

Another method to increase the gas permeability of the membranes is reducing the membrane thickness to increase the gas permeance [3]. Improving the permeance of the membranes can be achieved by depositing a thin selective LC layer onto a porous support,

where the thin selective layer provides the gas separation performances while the porous support provides mechanical strength to the membrane. However, challenges regarding pore intrusion in the porous support and alignment of the LC monomers can occur and have to be overcome.

This thesis only investigated the structure-property relations of nematic and smectic morphologies of thermotropic calamitic LCs. However, there are many other LCs (thermotropic and lyotropic) available with very different mesophases that could be used to fabricate LC membranes with different morphologies for gas separation. These membranes can have completely different gas separation performances compared to the LC membranes fabricated in this thesis. Using different LCs and their corresponding mesophases to fabricate LC membranes has already been studied for water separation/purification purposes. To show the potential of different sorts of LCs and their corresponding morphologies in more detail, the next section gives examples of reported LC systems that could potentially be used for water separations/purifications.

6.3 Liquid crystalline polymer membranes for water separations/purifications

This section is based on a review of how LCs can be used to design nanoporous membranes that are suitable for molecular separations. Contrary to the most frequently used membranes for gas separations, membranes for water separation are mostly porous. The fabrication of nanoporous networks that can potentially be used for water separations/purifications has been reported for both lyotropic and thermotropic LCs (Figure 6.1). For lyotropic LCs, the pore sizes in the polymerized network depend on the amount of solvent present in the organized mesophase [16]. While for thermotropic LCs, the most common strategy to obtain nanoporous membranes is to introduce the pores after polymerization. Generally, there are two distinct approaches for thermotropic LC networks to create pores: (1) Breaking non-covalent bonds such as hydrogen bonds in the LC network resulting in voids (for example by Coulomb repulsion) [17–19] or (2) the removal of a (non-) covalently linked template (porogen) from the LC network, resulting in uniform pores [17,18]. With these approaches, uniform pore sizes down to 1 nm are reported [17,20].

The morphology of the formed nanoporous structures is directly influenced by the type of mesophase (Figure 6.1). One-dimensional (1D) cylindrical pores can be prepared from

lyotropic and thermotropic discotic LCs in columnar mesophases (such as the columnar hexagonal and rectangular mesophases). Two-dimensional (2D) pores can be directly obtained by lyotropic lamellar mesophases or by thermotropic calamitic LCs that are polymerized in the smectic mesophase followed by a pore formation step. 1D and 2D nanoporous networks display a low tortuosity. However, to obtain well-defined continuous pores from top to bottom in the polymer membrane, the pores must be aligned perpendicular to the surface using surface-induced orientation or external forces, as mentioned before. In contrast to 1D and 2D systems where alignment is required to obtain continuous pores, nanoporous polymer networks with 3D geometries circumvent the requirement of LC alignment. Three-dimensional (3D) pores can be obtained with lyotropic and thermotropic LCs polymerized in the continuous cubic mesophase [17,18]. In the sections below, each type of morphology will be further discussed and examples of existing systems that have the potential for membrane applications, are shown.

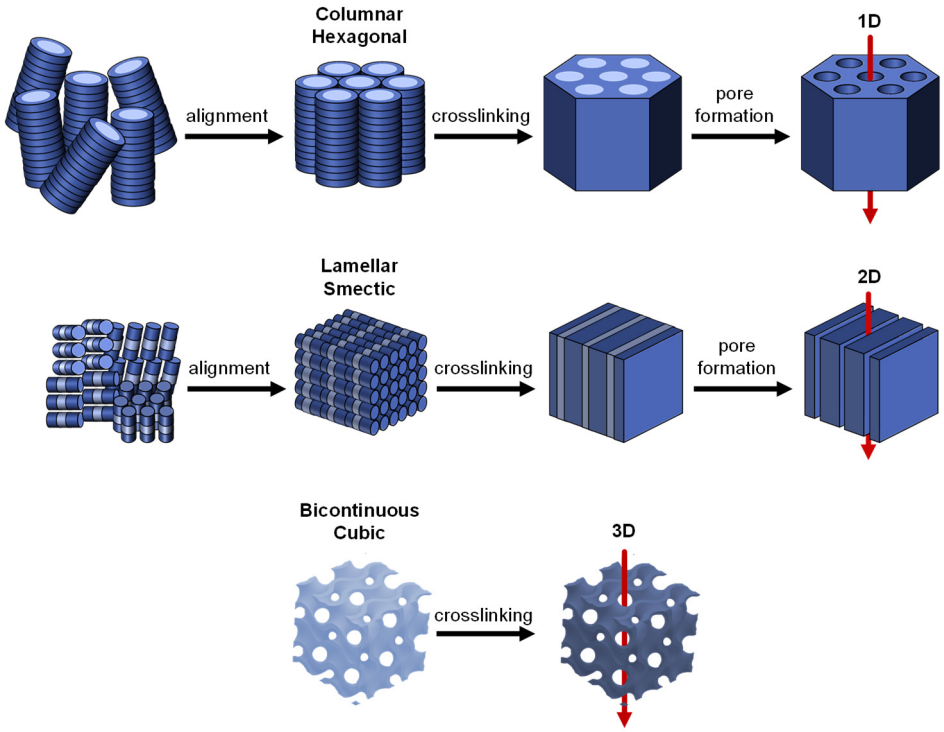

Figure 6.1: *Schematic overview of the fabrication methods for nanoporous LC networks with various morphologies.*

6.3.1 One-dimensional pores

A well-known strategy to obtain nanoporous materials with cylindrical 1D pores is by using a polymerizable wedge-shaped gallic acid-derived monomer. Pores are obtained by two different approaches. The first approach is based on converting the acid into a gallate salt, which can be used as a thermotropic or lyotropic LC [20–22]. Polymerization of the LC, in the hexagonal phase for the thermotropic processed salt and an inverted hexagonal phase for the lyotropic processed salt, results in cylindrical (aqueous) pores with an estimated diameter of 1 nm (Figure 6.2). This material can potentially be used as a selective layer e.g. nanofiltration applications [21].

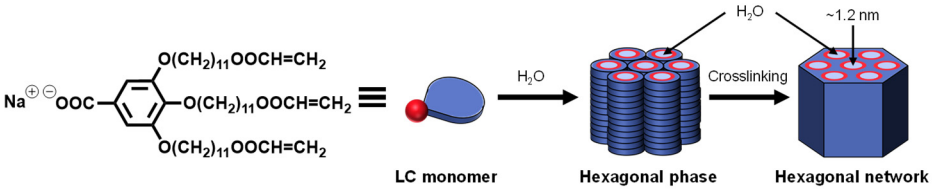

Figure 6.2: *Chemical structure of a lyotropic gallate salt and stepwise formation of a nanoporous hexagonal LC network.*

The second approach uses a complex of hydrogen bonded gallate acid monomers with a template molecule. After fixation of the morphology by polymerization, followed by the selective removal of a template molecule, nanoporous materials with pores in the size of the used template are obtained (Figure 6.3a and b) [23–26]. Using this approach, Bögels et al. obtained a nanoporous film that selectively binds sodium and potassium ions over lithium and barium, which have a larger hydrated radius (Figure 6.3c) [27]. Later Lugger et al. managed, at a small scale (cm^2 scale), to align these nanoporous films homeotropically by altering the LC-substrate interaction [28]. The effect of pore orientation was demonstrated by adsorption experiments in which the proper pore orientation (homeotropic alignment) showed a threefold increase in the initial uptake rate of a cationic dye compared to the nonideal pore orientation (planar alignment).

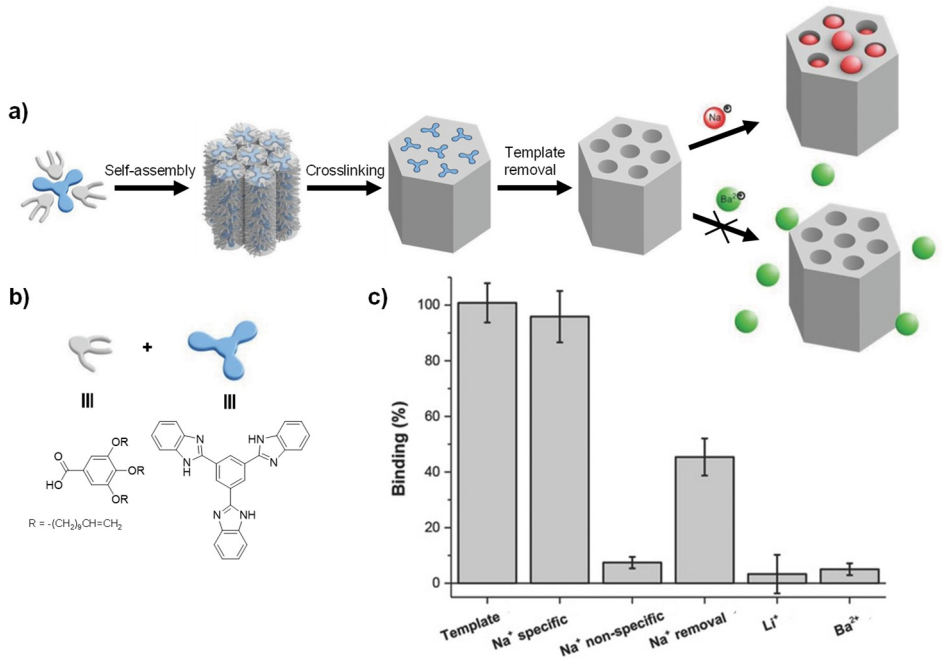

Figure 6.3: *Nanoporous hexagonal LC network using a gallic acid-derived monomer.* ***a)*** *Procedure for the fabrication of a nanoporous LC network using the template removal strategy and the selective ion uptake of the fabricated membrane.* ***b)*** *Chemical structure of the monomer and template used for self-assembly.* ***c)*** *Size-selective adsorption of ions as measured by using a quartz crystal microbalance. Adapted from Ref. [27] with permission of John Wiley and Sons, Inc.*

Li et al. explored the template strategy even further by complexation of a chiral template molecule with a gallate acid monomer (Figure 6.4) [29]. The chiral template was used to translate its chirality to a polymer host and by aligning the LCs in a magnetic field planar helical columns with an estimated diameter of 3.1 nm were obtained. By subsequent removal of the template pores were obtained. Adsorption experiments showed that various basic and cationic guest molecules can occupy up to 90% of the pores and order the guest molecules in a helical arrangement [29]. Although future work needs to be done regarding membrane studies and large-scale alignment in a homeotropic fashion, these examples show the potential of LCs as nanoporous membranes for the separation of ions and molecules or even chiral separations.

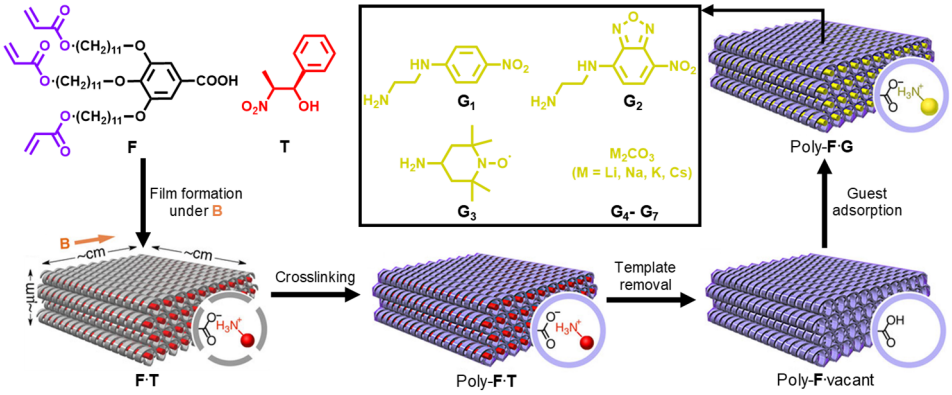

Figure 6.4: *The fabrication of chiral nanoporous LC networks. Schematic illustration of monomer self-assembly and alignment with a magnetic field, cross-linking, template removal and adsorption of guest molecules. Adapted from Ref. [29].*

The previous examples show the possibilities of nanoporous LC networks in terms of pore structure and functionality. However, in the examples above, the selectivity of the membranes was only determined using adsorption. The next step toward an application is the determination of the membrane properties in terms of permeation or rejection experiments. This requires the fabrication of selective thin LC films with a certain mechanical strength. To do so, thin LC layers are often coated on a porous support. This support gives the often brittle thin LC polymer layer mechanical strength, such that it can be used in membrane applications [30]. Gupta et al. used this strategy to prepare nanoporous LC membranes for virus rejection (Figure 6.5a) [31]. A 400 nm thin layer of a thermotropic wedge-shaped ionic LC with a photo-cleavable moiety was coated on top of a polysulfone microporous support. After the fixation of the LC structure and subsequent removal of the photo-cleavable moiety with a photocleavage and washing step, nanoporous films with pore sizes around 1.8 and 2.4 nm were obtained. The pore size and water flux (5 ± 2 and 9 ± 3 L m^{-2} h^{-1}, respectively) could be tuned by changing the alkyl length in the ionic moiety (Figure 6.5b). The rejection properties of the nanoporous films for the virus F-coliphage Qβ were evaluated. A virus removal effectiveness of more than 99.99% was obtained, which well exceeds the minimum required purity for drinking water according to the World Health Organization [31]. Separations of smaller molecules and ions were not yet explored with these membranes.

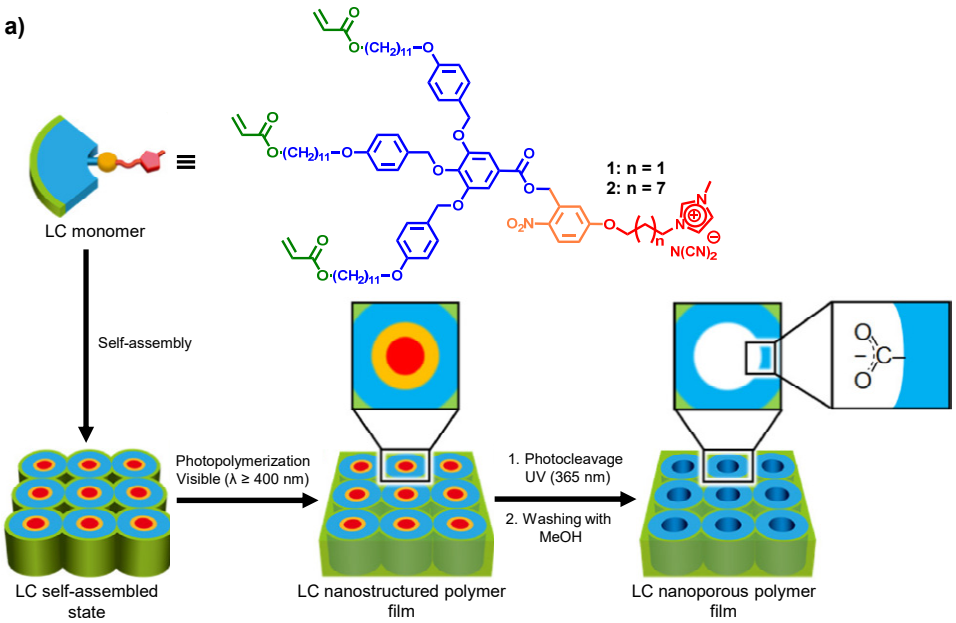

b)

Membrane (pore size)	Virus rejection [%]	Flux [L m^{-2} h^{-1}]
LC 1 (1.8 nm)	99.998	5 ± 2
LC 2 (2.4 nm)	99.997	9 ± 3

Figure 6.5: *1D Nanoporous LC membranes with variable pore sizes used for virus removal from water.* ***a)*** *Chemical structure of the monomer and schematic illustration of monomer self-assembly, photopolymerization and template removal by a photocleavage and washing step.* ***b)*** *Virus rejection rates and average flux over the first 6 hours of the two LC membranes. Adapted from Ref. [31] with permission of American Chemical Society.*

In a similar approach, Sakamoto et al. used thermotropic wedge-shaped ionic LCs on a porous polysulfone and nonwoven polyester support to obtain nanoporous LC membranes for water treatment [32]. Wedge-shaped LCs with different cationic moieties were developed that self-assemble into columnar hexagonal structures to obtain different pore functionalities. These structures were subsequently polymerized without alignment control by photopolymerization (Figure 6.6a). Single salt pressure-driven filtration measurements show a four times lower rejection of magnesium sulfate compared to the commercial NF membrane UTC-60 (Figure 6.6b). Surprisingly, sodium chloride rejection rates over 60%, depending on the pore functionality, are obtained, which is similar to the NF membrane

UTC-60. This is the first example of a membrane based on columnar thermotropic LCs that show similar results in sodium chloride rejections as commercial NF membranes. However, the fluxes of the LC membranes for both sodium chloride and magnesium sulfate are lower compared to the NF membrane UTC-60. Properties can be further improved by controlling the alignment of the mesophase.

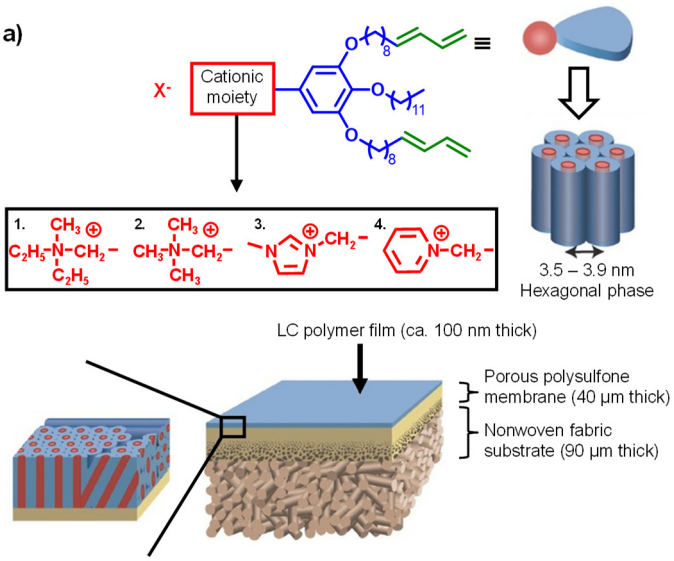

b)

Membrane	NaCl rejection		$MgSO_4$ rejection	
	Rejection [%]	Flux [L m^{-2} h^{-1}]	Rejection [%]	Flux [L m^{-2} h^{-1}]
LC 1	62 ± 2	29 ± 13	26 ± 2	26
LC 2	73 ± 3	9 ± 1	30 ± 2	22
LC 3	65 ± 10	30 ± 13	24 ± 3	45 ± 20
LC 4	46 ± 9	5 ± 2	26 ± 3	8 ± 3
UTC-60	79	65	99.6	58

Figure 6.6: *Composite membrane from thermotropic wedge-shaped ionic LC monomers.* ***a)*** *Chemical structure of the LC monomers and schematic illustration of the self-assembled monomer coated on a porous support.* ***b)*** *NaCl and $MgSO_4$ rejection and flux of the LC composite membranes and the commercial membrane UTC-60. Adapted from Ref. [32] with permission of John Wiley and Sons, Inc.*

The current greatest challenge for the application of columnar mesophases to form 1D nanoporous membranes is alignment control on larger scales (>cm^2). In recent years,

various alignment methods were reported to overcome this challenge. As mentioned before, surface confinement and magnetic fields are known methods to align discotic LCs [33]. Feng et al. used soft confinement to obtain 1 nm vertically aligned pores using the previously discussed sodium gallate salt (Figure 6.7) [34]. Highly aligned homeotropic monodomains were obtained by casting the discotic LC on a glass substrate and confining it with a PDMS substrate, before fixation of the morphology by a photo-polymerization. This approach shows potential for the alignment of 1D nanoporous membranes due to its easy scalability and ease of fabrication.

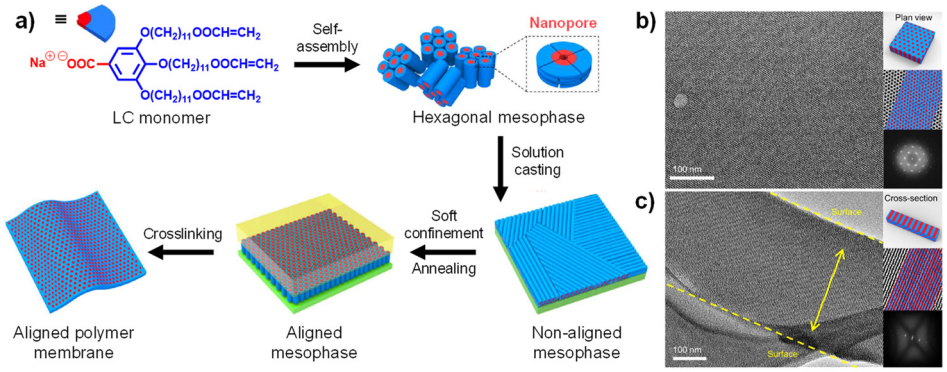

Figure 6.7: *The alignment of hexagonal ordered LCs by soft confinement.* ***a)*** *Schematic illustration of the alignment procedure.* ***b, c)*** *Transmission electron microscopy images of the aligned material microtomed along* ***b)*** *and perpendicular* ***c)*** *to the columns. Adapted from Ref. [34] with permission of American Chemical Society.*

Another powerful method to obtain well-organized nanopores is by alignment in magnetic fields [20,29,35,36]. Feng et al. obtained highly aligned LC films by rotating the film in a 3 - 6 T magnetic field, before a photo-polymerization to fixate the morphology. The influence of alignment on ion conductivity was demonstrated. The conductivity was 85 times higher for the homeotropic aligned films compared to nonaligned films [20]. These two alignment methods show that highly ordered nanoporous 1D LC networks can be obtained. However, the selectivity of these aligned films for small molecules or ion separations is not yet explored.

6.3.2 Two-dimensional pores

Two-dimensional (2D) pores are obtained from LCs with smectic or lamellar mesophases. Nanoporous polymer networks of smectic materials can be obtained by breaking chemical

bonds between the lamellar structures after fixation of the LCs. However, without a cross-linker between the lamellae sheets of the polymerized smectic layers, separation of the layers can occur. This will result in the collapse or disintegration of the lamellar structure [37]. To maintain the lamellar structure, Kishikawa et al. introduced reactive ”nanopillars” that act as a cross-linker to interconnect the layers [37]. These nanopillars are LC molecules with two polymerizable acrylate groups at each end and have similar sizes and shapes as the LCs with the hydrogen bonded template molecule (Figure 6.8a). A mixture containing a hydrogen bonded smectic LC and a covalent nanopillar LC was polymerized in the smectic mesophase and subsequent removal of the template yielded nanoporous polymer films (Figure 6.8b).

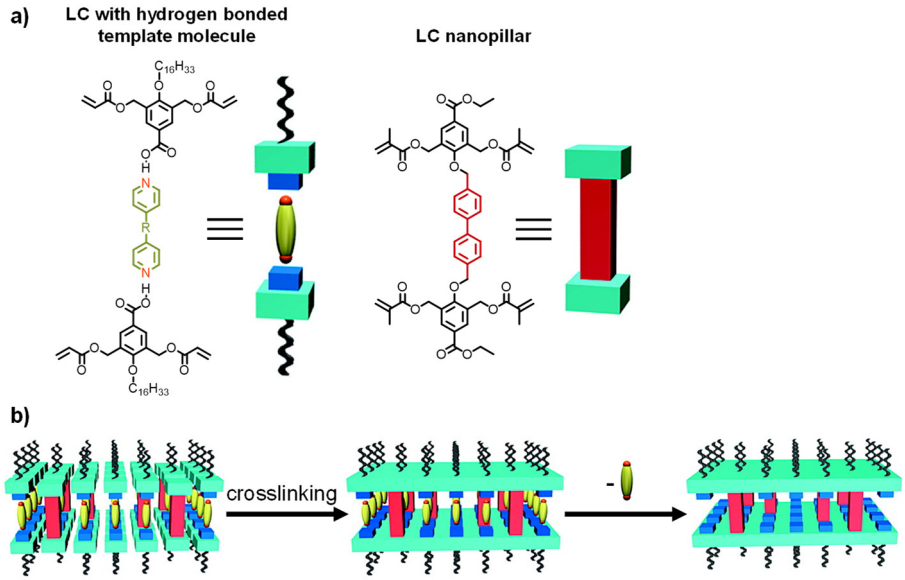

Figure 6.8: *Smectic LC-based nanoporous network using nanopillars.* ***a)*** *Structure of the hydrogen bonded LC and the nanopillar LC.* ***b)*** *Schematic illustration of monomer self-assembly, cross-linking and template removal. The nanopillar was used to provide structure and layer integrity. Adapted from Ref. [37] with permission of American Chemical Society.*

Using a similar approach, Mulder et al. presented nanoporous LC networks with neutral or positively charged pore interiors [38]. This approach relies on an LC heterodimer consisting of a polymerizable molecule with a pyridine functional group that forms a hydrogen bond with a non-polymerizable template molecule (Figure 6.9a). After cross-linking, the template is removed by breaking the hydrogen bonds between the dimers, resulting in a neutral

nanoporous network (Figure 6.9b). Next, the versatility of this system was demonstrated by protonation of the pyridyl nitrogen, which resulted in a positively charged pore interior.

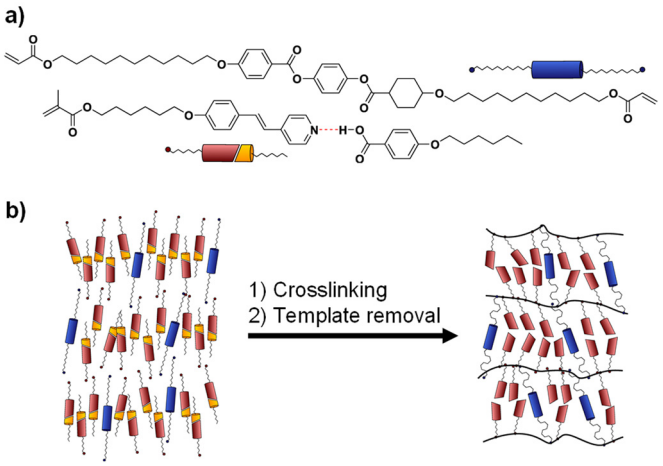

Figure 6.9: *Smectic LC-based nanoporous network using template removal strategy.* ***a)*** *Structures of the LC heterodimer with a hydrogen bonded template molecule and the cross-linker.* ***b)*** *Schematic illustration of monomer self-assembly, cross-linking and template removal. Adapted from Ref. [38].*

In another approach, Gonzalez et al. obtained a nanoporous network by breaking the hydrogen bonds between LC-hydrogen bonded dimers. This resulted in the formation of negatively charged carboxylate groups (Figure 6.10) [19]. In this approach, the breaking of the hydrogen bonds forms the pores based on Coulomb repulsion between the negatively charged carboxylate groups. This resulted in nanoporous networks with 2D pores of approximately 1 nm. Moreover, it was shown that the anionic pore interior of the nanoporous network can adsorb cationic methylene blue with a high occupation level (0.98 g of dye per gram of material), whereas anionic methyl orange and zwitterionic rhodamine B were respectively not or hardly adsorbed [39]. Furthermore, the adsorption of a cationic dye was highly dependent on the orientation of the pores [40]. The LC network with a proper pore orientation (planar alignment) had a significantly enhanced dye adsorption over the nonideal pore orientation (homeotropic alignment) (Figure 6.10c). This example highlights the importance of LC alignment and that pore orientation.

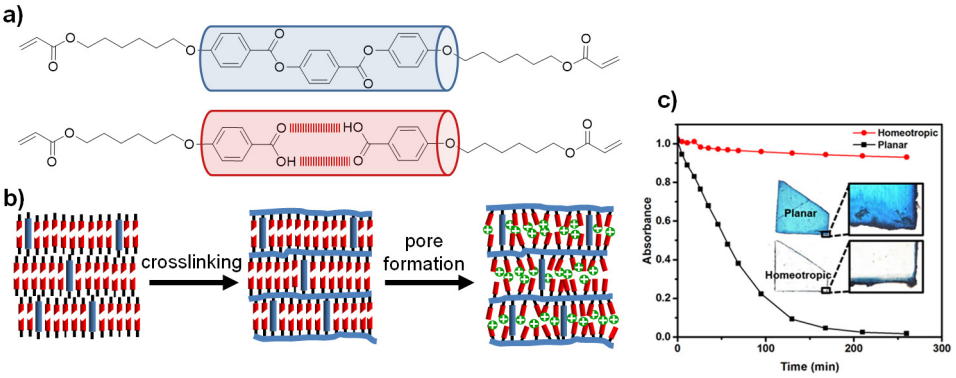

Figure 6.10: *Smectic LC-based nanoporous network using Coulomb repulsion.* ***a)*** *Structure of the LC dimer and the cross-linker.* ***b)*** *Schematic illustration of monomer self-assembly, cross-linking and pore formation due to the repulsion of the negatively charged carboxylate groups upon breaking of the hydrogen bonds [19].* ***c)*** *Cationic dye adsorption kinetics and microscopy pictures of the planar and homeotropic aligned network. Adapted from Ref. [40] with permission of American Chemical Society.*

The mentioned charge selectivity in the previous example seems promising for pressure-driven filtration of charged molecules. However, pressure-driven filtration requires strong mechanical films that are commonly achieved by the integration of a thin selective layer on a mechanically strong porous support [41]. Unfortunately, the fabrication of such membranes using smectic materials is unfeasible when combined with traditional alignment methods used in the LC display industry [42]. These techniques align LCs using surface-induced orientation in combination with confinement between two substrates. However, most porous supports do not act as an alignment layer or induce a nonideal pore orientation (homeotropic alignment). A possible solution for this challenge is using a porous scaffold as a support and alignment layer [43,44].

6.2.3.3 Three-dimensional pores

In contrast to 1D and 2D systems where large-scale alignment (>cm^2) is difficult to obtain and thereby limiting their applicability for a long time, nanoporous polymer networks with 3D geometries circumvent the requirement of LC alignment. However, the fundamental drawback of 3D geometries is that these systems display a higher tortuosity for molecular transport applications. Both lyotropic and thermotropic LCs can form bicontinuous mesophases that provide continuous nanochannels through the membrane. The most common approach to prepare membranes with 3D pores is by applying a thin LC layer in a bicontinuous mesophase on a porous support where the thin LC layer act as the selective

layer [32,45–48]. By subsequently fixating the LC morphology by a polymerization reaction, membranes with continuous small-diameter channels are formed. Henmi et al. used this approach to develop a thin separating layer based on a bicontinuous cubic polymer network [30]. A 50-100 nm thick layer of a thermotropic wedge-shaped LC monomer with a cationic triethylammonium head was coated on a polysulfone and nonwoven polyester support (Figure 6.11a-c). After polymerization of the LC structure, nanoporous films with pore sizes around 0.6 nm were obtained. Single salt pressure-driven permeation measurements show that these membranes have selective ion rejection. Surprisingly, small bromine anions were selectively rejected (83%), while larger sulfate ions (33% rejection) could pass the membrane (Figure 6.11d). Moreover, it was shown that the ions permeate predominantly through the 3D ionic pores. The permeability of ionic solutes is depending on specific interactions between the solute and the pore interior, making these membranes interesting for selective ion transport. In a later publication, Marets et al. showed that these materials could also be used for virus retention from water with a high efficiency, which expands the possible application range for these materials [49].

Using a similar approach, Zhou et al. coated a 40 µm thick layer of a gemini phosphonium lyotropic LC with a cubic morphology on a porous polyethylene fiber matte support [45]. After fixation of the morphology of the LC layer, 3D interconnected pores with an effective pore size of 0.75 nm were obtained (Figure 6.12a-b). The membrane properties were studied with dead-end water filtration measurements. It was shown that these membranes almost completely (95 to >99.9%) reject dissolved salt ions and neutral molecules in the 0.7-1.2 nm size range (Figure 6.12c). The solute rejections were comparable to a commercial RO membrane (AG series; not specified) and better than a commercial NF membrane (NF-270). Also the thickness-normalized water permeability (0.089 L m^{-2} h^{-1} bar^{-1} µm) was comparable to that of commercial RO membranes (AG series, 0.047-0.280 L m^{-2} h^{-1} bar^{-1} µm) [45,48]. Later Hatakeyama et al. showed that these LC membranes are also resistant to chlorine degradation and protein fouling [50]. However, a disadvantage of phosphonium systems is their difficult synthesis and the expensive reagents required to produce the gemini phosphonium lyotropic LC monomer [48]. To lower the production costs, ammonium-based gemini lyotropic LC monomers have been made. These LC monomers are significantly cheaper, easier to synthesize and more scalable compared to phosphonium-based lyotropic LCs, with only a slight penalty in membrane performance [48,51].

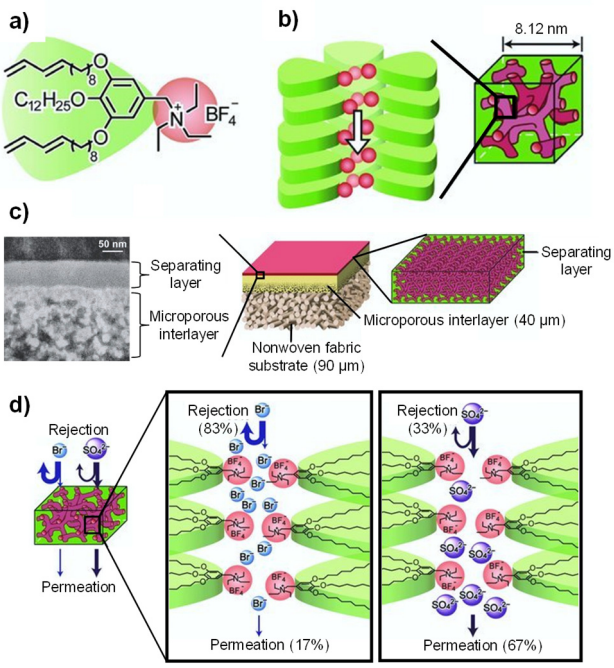

Figure 6.11: *A LC membrane with a thin separating layer based on a bicontinuous cubic morphology.* ***a)*** *Chemical structure of the thermotropic wedge-shaped LC molecule;* ***b)*** *Self-assembled bicontinuous cubic LC phase forming 3D interconnected pores;* ***c)*** *Schematic representation of the LC membrane;* ***d)*** *Schematic representation of selective rejection of anions through the membrane. Adapted from Ref. [30] with permission of John Wiley and Sons, Inc.*

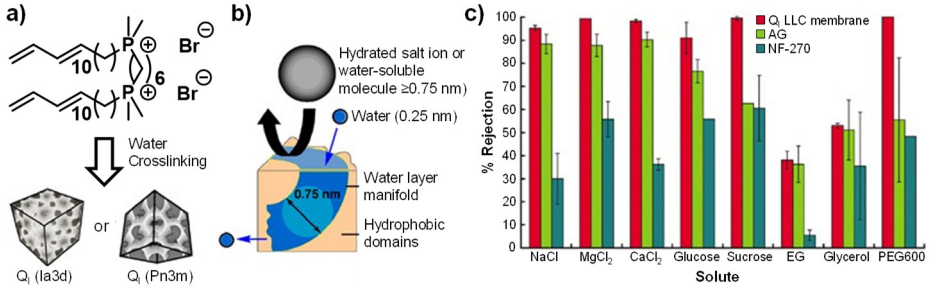

Figure 6.12: *Phosphonium-based LC membrane with a bicontinuous cubic morphology.* ***a)*** *Chemical structure of the phosphonium-based LC membrane with 3D interconnected pores, cross-linked in a bicontinuous cubic phase.* ***b)*** *Mechanism of water permeation through the LC membrane.* ***c)*** *Rejection properties of the LC membrane compared to commercial RO (AG series) and NF (NF-270) membranes. Adapted from Ref. [45] with permission of American Chemical Society.*

Later Dischinger et al. used an imidazolium-based lyotropic LC membrane with 1 nm pores for the treatment of hydraulic fracturing flowback water (Figure 6.13a) [52,53]. This wastewater is difficult to purify due to high concentrations of both salts and organic compounds. They showed that the imidazolium-based LC membrane thickness-normalized permeability (1.2 L m-2 h-1 MPa-1) was competitive with commercial RO (SW30HR, 0.7 L m-2 h-1 MPa-1) and NF membranes (NF-270, 1.9 L m-2 h-1 MPa-1) during filtration of flowback water. Remarkably, the imidazolium-based LC membrane showed different selectivity behavior compared to the commercial membranes (Figure 6.13b) [52]. The rejection of dissolved organic carbon (DOC) and total dissolved solids (TDS) are both lower for the imidazolium-based LC membrane compared to the SW30HR membrane. The selectivity of the imidazolium-based LC membrane shows a similar rejection of DOC as the NF-270 membrane but rejects TDS to a higher degree (75%) compared to the NF-270 membrane (10%). The higher TDS rejection of the imidazolium-based LC membrane compared to the NF-270 membrane is most likely explained by the uniform, charged pores in the nanostructured selective layer of the imidazolium-based LC membrane. These uniform pores allow the selective passage of uncharged solutes smaller than 1 nm by size exclusion. Meanwhile, the cations in solution are repelled by the cations forming the pore walls via charge repulsion. Consequently, by an unequal distribution of ions between the two sides of the membrane there is a potential build-up, resulting in the rejection of anions (Donnan exclusion). Therefore, the unique charged nanopore structure of the imidazolium-based LC membrane allows small organic compounds to permeate through the membrane while monatomic salts are rejected, showing the potential of this material as an alternative material to treat complex wastewaters.

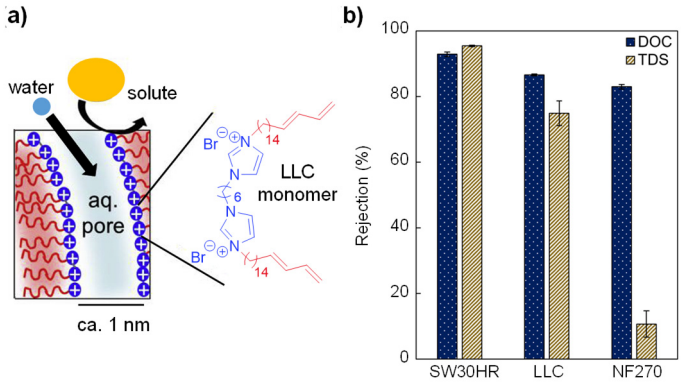

Figure 6.13: *Imidazolium-based lyotropic LC membrane with a bicontinuous cubic morphology.* ***a)*** *Chemical structure of the imidazolium-based LC membrane with 3D interconnected pores.* ***b)*** *Hydraulic fracturing flowback water rejection properties of the LC membrane compared to commercial RO (SW30HR) and NF (NF-270) membranes. Adapted from Ref. [52] with permission of Elsevier.*

Although all types of the discussed nanoporous LC networks show potential as membranes for ion transport, the separation of small (chiral) molecules and the removal of viruses for the production of drinking water, more research is needed toward actual filtration experiments with aligned membranes to demonstrate the true operating window of these membranes. Challenges for these systems include a combination of mechanical toughness and the control of alignment on large scales (≥cm^2). The often brittle nanoporous LC membranes need to be mechanically strong enough to withstand the mechanical pressure of pressure-driven filtration. In the ideal case, this challenge can be overcome by applying a thin LC layer on a polymer support, in which the LC layer acts as a thin selective layer and the support provides both mechanical strength and alignment of LCs. However, most current polymer supports have a negative effect on the alignment of LCs. Smart processing techniques and control of interactions between support and LCs can help to overcome this. In contrast to 1D and 2D systems, 3D nanoporous LC networks are obtained by using LCs with bicontinuous mesophases and provide continuous channels across the membrane without the need for alignment. These nanoporous films display a higher tortuosity compared to 1D and 2D nanoporous LC networks but can already compete with commercial reverse osmosis and nanofiltration membranes in terms of thickness-normalized permeabilities and retentions.

The discussed morphologies (1D, 2D and 3D systems) are not only interesting for water applications but can potentially, depending on their fabrication methods, also be used for the fabrication of non-porous membranes which can be used for gas separation. The above-mentioned morphologies offer the opportunity of using different chemistries to tailor the gas permeation properties of LC membranes and can lead to better gas separation performances compared to the LC membranes studied in this thesis.

6.4 Conclusion

In conclusion, this thesis describes the opportunities of using LCs to fabricate nanostructured membranes for gas separations of which the gas permeation properties can be easily tuned. A reliable method was found to fabricate and characterize the gas separation performances of these materials. Important properties such as the LC morphology, alignment and other subtle order differences provide control over the gas permeability and selectivity of LC membranes. However, given the many unique properties of LCs and their infancy in the field of gas separation, there is still a lot to explore regarding what these highly ordered materials can do in this field.

References

[1] G. Genduso, B.S. Ghanem, I. Pinnau, *Membranes (Basel).* **2019**, 9, 10.

[2] C.A. Scholes, J. Jin, G.W. Stevens, S.E. Kentish, *J. Polym. Sci. Part B Polym. Phys.* **2015**, 53, 719–728.

[3] R.W. Baker, *Ind. Eng. Chem. Res.* **2002**, 41, 1393–1411.

[4] B.W. Rowe, B.D. Freeman, D.R. Paul, *Polymer (Guildf).* **2009**, 50, 5565–5575.

[5] J.M. Hutchinson, *Prog. Polym. Sci.* **1995**, 20, 703–760.

[6] M. Galizia, W.S. Chi, Z.P. Smith, T.C. Merkel, R.W. Baker, B.D. Freeman, *Macromolecules.* **2017**, 50, 7809–7843.

[7] A.F. Ismail, W. Lorna, *Sep. Purif. Technol.* **2002**, 27, 173–194.

[8] A.C. Puleo, D.R. Paul, S.S. Kelley, *J. Membr. Sci.* **1989**, 47, 301–332.

[9] M. Mubashir, L.F. Dumée, Y.Y. Fong, N. Jusoh, J. Lukose, W.S. Chai, P.L. Show, *J. Hazard. Mater.* **2021**, 415, 125639.

[10] M. Houben, Z. Borneman, K. Nijmeijer, *Sep. Purif. Technol.* **2021**, 255, 117307.

[11] S.R. Reijerkerk, A. Arun, R.J. Gaymans, K. Nijmeijer, M. Wessling, *J. Membr. Sci.* **2010**, 359, 54–63.

[12] A. Car, C. Stropnik, W. Yave, K.V. Peinemann, *Sep. Purif. Technol.* **2008**, 62, 110–117.

[13] K. Ghosal, B.D. Freeman, *Polym. Adv. Technol.* **1994**, 5, 673–697.

[14] M.W. Hellums, W.J. Koros, G.R. Husk, D.R. Paul, *J. Membr. Sci.* **1989**, 46, 93–112.

[15] S.J.A. Houben, J. Kloos, Z. Borneman, A.P.H.J. Schenning, *J. Polym. Sci.* **2022**, 60, 803–811.

[16] G. Wang, C.J. Garvey, H. Zhao, K. Huang, L. Kong, *Membranes (Basel).* **2017**, 7, 37.

[17] J. Lugger, D.J. Mulder, R. Sijbesma, A. Schenning, *Materials (Basel).* **2018**, 11, 104.

[18] T. Kato, J. Uchida, T. Ichikawa, T. Sakamoto, *Angew. Chemie - Int. Ed.* **2018**, 57, 4355–4371.

[19] C.L. Gonzalez, C.W.M. Bastiaansen, J. Lub, J. Loos, K. Lu, H.J. Wondergem, D.J. Broer, *Adv. Mater.* **2008**, 20, 1246–1252.

[20] X. Feng, M.E. Tousley, M.G. Cowan, B.R. Wiesenauer, S. Nejati, Y. Choo, R.D. Noble, M. Elimelech, D.L. Gin, C.O. Osuji, *ACS Nano.* **2014**, 8, 11977–11986.

[21] M. Zhou, T.J. Kidd, R.D. Noble, D.L. Gin, *Adv. Mater.* **2005**, 17, 1850–1853.

[22] R.C. Smith, W.M. Fischer, D.L. Gin, *J. Am. Chem. Soc.* **1997**, 119, 4092–4093.

[23] H.K. Lee, H. Lee, Y.H. Ko, Y.J. Chang, N.K. Oh, W.C. Zin, O. Kim, *Angew. Chemie - Int. Ed.* **2001**, 40, 2669–2671.

[24] Y. Ishida, S. Amano, N. Iwahashi, K. Saigo, *J. Am. Chem. Soc.* **2006**, 128, 13068–13069.

[25] Y. Ishida, S. Amano, K. Saigo, *Chem. Commun.* **2003**, 3, 2338–2339.

[26] Y. Ishida, H. Sakata, A.S. Achalkumar, K. Yamada, Y. Matsuoka, N. Iwahashi, S. Amano, K. Saigo, *Chem. - A Eur. J.* **2011**, 17, 14752–14762.

[27] G.M. Bögels, J.A.M. Lugger, O.J.G.M. Goor, R.P. Sijbesma, *Adv. Funct. Mater.* **2016**, 26, 8023–8030.

[28] J.A.M. Lugger, D.J. Mulder, S. Bhattacharjee, R.P. Sijbesma, *ACS Nano.* **2018**, 12, 6714–6724.

[29] C. Li, J. Cho, K. Yamada, D. Hashizume, F. Araoka, H. Takezoe, T. Aida, Y. Ishida, *Nat. Commun.* **2015**, 6, 1–9.

[30] M. Henmi, K. Nakatsuji, T. Ichikawa, H. Tomioka, T. Sakamoto, M. Yoshio, T. Kato, *Adv. Mater.* **2012**, 24, 2238–2241.

[31] M. Gupta, Y. Suzuki, T. Sakamoto, M. Yoshio, S. Torii, H. Katayama, T. Kato, *ACS Macro Lett.* **2019**, 8, 1303–1308.

[32] T. Sakamoto, T. Ogawa, H. Nada, K. Nakatsuji, M. Mitani, B. Soberats, K. Kawata, M. Yoshio, H. Tomioka, T. Sasaki, M. Kimura, M. Henmi, T. Kato, *Adv. Sci.* **2018**, 5, 1–9.

[33] H.K. Bisoyi, Q. Li, *Prog. Mater. Sci.* **2019**, 104, 1–52.

[34] X. Feng, S. Nejati, M.G. Cowan, M.E. Tousley, B.R. Wiesenauer, R.D. Noble, M. Elimelech, D.L. Gin, C.O. Osuji, *ACS Nano.* **2016**, 10, 150–158.

[35] M.E. Tousley, X. Feng, M. Elimelech, C.O. Osuji, *ACS Appl. Mater. Interfaces.* **2014**, 6, 19710–19717.

[36] X. Feng, K. Kawabata, G. Kaufman, M. Elimelech, C.O. Osuji, *ACS Nano.* **2017**, 11, 3911–3921.

[37] K. Kishikawa, A. Hirai, S. Kohmoto, *Chem. Mater.* **2008**, 20, 1931–1935.

[38] D.J. Mulder, T. Liang, Y. Xu, J. Ter Schiphorst, L.M.W. Scheres, B.M. Oosterlaken, Z. Borneman, K. Nijmeijer, A.P.H.J. Schenning, *J. Mater. Chem. C.* **2018**, 6, 5018–5024.

[39] H.P.C. Van Kuringen, G.M. Eikelboom, I.K. Shishmanova, D.J. Broer, A.P.H.J. Schenning, *Adv. Funct. Mater.* **2014**, 24, 5045–5051.

[40] T. Liang, H.P.C. Van Kuringen, D.J. Mulder, S. Tan, Y. Wu, Z. Borneman, K. Nijmeijer, A.P.H.J. Schenning, *ACS Appl. Mater. Interfaces.* **2017**, 9, 35218–35225.

[41] R.W. Baker, *Membrane technologies and applications*, third ed., John Wiley & Sons, **2012**.

[42] J.M. Geary, J.W. Goodby, A.R. Kmetz, J.S. Patel, *J. Appl. Phys.* **1987**, 62, 4100–4108.

[43] A. Ryabchun, F. Lancia, A.D. Nguindjel, N. Katsonis, *Soft Matter.* **2017**, 13, 8070–8075.

[44] A. Bobrovsky, V. Shibaev, G. Elyashevitch, *J. Mater. Chem.* **2008**, 18, 691–695.

[45] M. Zhou, P.R. Nemade, X. Lu, X. Zeng, E.S. Hatakeyama, R.D. Noble, D.L. Gin, *J. Am. Chem. Soc*. **2007**, 129, 9574–9575.

[46] T. Ichikawa, M. Yoshio, A. Hamasaki, J. Kagimoto, H. Ohno, T. Kato, *J. Am. Chem. Soc.* **2011**, 133, 2163–2169.

[47] B.M. Carter, B.R. Wiesenauer, E.S. Hatakeyama, J.L. Barton, R.D. Noble, D.L. Gin, *Chem. Mater.* **2012**, 24, 4005–4007.

[48] B.R. Wiesenauer, D.L. Gin, *Polym. J.* **2012**, 44, 461–468.

[49] N. Marets, D. Kuo, J.R. Torrey, T. Sakamoto, M. Henmi, H. Katayama, T. Kato, *Adv. Healthc. Mater.* **2017**, 6, 1–6.

[50] E.S. Hatakeyama, C.J. Gabriel, B.R. Wiesenauer, J.L. Lohr, M. Zhou, R.D. Noble, D.L. Gin, *J. Membr. Sci.* **2011**, 366, 62–72.

[51] E.S. Hatakeyama, B.R. Wiesenauer, C.J. Gabriel, R.D. Noble, D.L. Gin, *Chem. Mater.* **2010**, 22, 4525–4527.

[52] S.M. Dischinger, J. Rosenblum, R.D. Noble, D.L. Gin, K.G. Linden, *J. Membr. Sci.* **2017**, 543, 319–327.

[53] S.M. Dischinger, J. Rosenblum, R.D. Noble, D.L. Gin, *J. Membr. Sci.* **2019**, 592, 117313.

Authorship statement

PhD candidate's name: ir. J.J.H. Kloos

First promotor: prof.dr.ir. D.C. Nijmeijer

Second promotor: dr.ing. Z. Borneman

Co-promotor: prof.dr. A.P.H.J. Schenning

Chapter 1 *Introduction.* I proposed the general idea of the content in my first draft. My promotors then gave general directions about defining the research question, aligning the contents and general storyline. Revisions were made based on the feedback from the promotors and co-promotor.

Chapter 2 *On the order and orientation in liquid crystalline polymer membranes for gas separation*. I proposed the research question, conducted the experiments, drafted the results into a manuscript and supervised a master student (co-author) who synthesized and characterized compound M1. Compound M2 was prepared and characterized by two co-authors. My promotors and co-promotor gave feedback on the manuscript and directed the discussion.

Chapter 3 *Molecular order determines gas transport through smectic liquid crystalline polymer membranes with different chemical compositions.* I formulated the research question based on findings from previous research. I conducted experiments, wrote the draft manuscript and supervised a master student who performed experiments. My promotors and co-promotor gave feedback on the manuscript and directions on how to present the results.

Chapter 4 *Tuning the gas separation performances of smectic liquid crystalline polymer membranes by molecular engineering.* I proposed the research question, performed the experiments and drafted the manuscript. All compounds in this chapter were synthesized and characterized by a co-author. My promotors and co-promotor gave feedback on the manuscript.

Chapter 5 *Nematic liquid crystalline polymer membranes for gas separation.* I formulated the research question, performed the experiments and drafted the manuscript. All compounds in

this chapter were synthesized and characterized by a co-author. My promotors and co-promotor gave feedback on the manuscript, directed the discussion and helped with how to present the results.

Chapter 6 *Epilogue.* I wrote the draft based on the directions from my promotors and co-promotor. Revisions were made based on the feedback from the promotors and co-promotor.

Acknowledgements

Een promotieonderzoek doen, dat klinkt cool, leuk en leerzaam. Vier jaar lang onderzoek doen met (hopelijk) leuke mensen, ondertussen mijn onderzoekskwaliteiten verbeteren en verder groeien als persoon. Dat was wat ik (ongeveer) dacht toen ik vier en een half jaar geleden besloot dat ik een promotieonderzoek wilde doen. Al het bovengenoemde bleek zeker waar: ik heb met geweldige mensen mogen samenwerken en leuke dingen mogen doen en ik ben de afgelopen jaren zowel op werk als op persoonlijk vlak ontzettend gegroeid. Maar de misschien naïeve ik vergat dat vier jaar een lange tijd is waarin veel kan gebeuren. Zo waren er de eerdergenoemde leuke dingen, maar ook minder leuke en moeilijke dingen en ervaringen. Ondanks alles is het na vier jaar eindelijk zo ver: het proefschrift is af! Ik wil daarom graag de komende pagina's van mijn proefschrift gebruiken om iedereen te bedanken die, op welke manier dan ook, mij de afgelopen vier jaar heeft geholpen of ondersteund. Zonder jullie zou dit proefschrift er niet zo hebben uitgezien!

Allereerst wil ik mijn promotoren prof. Kitty Nijmeijer en dr. Zandrie Borneman bedanken voor het mogelijk maken van mijn promotieonderzoek binnen de MMP-groep. Ondanks dat ik de schrijfopdracht tijdens mijn sollicitatie compleet had verknald, hadden jullie vertrouwen in mij en hebben jullie mij de kans gegeven mezelf te ontwikkelen. Bedankt hiervoor. De eerste twee jaar van mijn onderzoek waren niet bepaald makkelijk, omdat het toch lastiger bleek te zijn dan wij in eerste instantie dachten om van vloeibare kristallijne materialen membranen te maken. Maar jullie wisten mij toch altijd weer te motiveren en zo nodig bij te sturen tijdens onze meetings en verzekerden mij dat alles goed ging komen. Ik moet toegeven dat ik over dit laatste af en toe sceptisch was. Hoe ging ik in twee jaar vier experimentele hoofdstukken genereren? Nou de vier hoofdstukken zijn gelukt, dus ik kan nu zeggen dat jullie helemaal gelijk hadden. Buiten de wetenschappelijke bijdrage, wil ik jullie ook bedanken voor jullie steun en begrip toen mijn thuissituatie veranderde. Kitty, ik kan niet genoeg benadrukken hoezeer ik het waardeer dat ik altijd bij je kon langskomen voor 'korte' werkgerelateerde vragen of om gewoon mijn hart te luchten. Dit heeft mij enorm geholpen in lastige periodes en ik wil je hier dan ook heel erg voor bedanken. Zandrie, jouw 'out-of-the-boxdenken' was heel belangrijk voor mijn onderzoek en heeft mij vaker over moeilijke punten geholpen. Verder wil ik je bedanken dat ik altijd bij je terecht kon voor vragen. Dus Kitty en Zandrie: bedankt voor jullie hulp en de hele fijne samenwerking.

Ik wil mijn copromotor prof. Albert Schenning graag bedanken voor zijn tijd, steun, advies en medewerking tijdens mijn PhD-traject. Albert, jouw eeuwige enthousiasme, openheid en directheid heb ik altijd ontzettend gewaardeerd, het heeft een grote bijdrage gehad aan dit proefschrift. Bedankt dat ik altijd bij je kon langskomen met mijn korte vragen, die vaak toch niet zo kort waren of om gewoon mijn hart te luchten. Ik weet dat je van korte to-the-point stukken tekst houdt, dus ik zal het voor de verandering kort houden. Albert, bedankt voor je hulp en de hele fijne samenwerking.

Daarnaast wil ik ook dr. Johan Lub bedanken voor zijn hulp met hoofdstuk 2, 4 en 5. Johan, jouw hulp met het zoeken, maken en karakteriseren van verschillende vloeibaar kristallijne monomeren was van onschatbare waarde voor dit proefschrift. Jouw enthousiasme voor chemie is aanstekelijk en ik hoop dat ik mijn werk met net zo veel enthousiasme kan blijven doen als dat jij dit nog steeds doet. Ik ga onze gesprekken over vloeibaar kristallijne materialen missen.

I want to thank the members of the committee prof. Emiel Hensen, prof. Ivo Vankelecom, prof. José Luis Serrano, prof. Rint Sijbesma and dr. Hans Heuts for taking the time to carefully read and evaluate my thesis and attending my defense.

Ik wil ook graag mijn paranimfen Machiel en Menno bedanken. Mannen het is bijna zover, ook jullie ‘gasscheidingsbaby’ en de laatste van de drie musketiers is bijna klaar. Machiel, Chiel, Chielke, jij was de eerste persoon die ik tegenkwam op mijn eerste dag toen ik aan mijn promotieonderzoek begon. Vanaf het moment dat je met een van je ijsbrekers het ijs brak, was het voor mij al duidelijk dat je een topkerel bent. Jouw enthousiasme, creativiteit, nuchterheid en relaxte houding zijn eigenschappen die ik zeer waardeer en waar ik nog veel van kan leren. Onze (te korte) tijd als kantoorgenoten was gezellig, misschien iets te gezellig, en ik zal je fructose-experiment nooit vergeten. We hebben ook veel leuke momenten buiten werk gehad, zoals het voorbereiden van Menno’s verdediging, broeken passen in te kleine pashokjes en pannenkoeken eten op kerstavond. Dit zijn momenten waar ik met plezier aan terugdenk. Anneloes, ik wil jou ook bedanken voor alle steun en leuke momenten van de afgelopen jaren. Jouw ideeën, inzet maar vooral uitvoering tijdens de fotoshoot voor Machiels fotoboek waren goud! Menno, Houb, Houbie, Houbje, Houbinator (en nog veel meer), onze ‘bromance’ is begonnen toen we samen de DSC probeerden te maken. De DSC heeft het niet gered, maar hier is wel een goede en zeer gewaardeerde vriendschap uit voortgekomen. Zonder jou zou dit proefschrift er heel anders uit hebben gezien, aangezien jij iets meer dan

twee jaar geleden met het idee kwam om over te stappen naar gasscheiding. Hierdoor hebben we nog meer kunnen samenwerken, wat heeft geresulteerd in vier publicaties. Wie had dat gedacht op die vrijdagmiddag. Jouw bereidheid om te helpen, je nuchterheid en kennis waren heel belangrijk voor het tot stand komen van dit proefschrift, bedankt hiervoor. Naast werk, hebben we ook veel leuke momenten gehad. Onze (bijna wekelijkse) filmdagen met sushi waren top, maar de vakantie naar Markelooo en daarna de roadtrip in Amerika waren legendarisch. Machiel en Menno, ontzettend bedankt voor jullie hulp, steun, de gezellige avonden en het feit dat jullie mijn paranimfen willen zijn.

Tijdens mijn PhD heb ik ook een aantal studenten mogen begeleiden bij hun afstuderen of bachelor-eindproject. Daphne, Sandra en Nico, jullie hebben allemaal bijgedragen aan dit proefschrift en ik wil jullie daarvoor bedanken. Nico, ik wil jou nog even apart benoemen, jouw inzet en harde werken hebben hoofdstuk 2 en 3 mogelijk gemaakt. Hier mag je echt trots op zijn! Ik wens jullie allemaal veel succes in jullie verdere carrière.

Small research groups will eventually become larger research groups. To all (former and new) MMP members and colleagues from other groups: Thank you for all your help, support and fun moments over the last four years. Next to work, I enjoyed all the good moments we shared such as our breaks/lunches, borrels and activities.

Anna banana, four years ago we started on the same day on the same project. And ohh boy, I think I can say that the original project was a real challenge for both of us. Luckily we started together and learned a lot of new things, how to work together with a very stubborn person, patience and the density of water are some examples. Thank you for all the nice food and your willingness to help and support me in difficult times. I am looking forward to party with you and Rémy when we are all finished.

Rémy, you are the smartest clown that I know. Although our topics were less intertwined, you were always willing to help me when needed. I will never forget the setup you built to remove solvent in our first year. Thank you for the good time and enjoy your new house!

Niki, jij bent een van de meest energieke en positieve mensen die ik ken. Tijdens de coronalockdown hebben we samen een reviewartikel geschreven, dat ik heb gebruikt in hoofdstuk 1 en 6. Dit ging naar mijn idee heel gemakkelijk en het was dan ook heel fijn om dit samen met jou te doen. Bedankt voor je positieve mindset in ons kantoor en voor het feit dat je altijd met mij wilde wandelen tijdens de lunchpauze.

Cees, your belly is never full. Where there is cake, there is Cees. Ik daag je uit voor een all-you-can-eat-sushi-eetwedstrijd. Naast dat je altijd een leuke kantoorgenoot bent geweest, wil ik je ook bedanken voor al je technische hulp met mijn experimenten.

Sjoukje, bedankt voor de gezellige gesprekken op het lab en al je technische hulp met mijn experimenten. Veel succes met je nieuwe baan!

Daniëlle, mijn partner in crime wat betreft (koffie)pauzes. Je was er altijd voor in om onder het genot van een kopje koffie al mijn zorgen aan te horen of om een of ander random onderwerp voor de tiende keer te bespreken. Dit maakte het werk echt veel leuker en ik ga onze 'positieve' gesprekken echt missen. Gelukkig bestaat er zoiets als een telefoon en anders weet ik je vast wel mee te lokken naar het terras voor een drankje. Bedankt voor al je hulp en steun en blijf vooral jezelf.

Maxime, jij was mijn partner in crime wat betreft het geven van de werkcolleges van Scheidingstechnologie. We hebben samen een flink aantal tentamens en opdrachten nagekeken met een eendjesdouchegordijn tussen ons in, dit blijft toch een aparte ervaring. Verder was je altijd in voor een kop koffie of voor een drankje in de Fort, of nou ja, je zorgde dat iedereen meekwam naar de Fort. Bedankt voor de gezellige avonden!

Nadia(aaa), jij bent echt een topper. Ik heb altijd ontzettend moeten lachen om je droge humor, ga zo door. Verder ben ik blij dat je huidige kantoorgenoten (Woutje en Marrit) doorgaan met onze 'zingwedstrijden'.

Caroline, jij bent de heldin van MMP. Bedankt voor al je hulp en steun de afgelopen jaren, ik vond het heel fijn dat je alles binnen de groep zo soepel liet verlopen en dat ik met al mijn vragen bij je langs kon komen. Verder wil ik je bedanken voor de snoepjes die je elke dag bijvult op je bureau, hier heb ik goed gebruik van gemaakt.

Simon, ik zie ons nog prutsen tijdens de organische-chemievakken bij Zuyd en ik ben er nog steeds trots op dat wij als enige van ons jaar het molecuul hebben gemaakt dat daadwerkelijk de bedoeling was. Beginnersgeluk I guess. Hoe toevallig was het dan ook dat we ook nog eens aan hetzelfde onderwerp werkten voor ons proefschrift. Hier hadden we beiden wat minder geluk, maar uiteindelijk zijn we er wel gekomen. Bedankt voor al je hulp en steun in het lab, maar ook voor de mentale ondersteuning toen alles wat minder ging.

Patricia, in your thesis acknowledgements you said that I have a positive and cheerful attitude in life. Although I completely agree with this statement, it was you that made the membrane meetings more fun due to your enormous amount of positive energy! Thank you for this and the fact that you were always willing to help me.

Sterre, vijf jaar geleden hebben wij ons afstudeerproject bij Ellen gedaan. Vanaf dag één gingen we als Jut en Jul aan het werk. Dat was echt een toptijd en ik was dan ook heel blij dat Albert je zover kreeg om ook een promotieonderzoek te doen. Tijdens ons promotieonderzoek waren we geen Jut en Jul meer, maar waren de koffiepauzes nog altijd even gezellig. Bedankt voor het aanhoren van al mijn geklaag en ik wens je veel succes met het afronden van je proefschrift.

Roel, wij hebben elkaar pas echt leren kennen toen we paranimfen van Simon waren. Ik blijf erbij dat we meer dan zes potten pindakaas voor Simon hadden moeten bestellen. Bedankt voor de wetenschappelijke discussies en de koppen koffie. Jij ook succes met het afronden van je proefschrift.

Arne, jij was mijn labpartner wanneer ik bij SFD aan het werk was. Hoe vaak wij wel niet samen op het lab hebben gestaan om ‘even’ iets nieuws te proberen, om er vervolgens een hele week (waarschijnlijk langer) mee bezig te zijn. Dat was iets wat ons beiden voortdurend overkwam. Gelukkig konden we tussendoor onze frustratie kwijtraken met een kop koffie of een biertje in de Fort, samen met Sterre en Yari. Het samen prutsen in het lab is echt iets wat mij altijd goed heeft gedaan en ik wil je dan ook bedanken voor de afgelopen jaren.

Yari, samen met Arne vormden jullie het Belgenfront in SFD. Aanvankelijk moest ik even wennen aan je voor mij exotische taalgebruik; muren behangen zal nooit meer hetzelfde zijn, maar ik heb altijd heel erg om jou en Arnes droge humor moeten lachen. Dit maakte het werk echt een stuk leuker. Ook onze momenten in het Fort waardeer ik zeer, Belgen met hun bier. Bedankt voor alles en veel succes met het verbouwen en behangen van je pas gekochte huis in Diepenbeek!

Zonder familie zou ik nooit tot dit punt zijn gekomen. Mam, pap, Angel, Eddy, Shane, Anush en Lance bedankt voor al jullie onvoorwaardelijke steun, eerst met het boogschieten en daarna met mijn promotieonderzoek. Jullie waren altijd geïnteresseerd in wat ik deed en hoe het ging, ook al hadden jullie vaak geen idee waar het nou precies over ging. Ook toen ik tijdens het behandeltraject van Brechtje druk was - zowel op werk als thuis - hebben jullie ons

altijd gesteund en geholpen door bijvoorbeeld eten te komen brengen. Dit waardeer ik (en Brechtje) ontzettend en ik mag dan ook heel blij zijn dat ik jullie als familie heb. Bedankt voor alles!

Ook wil ik mijn schoonouders bedanken voor al hun hulp in de afgelopen jaren. Roel en Margriet, zonder jullie hulp tijdens het behandeltraject van Brechtje zou dit proefschrift nooit op tijd af zijn geweest. Verder wil ik jullie bedanken voor de mentale steun en alle leuke momenten die we hebben gehad de afgelopen jaren.

Brechtje, al ruim acht jaar ben jij mijn grootste steun en toeverlaat. Je hebt mij altijd gesteund, liefde gegeven en mij af en toe tegen mezelf beschermd. Toen ik begon aan mijn promotieonderzoek wisten we beiden dat dit niet altijd even makkelijk zou zijn. Er zouden moeilijke periodes komen, maar die zouden we samen overwinnen. Nou die zijn er zeker geweest. Vooral de afgelopen twee jaar waren niet makkelijk en die periode heeft ons leven totaal veranderd. Ik ben supertrots op je hoe je door alles heen bent gegaan en hoe hard je hebt gewerkt om te herstellen. Jouw enorme doorzettingsvermogen heeft mij altijd gemotiveerd om door te gaan en jouw steun heeft ervoor gezorgd dat het proefschrift op tijd af is. Bedankt voor alles. Nu is het tijd om samen nieuwe avonturen aan te gaan en om te genieten van ons huisje in Sterksel.

“I am going on an adventure!”

— Bilbo Baggins

About the author

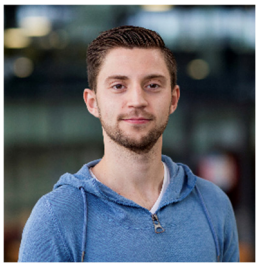

Joey Kloos was born on the 31st of March 1993 in Maastricht, The Netherlands. After graduating from high school, he started his education in Chemical Engineering at Zuyd University of Applied Sciences in Heerlen where he received his Bachelor of Science degree. Thereafter, he moved in 2015 to Eindhoven and continued with his master's education at the Eindhoven University of Technology (TU/e) following the Molecular Systems and Materials Chemistry track. In May 2018, he successfully defended his master's thesis entitled: "Temperature responsive coatings for infrared reflecting windows" in the group Stimuli-responsive Functional materials and Devices (SFD) of prof.dr. Albert Schenning under the supervision of Ellen van Heeswijk and obtained his Master of Science degree. In 2018, he joined the Membrane Materials & Processes (MMP) group at the same university as a PhD candidate under the supervision of prof.dr.ir Kitty Nijmeijer and dr.ing. Zandrie Borneman and investigated the structure-property relationships of liquid crystalline polymer membranes for gas separation applications. The most important results of this research are presented in this thesis.

List of publications

Publications related to this thesis

J. Kloos, N. Joosten, A. Schenning, K. Nijmeijer, Self-assembling liquid crystals as building blocks to design nanoporous membranes suitable for molecular separations, *J. Membr. Sci.* **2021**, 620, 118849.

J. Kloos, N. Jansen, M. Houben, A. Casimiro, J. Lub, Z. Borneman, A.P.H.J. Schenning, K. Nijmeijer, On the order and orientation in liquid crystalline polymer membranes for gas separation, *Chem. Mater.* **2021**, 33, 8323–8333.

J. Kloos, N. Jansen, M. Houben, K. Nijmeijer, A.P.H.J. Schenning, Zandrie Borneman, Molecular order determines gas transport through smectic liquid crystalline polymer membranes with different chemical composition, *ACS Appl. Polym. Mater.* **2022**, 4, 7426–7436.

J. Kloos, M. Houben, J. Lub, Z. Borneman, K. Nijmeijer, A.P.H.J. Schenning, Tuning the gas separation performances of smectic liquid crystalline polymer membranes by molecular engineering, *Membranes (Basel).* **2022**, 12, 805.

J. Kloos, J. Lub, M. Houben, Zandrie Borneman, K. Nijmeijer, A.P.H.J. Schenning, Nematic liquid crystalline polymer films for gas separation, *Liq. Cryst.* **2022**, 1–9.

Other publications

E.P.A. van Heeswijk, J. Kloos, J. de Heer, T. Hoeks, N. Grossiord, A.P.H.J. Schenning, Well-adhering easily producible photonic reflective coatings for plastic substrates, ACS Appl. *Mater. Interfaces.* **2018**, 10, 30008–30013.

E.P.A. van Heeswijk, J. Kloos, N. Grossiord, A.P.H.J. Schenning, Humidity-gated, temperature-responsive photonic infrared reflective broadband coatings, *J. Mater. Chem. A.* **2019**, 7, 6113–6119.

S.J.A. Houben, J. Kloos, Z. Borneman, A.P.H.J. Schenning, Switchable gas permeability of a polypropylene-liquid crystalline composite film. *J. Polym. Sci.* **2022**, 60, 803–811.

M. Houben, J. Kloos, M. van Essen, K. Nijmeijer, Z. Borneman, Systematic investigation of methods to suppress membrane plasticization during CO_2 permeation at supercritical conditions. *J. Membr. Sci.* **2022**, 647, 120292.